STRUCTURE STUDIES OF NUCLEI USING SELF CONSISTENT MEAN FIELDS

Thesis submitted to the University of Calicut
in partial fulfillment of the requirements
for the award of the degree of

Doctor of Philosophy
in
Physics
under the Faculty of Science

by

NITHU ASHOK

Department of Physics
University of Calicut
Kerala

December 2018

CERTIFICATE

This is to certify that the corrections/suggestions from the adjudicators have been incorporated in the thesis entitled "STRUCTURE STUDIES OF NUCLEI USING SELF CONSISTENT MEAN FIELDS" submitted to the Department of Physics, University of Calicut by Ms. Nithu Ashok.

University of Calicut
Date:

Prof. Antony Joseph
(Supervising Guide)
Department of Physics
University of Calicut.

CERTIFICATE

Certified that the work presented in this thesis entitled 'Structure studies of nuclei using Self Consistent Mean Fields' is a bonafide work done by Ms. Nithu Ashok, under my guidance in the Department of Physics, University of Calicut and that this work has not been included in any other thesis submitted previously for the award of any degree.

University of Calicut
Date:

Prof. Antony Joseph
(Supervising Guide)
Department of Physics
University of Calicut
Calicut University P.O.
Malappuram, Kerala
email: aj@uoc.ac.in
Ph. no.: 9446164109.

DECLARATION

I hereby declare that the work presented in this thesis entitled 'Structure studies of nuclei using Self Consistent Mean Fields' is based on the original work done by me under the guidance of Prof. Antony Joseph, Department of Physics, University of Calicut, and has not been included in any other thesis submitted previously for the award of any degree.

University of Calicut
Date: Nithu Ashok

blank

Dedicated to

My family

Acknowledgements

First of all I would like to express my sincere gratitude to my guide Dr. Antony Joseph who introduced me into the fascinating world of nuclear physics. It is his continuous support, motivation and guidance throughout my research helped me to complete my Ph.D. I also thank him for providing oppurtunities for scientific discussions with eminent personalities of the field.

I am utmost thankful to Dr. Jhilam Sadhukhan, for his constant support to reach my potential when I thought I couldn't reach my goals. I am extremely grateful to him for providing an oppurtunity to work with him. Words are not enough to express my gratitude towards him.

I would like to thank Dr. Mrutunjaya Bhuyan for giving me reply to all my mails without any hesitation regarding doubts. I am also grateful to Dr. Raja Nisar Ali, for his valuable suggestions during my early stages of research. He is the one who gave me confidence so that I was able to begin my journey. I would like to thank my beloved friend Dr. Arunabha Saha for rendering all the help during the period I spend at VECC.

I acknowledges VECC, Kolkata for their warm hospitality and for providing the necessary computing facilities.

I also acknowledges, UGC, Govt. of India for providing financial support under JRF scheme for pursuing my research.

I express my sincere gratitude to Dr. Lajish V. L., Department of Computer Science, University of Calicut for making me available the cloud computing server RX 2530 M2 Xeon for carrying out a part of our computations.

I would like to say my heartfelt gratitude to my dear sweet lovely friend Anju who was there for me with a helping hand and a sweet smile on face. I would like to thank my travel companions Sanila, Vishnu, Shan and Sebastian for giving me some memorable moments in my life. I also like to acknowledge Sreejith, Senthil and Bhabina for their helping hands during my journey of PhD. I would like to thank my beloved friend Pankajakshy for being with me throughout my hardships.

I thank my friends Deepthy, Ramsiya, Usha, Vidya, Sahra, Sreepriya, Bintu, Divya, Raseen, Prasanth, Sravan, Shabeer, Arjun and many more for their care and support during my research period. Neverthless, I am also grateful to my dearest Manu and Sajith. It is a blessing to have you both to turn any crucial phase of life into happiness. I also thank my cousins Pooja, Keerthana and her friends for their invaluable help during the last stage of my research.

I also would like to express my sincere gratitude to all the teachers and non-teaching staff of the department for giving me their kind support. I am also grateful to my colleagues for their support during the last year of my Ph.D. I would like to thank each and every person who directly or indirectly helped me in the completion of my PhD.

Last but not least, I would like to thank my family: my parents and my sister for supporting and encouraging me throughout my life in fulfilling my dreams.

Nithu Ashok

Contents

List of Figures

List of Tables

List of Publications

Contributions related to thesis

1. "Cluster decay in Osmium isotopes using Hartree-Fock-Bogoliubov theory", **Nithu Ashok**, Deepthy Maria Joseph and Antony Joseph, Mod. Phys. Lett. A, 31, 1650045(2016).

2. "Alpha and cluster decay half-lives in tungsten isotopes: A microscopic analysis", **Nithu Ashok** and Antony Joseph, Nucl. Phys. A, 977, 101(2018).

3. "A systematic study of alpha and cluster decay in Platinum isotopes", **Nithu Ashok** and Antony Joseph, Int. J. Mod. Phys. E, 27, 1850098 (2018).

4. "Shape evolution of neutron rich nuclei in sub-lead region around neutron shell closure". **Nithu Ashok**, Jhilam Sadhukhan and Antony Joseph, Communicated (Nucl. Phys. A, 2019).

5. "A systematic study of the ground state properties of W, Os and Pt isotopes using HFB theory". **Nithu Ashok** and Antony Joseph, Under review (Int. J. Mod. Phys. E, 2019).

Other contributions

6. "A systematic study of proton, alpha and cluster decays in Rhenium isotopes using the effective liquid drop model", Deepthy Maria Joseph, **Nithu Ashok** and Antony Joseph, Mod. Phys. Lett. A, 31, 1650031(2016).

7. "A theoretical study of cluster radioactivity in platinum isotopes", Deepthy Maria Joseph, **Nithu Ashok** and Antony Joseph, Eur. Phys. J. A, 54,

8(2018).

8. "Study of level density and reaction cross-sections in Thorium isotopes" Erumban Ummukulsu, **Nithu Ashok** and Antony Joseph, Mod. Phys. Lett. A, 34, 1950091(2019).

Papers in conferences/symposia

9. "A study of alpha decay and cluster radioactivity from Osmium isotopes", **Nithu Ashok**, Deepthy Maria Joseph and Antony Joseph, National Seminar on Isotopes and Nuclear Techniques-Application to Basic and Applied Sciences during March 11-12, 2014 at M.A.M.O. College, Calicut, Kerala.

10. "Cluster radioactivity from Osmium isotopes", **Nithu Ashok**, Deepthy Maria Joseph and Antony Joseph, 75 years of Nuclear Fission Conference during May 8-10, 2014 at BARC, Mumbai.

11. "Theoretical study of cluster radioactivity in Re isotopes", Deepthy Maria Joseph, **Nithu Ashok** and Antony Joseph, 75 years of Nuclear Fission Conference during May 8-10, 2014 at BARC, Mumbai.

12. "Ground state properties of Osmium isotopes upto 2n drip line", **Nithu Ashok**, Deepthy Maria Joseph and Antony Joseph, two-day National Seminar on Nuclear, Astro and High Energy Physics during October 29-30, 2015 at Kuriakose Elias College, Mannanam, Kerala.

13. "Neutron skin in Osmium isotopes", **Nithu Ashok**, Deepthy Maria Joseph and Antony Joseph, in DAE-BRNS symposium on Nuclear Physics, during December 7-11, 2015 at SSSIHL, Prasanthi Nilayam, Puttaparthi, Andra Pradesh.

14. "Investigation of probable decays in Rhenium isotopes", Deepthy Maria Joseph, **Nithu Ashok** and Antony Joseph, DAE-BRNS symposium on Nuclear Physics, during December 7-11, 2015 at SSSIHL, Prasanthi Nilayam, Puttaparthi, Andra Pradesh.

15. "Neutron skin in Platinum isotopes", **Nithu Ashok**, Deepthy Maria Joseph and Antony Joseph, 28th Kerala Science Congress during January 28-30, 2016 at University of Calicut, Kerala.

16. "Ground state properties of Praseodymium isotopes within Hartree-Fock-Bogoliubov theory", **Nithu Ashok** and Antony Joseph, in the Symposium: A journey from nuclei to quarks during June 28-29, 2016 at Variable Energy Cyclotron Centre, Kolkata.

17. "One quasiparticle states in Lanthanum isotopes", **Nithu Ashok**, Deepthy Maria Joseph and Antony Joseph, DAE-BRNS symposium on Nuclear Physics, during December 5-9, 2016 at Saha Institute of Nuclear Physics, Kolkata.

18. "Shape co-existence in tungsten isotopes", **Nithu Ashok**, Jhilam Sadhukhan and Antony Joseph, DAE-BRNS symposium on Nuclear Physics, during December 20-24, 2017 at Thapar University, Punjab.

19. "Probable exotic decays in Tungsten isotopes", Deepthy Maria Joseph, **Nithu Ashok** and Antony Joseph, DAE-BRNS symposium on Nuclear Physics, during December 20-24, 2017 at Thapar University, Punjab.

20. "Structure studies of nuclei using Self consistent mean fields", **Nithu Ashok**, DAE International Symposium on Nuclear Physics, during December 9-14, 2018 at BARC, Mumbai.

21. "Study of level density and reaction cross sections in Thorium isotopes", E. Ummukulsu, **Nithu Ashok** and Antony Joseph, DAE International Symposium on Nuclear Physics, during December 9-14, 2018 at BARC, Mumbai.

Preface

Self Consistent Mean Field theory (SCMF) is one of the leading theories which help in studying and predicting the properties of medium and heavy mass nuclei nowadays. The basis of all mean field theories is Hartree-Fock (HF) theory. Pairing correlations are included with the help of Bardeen-Cooper-Schrieffer (BCS) theory. HF+BCS theory is well suited for nuclei around the beta stability line but fails towards the drip-line due to the inability to account for the continuum effect there. A generalized version of HF+BCS theory, the Hartree-Fock-Bogoliubov (HFB) theory, in which the mean field and pairing part are given equal status, can successfully describe nuclei away from the beta-stability line. Nuclei in the region $A \sim 190$ are found to exhibit structural changes between prolate, oblate and spherical configurations. This made these nuclei an interesting topic of study. We have selected W, Os and Pt isotopes as the representatives of this region. Moreover, these nuclei are near to the proton shell closure Z=82. The present thesis is devoted to the study of the structural properties of some transitional nuclei with the aid of HFB theory, with zero-range Skyrme interaction. The work can be divided into three parts.

In the first part, we analysed the shape transition of these isotopes using various Skyrme interactions. The study mainly concentrates on the isotopes around the neutron shell closure N=126. A strong competition between various shapes are found to occur in this particular region. Initially, axial calculations have been carried out. As some signatures of triaxiality is observed to occur in this region, triaxial calculations have also been done with the aid of UNEDF1 parametrization. A transition from prolate to spherical configurations via a γ-soft region is observed.

The second part of the study is devoted to the microscopic description of alpha and cluster decay in these isotopes. The emission of clusters of protons and neutrons heavier than alpha particle and lighter than the lightest fission fragment is called cluster radioactivity. It is observed that isotopes belonging to the region

between proton drip-line and beta-stability line are unstable against several decay modes. The emission of clusters like ^{8}Be, ^{12}C, ^{16}O, ^{20}Ne and ^{24}Mg from these nuclei have been predicted. The rate of emission of a cluster diminishes with the neutron number of the parent. The decay rate is maximum for the decay mode leading the magic daughter nuclei. This observation emphasises the role of shell closure in cluster radioactivity.

In the third part, we have extended our investigation to neutron rich region of W, Os and Pt isotopes. On moving away from the beta-stability line, neutron number exceeds that of protons and the n-p interaction is not strong enough to hold these excess neutrons inside the nucleus. This results in the spatial extension of neutrons around the bulk nuclear matter. As a result of this a thin layer of neutrons, called neutron skin, will be formed around the core. It is characterised by the difference between neutron and proton rms radii. It is observed that as we move away from the beta-stability line, width of this layer increases and reaches to a value of 5-6 fm near the neutron drip-line. The same have been observed with the help of neutron and proton density distributions. We have also predicted N=184 as the magic neutron number, next to N=126, based on the 2n-separation energy.

In summary, we have analysed the sensitivity of various Skyrme forces in predicting the structural properties of W, Os and Pt isotopes throughout the isotopic chain. We can observe various characteristic properties along the isotopic chain. Some dominate at neutron deficient region, some at neutron rich region while certain other characteristics are prominent near the beta-stability line. Thus a qualitative study of various properties of a set of heavy nuclei has been accomplished and is presented here.

Chapter 1

Introduction

The nucleus is the centre of the atom. It is a self-bound system which is composed of positively charged protons and electrically neutral neutrons, which are together called as nucleons. They are surrounded by negatively charged electron cloud. Nucleons are held together inside the nucleus through the strong interaction. Almost the whole mass of an atom resides within the nucleus. The word nucleus means 'kernel of a nut'. The discovery of the electron by J. J. Thomson provided the first significant insight into the structure of an atom. Later, Rutherford, by his alpha particle scattering experiment, gave first information about the structure of the nucleus. According to him, nucleus, a positively charged part, is concentrated in a small volume at the centre of the atom and is surrounded by a cloud of negatively charged electrons. The size of the atom is about $10^{-10}m$ whereas the nuclear size is about Fermi range $\sim 10^{-15}m$[1].

Though it is a known fact that nuclei are composed of neutrons and protons, any combination of neutrons and protons will not make up a nucleus because of the effect of some forces and symmetries. Figure 1.1 shows the nuclear landscape, which presents the nuclei which are known to exist as well as the nuclei which are expected to exist. Neutron number and proton number are shown in x-axis and y-axis respectively. The black region corresponds to the beta-stability line where the stable, long-lived nuclei exist. Here, the light stable nuclei lie along N=Z line and for heavy nuclei, the beta-stability line will deviate a little towards the neutron-rich side ($N > Z$). Around 300 nuclei lie in this valley of beta-stability.

The horizontal and vertical red lines show the nuclei with magic numbers (2, 8, 20, 28, 50, 82, 126), which are stable and have spherical shape. The yellow region shows nuclei which are experimentally observed through various nuclear reactions. The green area represents 'terra incognita', which contain nuclei far from the stability line and which are yet to be explored. On moving away from the beta-stability line on either side, with the addition or removal of neutron or proton, we reach the boundary of nuclear stability, called the drip-lines. On the right side, there is neutron drip-line, where the binding energy of the last neutron becomes zero. Similarly, towards the left side, proton drip-line exists, where the binding energy of the last proton vanishes.

Despite its minimal size, the nucleus exhibits a lot of interesting phenomena like shape-phase transition, radioactivity, fission, fusion, giant resonance, chirality, wobbling etc. Towards the nuclear drip-line, they show several interesting phenomena like halo, skin, shell quenching etc. Moreover, the nucleus can exist in various shapes. The stable nuclei will be in spherical configuration with nucleon number either singly or doubly magic. They can also exist in prolate and oblate configurations. Some higher deformed states like the pear shape and pyramid shapes are also experimentally observed in recent years.

For having an in-depth knowledge of factors underlying these phenomena, we should have an idea of the strong nuclear force which holds the nucleons inside the tiny nucleus. Unfortunately, till today no complete theory has been developed to understand the nature of the force that governs such a strong interaction inside this small entity. However, different models have been proposed over the years to solve the mystery behind the nucleus. A brief account of some well-established models are given below.

One of the widely accepted earlier models is the liquid drop model. Here, the nucleus is compared with the drop of an incompressible fluid having high density. This model successfully explained the binding energy, nuclear fission etc. The semi-empirical mass formula for finding the binding energy of the nucleus is given

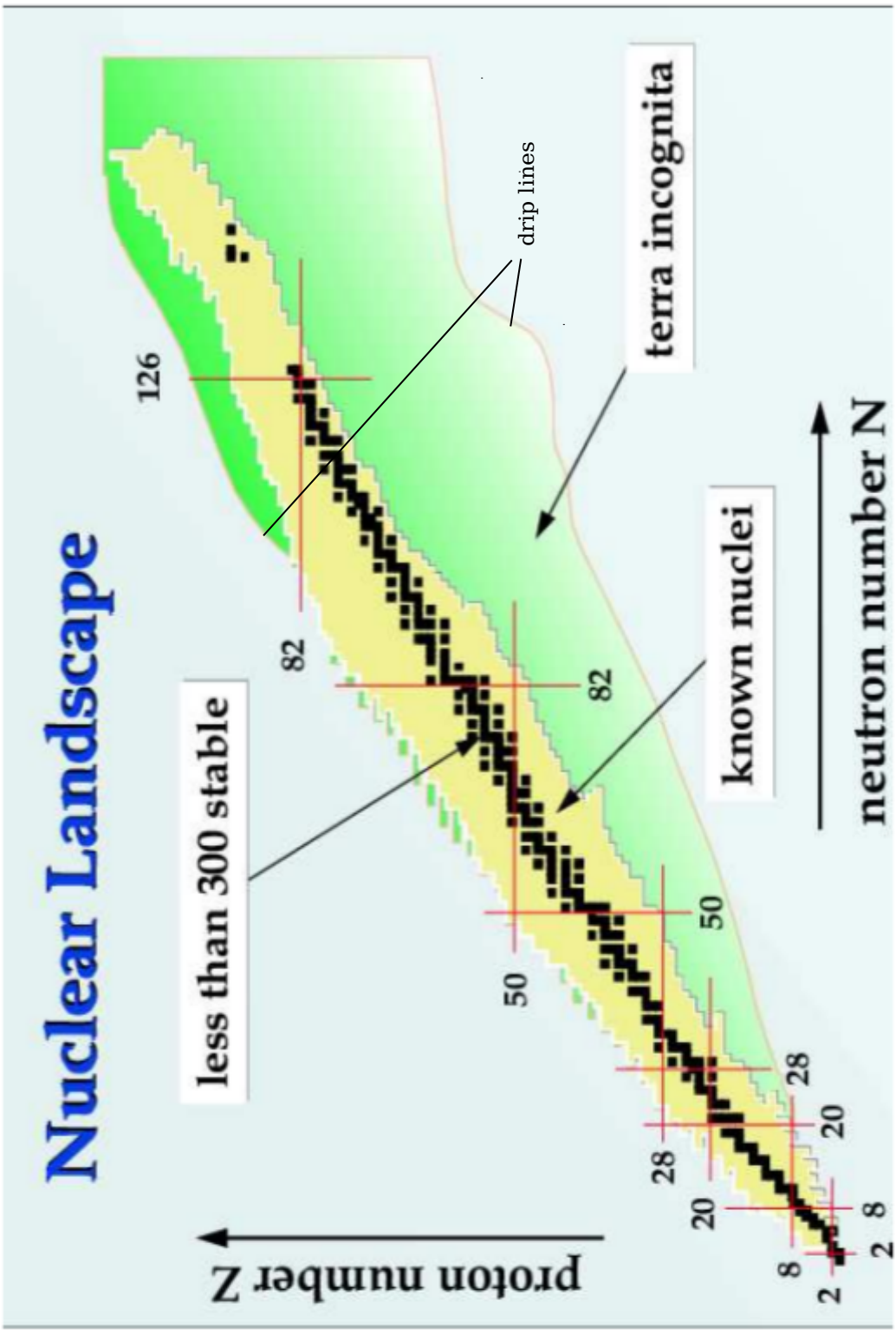

Figure 1.1: The nuclear landscape .

by,

$$BE = a_v A - a_s A^{2/3} - a_c \frac{Z(Z-1)}{A^{1/3}} - a_a \frac{(A-2Z)^2}{A} \pm \frac{a_p}{A^{3/4}} \tag{1.1}$$

Here the first term is the volume energy, which depends on the number of nucleons. Its contribution increases the binding energy because as the number of nucleons increases, the force which holds the nucleons inside the nucleus also increases. The second term, which is the surface energy, lowers the binding energy, as the nucleons at the surface is very less bound compared to those in the interior because they are not surrounded by other nucleons as in the interior. The third term represents the Coulomb energy which arises due to the repulsion of protons. This will reduce the binding energy. The fourth term shows the asymmetry energy, which points towards the stability of the nuclei. It also reduces the binding energy. The last term is the pairing energy which shows the spin or odd-even effect of the nucleus. But this model fails to predict the underlying shell structures of the nucleus. It cannot explain the magic numbers, spin, parity, magnetic moment etc.

The Fermi gas model considers the nucleus as a degenerate gas of protons and neutrons. This statistical model is based on the assumption that each nucleon moves in an attractive potential with constant depth. The behaviour of neutrons and protons are explained based on Fermi-Dirac distribution. This model helps to study the properties of nuclei in excited states but fails in the case of low lying nuclear states.

In 1949, the shell model (independent particle model) was developed by Eugene Paul Wigner, Maria Goeppert Mayer and J. Hans D. Jensen, which emphasises the shell structure of the nucleus. It was observed that nuclei with a certain number of protons or neutrons (2, 8, 20, 50, 82 and 126) are stable. These numbers called magic numbers were explained clearly by the shell model. Here it is assumed that nucleons move in a net nuclear potential produced by all the other nucleons. The actual form of the potential is the Woods-Saxon potential. But as

the eigen-value of this is not obtained in a closed form, square-well and harmonic oscillator potential are employed. Here all the three potentials considered are spherically symmetric. With the use of square well potential, they were not able to reproduce magic gaps at 28, 50, 82 and 126. The use of harmonic oscillator potential also failed to reproduce the magic numbers above 20. To obtain the required magic numbers, Meyer and Jenson independently proposed the inclusion of the spin-orbit interaction. Thus all the magic numbers were successfully reproduced. The shell model can successfully predict the ground state spin and parity, magnetic moment, quadrupole moment etc[2].

The collective model combines some of the features of the liquid drop model and the shell model. Here it is assumed that nucleons in the unfilled shells move around the core of the nucleus in a net potential produced by the core. The interaction between the extra nucleons and the core leads to the deformation of the nucleus. The coupling between collective motion of core and nucleons outside the core will be weak for spherical nucleus. This interaction increases in the case of deformed nuclei. The net potential due to the core is not spherically symmetric, instead it get modified to incorporate the deformation of the nuclei. The motion of extra nucleons and the collective motion of core leads to shape oscillations. The rotational and vibrational energy states arises due to the collective motion of the core and the motion of the extra nucleons outside the core leads to nucleonic energy state. This model explains the deviations of experimental magnetic moments from Schmidt lines, rotational and vibrational energy levels, quadrupole moments of highly deformed nuclei etc[3].

Nilsson model, introduced by S. G. Nilsson, is a generalizaton of the shell model. This model describe the single particle motion of nucleons in a deformed potential. Here instead of isotropic harmonic oscillator potential, anisotropic harmonic oscillator potential is considered. In addition to this, they also considered spin-orbit and centrifugal potentials. This model provides the information about the energy states of deformed nuclei. In the limit of large deformations, shell closures of spherically symmetric potential breaks[4].

1.1 Objectives of the present work

The broad aim of the present work is to study the macroscopic properties of some transitional nuclei.

Nuclei in the region $A \sim 190$ are found to exhibit a structural change between prolate, oblate and spherical configuration. This made nuclei in this region an interesting topic of study. We have selected W, Os and Pt isotopes as the representatives of this region. Moreover, these nuclei are near to proton shell closure Z=82. We have studied various structural aspects of these nuclei along the isotopic chain within the framework of Skyrme HFB theory. Isotopes lying far from β-stability line have much importance in nuclear astrophysics.

With the above intentions in mind, we have carried out studies related to three structural aspects of W, Os and Pt isotopes. They are

- Structural evolution of selected isotopes of W, Os and Pt around N=126 and also to analyse the presence of triaxiality in these nuclei.
- The feasibility of alpha and cluster radioactivity in W, Os and Pt isotopes. The reasoning behind this is that any structural characteristc of nuclei become eloquent through their decay processes.
- The evolution of neutron skin thickeness of W, Os and Pt isotopes and prediction of the magic number next to N=126.

1.2 A review on earlier works

1.2.1 Shape evolution

The study of the evolution of nuclear shapes with nucleon number has become a very interesting area of research nowadays. Nuclei, inspite of its small size can exhibit spherical, quadrupole, octupole and other higher order deformed shapes. The nuclear deformation is due to the interplay between the surface oscillation of the nuclear core and the motion of the individual valence nucleons. Or we

can say it is due to the polarization of the nuclear core by the valence nucleons. This leads to the spontaneous symmetry breaking which is called as the Jahn-Teller effect[5]. When the surface energy dominates, nuclei will have spherical configuration.

The nuclear surface is usually expressed in terms of the spherical harmonics $Y_{\lambda\mu}(\theta, \phi)$ and is given by

$$R = R_0(1 + \sum_{\mu} \beta_{\lambda\mu} Y_{\lambda\mu}(\theta, \phi)) \tag{1.2}$$

Here $\beta_{\lambda\mu}$ is the deformation parameter. When $\lambda = 2$, we have quadrupole deformation, which is the dominant mode of deformation of atomic nuclei. Here axially symmetric oblate and prolate configurations are the dominant deformation modes. $\lambda = 3$ gives rise to the octupole deformation, which is due to the spontaneous breaking of reflection symmetry and parity. Various shape deformations which are observed to occur in the atomic nuclei are shown in fig. 1.2 [6]. From this figure we can see that atomic nuclei exhibit axial as well as non-axial symmetry. This figure shows spherical, prolate, oblate, hexadecupole, triaxial ellipsoid, octupole, tetrahedron and highly deformed asymmetric octupole shapes, exhibited by the nuclei throughout the nuclear chart, respectively.

Nuclei can exhibit different types of phase transitions. The phase transition associated with the shape is the zero temperature phase transition[7]. They occur due to quantum fluctuations and hence termed as quantum phase transitions. Figure 1.3 shows the phase transition occuring in the atomic nucleus which is termed as Casten triangle.

The shape-phase transition of a nucleus had been explained based on dynamical symmetries by various groups. This transition corresponds to the breaking of dynamical symmetries [8]. These symmetries are usually employed in Interacting Boson Model (IBM). In IBM, the dynamical symmetries corresponding to spherical, axially deformed and $\gamma-$ soft shapes are U(5), SU(3) and SO(6) respectively. Iachello[9] had proposed X(5) and E(5) symmetries to study the shape-

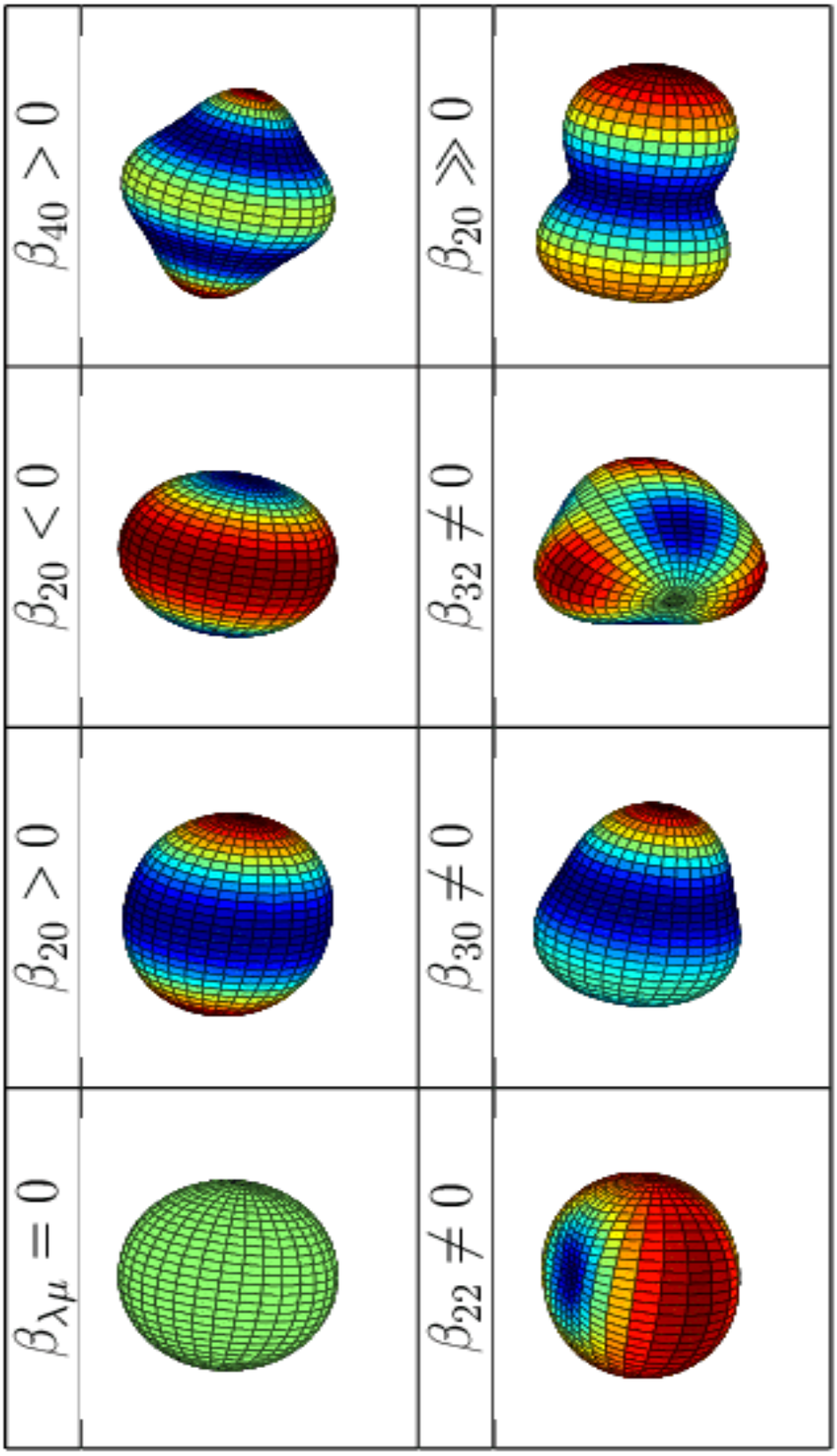

Figure 1.2: A schematic figure showing various nuclear shapes.

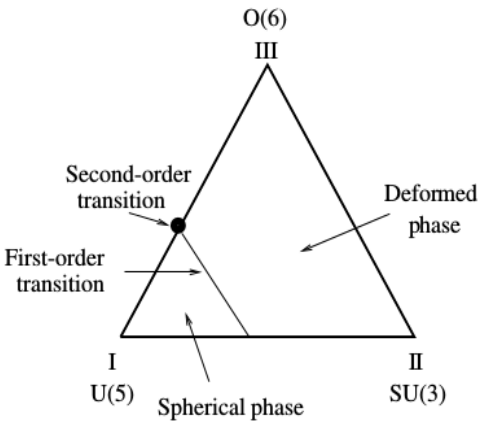

Figure 1.3: Casten triangle.

phase transitions in nuclei. X(5) symmetry explains the critical point showing the transition from spherically (U(5)) to axially deformed (SU(3)) shape. E(5) symmetry is for the critical point nuclei which shows the transition from spherical to $\gamma-$ soft (SO(6)) shapes. The transition from spherical to axially deformed shapes is the first order phase transition and from spherical to $\gamma-$ unstable state is the second order phase transition.

Geometrical interpretation of shapes have been done with the help of two shape parameters β and γ. β is the deformation parameter which is related to the axial deformation of the nuclei and γ is the triaxial parameter which shows the deviation from the axial deformation [10].

Experimental signatures for shape transitions can be obtained from the ratio of the excitation energy of first 4^+ to first 2^+ states. Experimental ratio E_{4^+}/E_{2^+} [11] are given in fig. 1.4. Nuclei will be axially symmetric deformed rotor, spherical vibrator and triaxial rotor if the ratio is 3.33, 2.0 and 2.5 respectively.

A brief review on experimental and theoretical studies are discussed below.

Survey on experimental studies of shape evolution

Y. Tanaka et al.[12] experimentally determined the ground state quadrupole deformation of some rare earth nuclei using quadrupole hyperfine splitting of muonic transition. The shape transition in the neutron-rich Os isotopes is

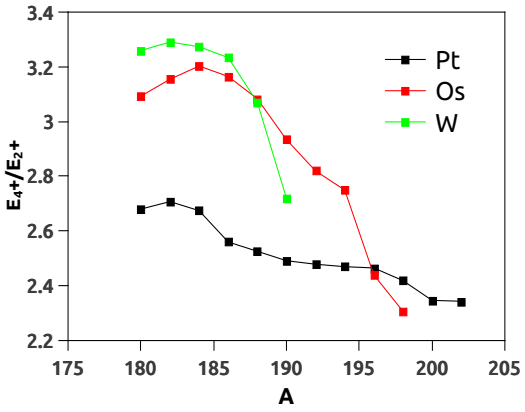

Figure 1.4: Experimental ratio of excitation energy of first 4^+ to 2^+ state.

studied by investigating the neutron-rich ^{196}Os nucleus through in-beam γ-ray spectroscopy using a two-proton transfer reaction from a ^{198}Pt target to a ^{82}Se beam[13]. γ -unstable/triaxial rotor yrast band was observed with the help of γ- ray spectroscopy. Some of the recent experimental studies show that ^{190}W (N=116) shows a transition from prolate to γ-soft system [14]. Experimental studies on Os isotopes shows that, ^{192,194}Os exhibit oblate configuration [15]. Prolate-oblate shape coexistence is found to exist in $^{176-188}$Pt by the analysis of yrast bands [16]. Isotope shift and hyperfine structure measurements show a shape co-existence in neutron deficien Pt isotopes [17]. Lifetime measurements show that ^{188}Pt exhibit prolate-oblate shape transition [18, 19]

Survey on theoretical studies on shape evolution

From theoretical point of view, the shape transition from prolate to oblate and vice versa, of isotopes around W, Os and Pt have been investigated by using different models. With the help of pairing plus quadrupole model, Kumar et al.[20] studied the transition of shapes in W, Os and Pt nuclei. Ansari [21], studied the shape transition in Os and Pt isotopes in the mass range A=186-196 using HFB theory with pairing plus quadrupole plus hexadecapole interaction. Shape transition and shape co-existence in even-even Pt and Hg isotopes with

neutron number ranging from N= 98 to 120 have been studied by R. Bengtsson et al. [22] with the help of Woods-Saxon potential and Nilsson potential. Bonche et al.[23] studied the shape isomerism of Os, Pt and Hg isotopes with the help of Skyrme HF+BCS approach. Stevenson et al.[24] have studied the nuclear shape evolution of even-even nuclei in the vicinity of ^{190}W using Hartree-Fock theory with separable monopole interaction. Sarriguren et al.[25] studied shape transition of W from N=110 to 122 using Skyrme HF+BCS model. Robledo et al.[26] with the help of HFB under triaxial symmetry studied the shape evolution of Yb, Hf, W, Os and Pt isotopes, having neutron number in the range N=110 to 122. Gogny as well as Skyrme interactions were used for their study. Similar study using axially symmetric relativistic and non relativistic mean field theory with angular momentum projection for Hf, W and Os isotopes have been carried out by Naik et al.[27]. HFB+Gogny interactions again stress the presence of triaxiality in Pt isotopes ranging from A=184 to 196 [28]. Interacting Boson Model (IBM), derived from HFB-Gogny have shown that Pt isotopes are more triaxial in nature as compared to Os and W isotopes [29, 30, 31]. Nomura et al. [32] also investigated the prolate to oblate shape transition in neutron-rich odd mass Pt, Os and Ir isotopes. Anuradha et al.[33] have studied the quadrupole deformation of proton emitters in the region $50 < Z < 80$ using triaxially deformed Cranked Nilsson Strutinsky method and they observed shape transition in Z=67-73 nuclei. Structural and decay properties of nuclei in the region Z=70-90 was studied using relativistic mean field theory by Mahapatro et al.[34].

1.2.2 Cluster radioactivity

The spontaneous emission of clusters heavier than alpha particle and lighter than the lightest fission fragment is defined as cluster radioactivity. This phenomenon takes place without the emission of neutrons[35]. In this particular phenomenon, the parent nucleus (N,Z) will spontaneously break into two fragments, a daughter nucleus (N_d, Z_d) and a light fragment (N_c, Z_c). The light fragment is termed as

cluster. Since the cluster decay mode is very rare, they are termed as exotic decay. Usually nuclear decay processes fall into two categories. They are cold and hot decays. In hot decays, daughter nuclei will be in excited states while in cold decays both parent and daughter will be in ground state. Here only a rearrangement of nucleons will takes place from the initial configuration to the final one. Since both the parent and the cluster are in ground states, total kinetic energy of the fragments is equal to the Q-value of the reaction. Cluster decay is an intermediate process between alpha decay and spontaneous fission. Cluster emission is a very rare process compared to alpha decay. The ratio of the rate of cluster emission to alpha emission is termed as branching ratio. The branching ratio decreases as the cluster becomes heavier. The experimental branching ratio for different decay modes vary between 10^{-9} and 10^{-17}.

Cluster decay can be explained on the basis of α-decay models or fission-like models. Studies on cluster decay have shown that there are two islands of cluster radioactivity. They are trans-tin region and trans-lead region. Because of this, cluster radioactivity is at times called tin-radioactivity or lead-radioactivity. The most probable decay modes lead to the formation of daughter nuclei which may be either in the tin region (^{100}Sn/^{132}Sn) or in the lead region(^{208}Pb). This is because of the stability due to shell effects of these magic nuclei. Experimentally clusters from ^{14}C to ^{34}Si were detected.

Many theoreticals models have been developed to study this phenomenon. In spite of all the differences, all these models stems from Gamow's theory of α decay. Theoretical models used to describe the phenomena of cluster radioactivity can be broadly classified into two - Unified Fission Model (UFM) and Preformed Cluster Model (PCM). A brief description of both the models are given below.

Unified Fission Model

Alpha decay, cluster decay and cold fission are treated in a similar way under UFM. They differ on the basis of the asymmetry in mass. In this model, parent nucleus undergoes gradual deformation until it attains the scission configuration

and finally it splits into two separate nuclei. The preformation probability is taken as unity. Based on the interacting potential, several research groups have developed different versions of UFM.

Poenaru et al. [36, 37, 38] used Analytical Super Asymmetric Fission Model (ASAFM) in which the potential energy for the overlapping region is approximated by a second order polynomial in the intra-nuclear distance R and for the separation region, this is taken to be equal to the sum of Coulomb interaction energy and the centrifugal potential. Shanmugham et al. [39] had used finite range Yukawa plus exponent potential to study the half-life as well as the deformation of parent and daugter nuuclei. Shi et al. [40, 41] used Coulomb energy and the proximity potential for the seperation region and simple power law interpolation for the overlapping region. Pik-Pichak used an asymmetric fission model to estimate the cluster decay probabilities[42]. Royer et al. [43] developed the Generalised Liquid Drop Model(GLDM), where the potential is taken as the sum of volume, surface, Coulomb, proximity and rotational energy. Here shell correction and pairing energy were also taken into account. Goncalves et al. [44] developed the Effective Liquid Drop Model(ELDM), in which the total potential energy is taken as the sum of Coulomb, surface and centrifugal potential.

In our work we have used the phenomenological model called ELDM for comparing the half-lives of alpha and cluster decay obtained from the microscopic analysis (HFB theory). A brief theoretical explanation of ELDM is given below.

Effective Liquid Drop Model

In ELDM, α and cluster decay are explained in a unified framework. These processes are explained by considering different inertial coefficients according to the shape parametrization chosen to explain the dynamical evolution of the system. Four independent coordinates are selected to explain the shape parametrization. As shown in fig. 1.5, they are the radii of spherical fragments R_1 and R_2, the distance between their geometrical centres ζ and the distance of the plane of intersection from the geometrical centre of the massive fragment ξ. Applying

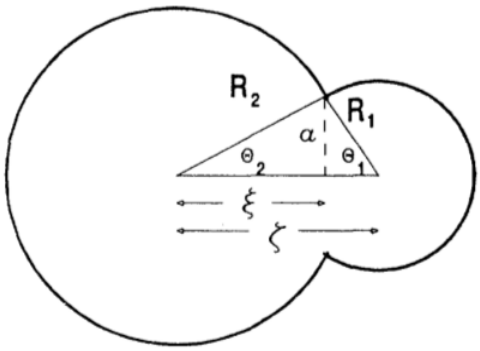

Figure 1.5: Schematic representation of shape parametrization of nuclear deformation.

three constraints, the 4-D problem is reduced to 1-D problem[44].

In ELDM, the potential energy contribution includes the Coulomb, surface and centrifugal components. The Coulomb energy which was developed by Gaudin[45] is given by

$$V_c = \frac{8}{9}\pi a^5 \varepsilon(x_1, x_2)\rho_c \tag{1.3}$$

where ρ_c is the initial charge density, a is the neck radius and $\varepsilon(x_1, x_2)$ is a function of the angular variables x_1 and x_2 which are defined in terms of angles θ_1 and θ_2 are expressed as

$$x_1 = \pi - \theta_1$$

and

$$x_2 = \theta_2 - \pi$$

The surface potential used here is expressed as[44]

$$V_s = 4\pi\sigma_{eff}(R^2 - R_1^2 - R_2^2) \tag{1.4}$$

with σ_{eff} being the effective surface tension and R, R_1 and R_2 are the radii of

parent, daughter and cluster respectively. The effect of centrifugal potential is not included in the molecular phase. It is considered only after the scission point. It is given by

$$V_l = \frac{\hbar^2}{2\mu}\frac{l(l+1)}{\zeta^2} \tag{1.5}$$

The total potential in 1-D case is given by

$$V = V_c + V_s + V_l - V_o \tag{1.6}$$

Here V_o the reference of potential corresponding to the sum of self potential energies (Coulomb and surface) of each fragment in the asymptotic configuration.

The barrier penetrability factor P is calculated using WKB approximation[46]

$$P = exp\{-\frac{2}{\hbar}\int_{\zeta_1}^{\zeta_2}\sqrt{2\mu(V-Q)}d\zeta\} \tag{1.7}$$

The limits of integration corresponds to inner and outer turning points. Q is the Q-value ie. the energy released during the disintegration. Q-value is calculated using the mass excess taken from AME 2012[47]. The inertia coefficient μ is determined using Werner-Wheeler inertia coefficient[48]. The decay constant is calculated as

$$\lambda = \nu_0 P \tag{1.8}$$

where ν_0 is the assault frequency ($\nu_0 \approx 10^{22}s^{-1}$)[49]. Finally, the half-life for the decay is obtained as

$$T_{1/2} = \frac{ln2}{\lambda} \tag{1.9}$$

Preformed Cluster Model

In PCM, the cluster is assumed to be preformed inside the nucleus. The preformation probability associated with the formation of each cluster is different.

The cluster formed inside the nucleus will tunnel the nucleus irrespective of the size or shape of the nucleus. Different groups of researchers used different forms of the potentials for studying this phenomenon.

Blendowske et al. [50, 51, 52] have chosen the interacting potential as the sum of semi-empirical heavy-ion potential, Coulomb and centrifugal potentials. Gupta et al. [53] have considered this as a two step process. i.e, cluster formation and penetration through the barrier. They have used the Coulomb energy, proximity potential and experimental binding energy as the interaction energy. In the cluster model of Buck et al.[54, 55] they have used simple local potential as interacting potential. Sandulescu et al.[56] used double folded Michigan plus three Yukawa potential model for studying the phenomena of cluster decay.

Semi-empirical formulae

Several semi-empirical formulae are in use to predict the half-lives of alpha decay and different modes of cluster decay [57]. They are of two types: model dependent and model independent. In this section we have presented some of the widely used semi-empirical formulae used for studying alpha and cluster decay.

The first attempt to study alpha decay systematically was done by Geiger and Nuttal in 1911. They experimentally confirmed the relation between the range R of alpha particles and the decay constant λ, which is the Geiger-Nuttal (GN) law[58]. This law can be expressed in terms of the logarithmic half-lives and Q values of the decays. The Geiger-Nuttal law, which is a linear relationship between logarithmic half-lives and Q-values is given by,

$$log_{10}T_{1/2} = aQ_{\alpha}^{-1/2} + b \tag{1.10}$$

Brown[59], in 1992, tried to study the relation between alpha decay half-lives and alpha disintegration energy. They also found a linear relation similar to the Geiger-Nuttal law, but in terms of the atomic number of the daughter nucleus and Q_{α}- values. It is given by,

$$log_{10}T_{1/2} = (0.954\frac{Z_d^{0.6}}{\sqrt{Q_\alpha}} - 51.37) \tag{1.11}$$

Compared to G-N relation, this relation provides less scatter of data.

Later in 1996, Viola et al.[60] derived a semi-empirical formula based on the square well nuclear model and hindrance factor for unpaired nucleons. The half-lives are expressed as

$$log_{10}T_{1/2} = A_Z Q_{eff}^{-1/2} + B_Z + logF \tag{1.12}$$

where $A_Z = 2.1133Z - 48.9879$, $B_Z = -0.39004Z - 16.9543$, $logF$ is the hindrance factor for nuclei with unpaired nucleons. Q_{eff} is the sum of alpha particle energy, recoil energy of the daughter nucleus and the orbital electron screening correction. The value of $logF$ is given below,

$$\begin{aligned} logF &= 0,\ even - even \\ &= 0.772,\ odd\ Z, even\ N \\ &= 1.066,\ even\ Z, odd\ N \\ &= 1.114,\ odd - odd. \end{aligned} \tag{1.13}$$

Later these values had been modified by Sobiczewski et al.[61]. The new values are $A_Z = 1.6617Z - 8.5166$ and $B_Z = -0.2023Z - 33.9069$. No change for $logF$ values. These new values reproduce the half-lives in a better way, by upto about one order of magnitude for some of the nuclei.

Horoi et al.[62] developed a new scaling law for alpha as well as cluster decay of even-even heavy nuclei. This is a model independent law. It is shown that half-lives depend on the scaling factor $(Z_c Z_d)^{0.6}/\sqrt{Q}$ and the reduced mass μ of daughter and cluster nuclei. The reduced mass has a very important role in cluster decay. It is expressed as,

$$log_{10}T_{1/2} = (a_1\mu^x + b_1) + [(Z_c Z_d)^y/\sqrt{Q} - 7] + (a_2\mu^x + b_2) \tag{1.14}$$

where a_1=9.1, b_1=-10.2, a_2=7.39, b_2=-23.2, x=0.416 and y=0.613.

Balasubramaniam et al.[63], in 2004 proposed a model-independent semi-empirical formula to evaluate the cluster decay half-lives using only three parameters. They have used mass and charge of parent and daughter as well as the Q-value of the decay process. The equation can be expressed as,

$$log_{10}T_{1/2} = \frac{aA_2\eta + bZ_2\eta_z}{\sqrt{Q}} + c \tag{1.15}$$

where a=10.603, b=78.027 and c=-80.669.

In 2009, Qi et al.[64] proposed a new semi-empirical formula which depends on the Q-value for the cluster emission and also on the charge and mass of the daughter and cluster nuclei. This is found to be a generalisation of Geiger-Nuttal law. So it is called as Universal Decay Law(UDL). This law predicts with high accuracy the half-lives of alpha as well as cluster decays. Using UDL, we can estimate the half-life of all the nuclei in the nuclear chart, with the help of binding energy. The UDL is given by the expression,

$$log_{10}T_{1/2} = aZ_cZ_d\sqrt{\frac{A}{Q}} + b\sqrt{AZ_cZ_d(A_d^{1/3} + A_c^{1/3})} + c \tag{1.16}$$

where a=0.4314, b=-0.4087 and c=-25.7725. Z_c, Z_d are the atomic number of cluster and daughter nuclei, A_c, A_d are the mass number of cluster and daughter nuclei and

$$A = \frac{A_cA_d}{A_c + A_d} \tag{1.17}$$

Here Q is the Q-value of the decay.

Poenaru et al.[65] developed a Universal curve by extending fission theory to large mass asymmetry, which is based on quantum mechanical tunnelling process. They have obtained a single line of universal curve for alpha and cluster decay, by plotting the sum of the logarithm of half-lives and cluster preformation

probabilities against the logarithm of penetrability of external barrier.

$$log_{10}T(s) = -log_{10}P - log_{10}S + [log_{10}(ln2) - log_{10}\nu] \tag{1.18}$$

where P is the penetrability, S is the pre-formation probability of the cluster and ν is the assault frequency.

A brief review of experimental as well as theoretical advancements taken place in this field is given below.

Survey on experimental studies of cluster radioactivity

Since cluster radioactivity is a rare process, with an intense background of α particles, highly efficient and highly selective detectors should be used for the detection of such decay modes. Solid State Nuclear Track Detector (SSNTD) are the most efficient detectors for studying cluster radioactivity because they can effectively reject the events due to α particles. CR-39 and Lexan are the mostly used detectors in this category. In addition to this, some experimentalists used polyethylene teraphthalate (dielectric) detectors, polycarbonate track recording films and phosphate glass detectors for studying the phenomenon of cluster decay.

This exotic decay was first experimentally observed by Rose and Jones[66] in 1984, with the emission of ^{14}C cluster from ^{223}Ra. They used solid state counter telescope to identify the emitted particles. They had observed a branching ratio of $(8.5 \pm 2.5) \times 10^{-10}$ with respect to α decay. Later in the same year, Aleksandrov et al.[67] also observed the same process using $\Delta E - E$ type telescope and obtained a branching ratio of $(7.6 \pm 3.0) \times 10^{-10}$ relative to α decay. Gales et al. [68] have repeated the experiment but used superconducting magnetic solenoid spectrometer inorder to suppress α particles. Kutschera et al.[69] used Enge split-pole magnetic spectrograph for suppressing α particles. The experiments done by these groups have thus confirmed the emission of clusters from parent nuclei.

Later several other decay modes had been observed by different groups of

scientists throughout the world. Barwick et al.[70, 71] had observed ^{14}C and ^{24}Ne decay from ^{226}Ra and ^{232}U respectively. Price et al. [72, 73, 74] experimentally observed ^{14}C decay from ^{222,224}Ra. Bonetti et al.[75, 76, 77], in 1990s, done a couple of experiments and observed that different clusters like ^{14}C, ^{20}O, $^{22,24-26}$Ne, $^{28-30}$Mg are emitted from parents like ^{225}Ac, ^{228}Th, ^{221}Fr, ^{221}Ra and ^{230,232,236}U. Tretyakova et al.[78, 79] had observed clusters like Ne and Mg from heavy nuclei with $Z > 90$. Moody et al.[80] using phosphate glass detectors analysed the rare decay modes of ^{242}Am. In all these decays the daughter nuclei are ^{208}Pb or its neighbours.

Another region of interest in the field of cluster radioactivity is the trans-tin region. Here the daughter nuclei formed will fall in the vicinity of ^{100}Sn or ^{132}Sn which are doubly magic. Experimental data available in this region is very limited. Oganession et al. [81] observed the emission of ^{12}C cluster from ^{114}Ba with a half-life $\geq 10^3$s. Guglielmetti et al. [82] had observed that ^{12}C cluster is emitted from ^{114}Ba with a half-life $\geq 1.1 \times 10^3$ s while in another experiment [83] they obtained a half-life of 1.7×10^4s. La Commara et al. [84] had investigated neutron deficient isotopes near ^{100}Sn using heavy ion-induced fusion-evaporation reaction followed by light particle emission and cluster decay.

Survey on theoretical studies of cluster radioactivity

This phenomena was first predicted by Sandulescu et al. in 1980 on the basis quantum mechanical fragmentation theory[85]. Cluster radioactivity is a rare cold nuclear phenomenon explained based on quantum mechanical fragmentation theory(QMFT)[86, 87]. The probability of formation of a cluster is mainly determined by its binding energy. Binding energy of an α particle is 28.296 MeV. This implies that among all the possible clusters, α cluster is the most prominent one.

Cluster radioactivity falls mainly in two regions - trans-tin and trans-lead. A brief review on the theoretical studies done so far by different research groups throughout the world is given below.

Poenaru et al. had made pioneering studies in the field of cluster radioactivity theoretically, using Analytical Super Asymmetric Fission Model (ASAFM). They had shown that nuclei with $Z > 40$ are metastable with respect to cluster decay and also calculated their half-lives and kinetic energies[88] and later made a unified description of alpha, cluster decay and spontaneous fission[89]. They had discussed half-lives of ^{14}C, ^{24,25,26}Ne and ^{28,30}Mg and ^{32}Si. They also mentioned that shell effects is the reason not only for cluster decay in the trans-lead region but also for cold fusion reactions[90].

Sandulescu presented a unified description for different decay modes like alpha decay, cluster radioactivity and new type of symmetric fission with compact shapes in which one or both fragments have Z or N equal to the magic numbers or near to the magic numbers[91]. In the very next year, with the help of open quantum nuclear dynamics (fragmentation theory), he had explained the new natural radioactivity called cluster radioactivity with the emission of clusters like ^{14}C, ^{24}Ne and ^{28}Mg[92].

Buck et al.[54] studied the exotic decay with the aid of cluster model, in which a local, effective cluster-core potential based on folding procedure was used. They had predicted the ^{14}C and ^{24}Ne decay from $^{221-224,226}$Ra, ^{231}Pa and ^{232,233}U. They had also studied how the size of the emitted clusters affect the decays[55]. Later, in 1991, they proposed a unified model for alpha and cluster decay[93]. They also showed that in the case of even-even nuclei, the g.s to g.s decay is well explained by their model. But for the case of odd-A nuclei, the decay is observed to be from g.s to excited state[94, 95].

Patra et al. [96] have studied the cluster structures in heavy nuclei like ^{222}Ra, ^{232}U, ^{236}Pu, ^{242}Cm and in super heavy nuclei with Z=114 and N=172,176,180 and 184 using the axially deformed relativistic and non-relativistic mean field formalism.

Santhosh et al. [97, 98, 99, 100, 101] have studied the feasibility of $^{244-260}$Fm against alpha and cluster decay. They showed that the inclusion of quadrupole and hexadecupole deformation decreases the height and shape of the potential

barrier and hence the corresponding half-lives. They had shown that alpha-like clusters are the most probable ones in trans-tin region and non-alpha like in trans-lead region. They also investigated the probable cluster decay in Ra, Ac, Th, Pa, Np, Cf etc.

So far we have presented the studies done on tran-lead region. Many theoretical studies have been carried out in trans-tin region also in recent decade. A brief discussion on trans-tin region is given below.

Poenaru et al. have also made valuable contibutions in the field of tin radioactivity theoretically using Analytical Super Asymmetric Fission Model (ASAFM). They observed the emission of clusters like ^{12}C, ^{16}O, ^{30,32}Si, ^{48,50}Ca and ^{68}Ni from nuclei with $Z > 60$ leading to the daughter nuclei in the region Z=50-58[102]. Later they have studied nuclei in the range Z=52-122 by taking into account odd even effect[103]. They also predicted a new region of cluster radioactivity exhibited by proton rich nuclei in the region Z=56-64 leading to the formation of daughter in the neighbourhood of ^{100}Sn[104]. Later they have studied the influence of masses, radii and interaction potential on ^{12}C decay of ^{114}Ba[105]. They have made an analysis on cluster decay in Ba, Ce, Nd, Sm, Gd and Dy isotopes which leads to Tin radioactivity[106].

Gupta et al. [107] studied cluster decay of nuclei in the region $50 < Z < 82$ using PCM. Satish Kumar et al. [108, 109, 110] using PCM had studied cluster decay in Xe, Ba, Ce, Nd, Sm and Gd. They had also studied, with the help of PCM, Sn radioactivity from ^{146}Ba, ^{152}Ce, ^{156}Nd, ^{160}Sm and ^{164}Gd. They have observed that for ^{100}Sn radioactivity, alpha-like clusters are more probable and in ^{132}Sn radioactivity, non-alpha like clusters are more probable. Santhosh et al. [111, 112, 113, 114] studied the phenomena of cluster decay using Coulomb plus Proximity potential model. They had predicted cluster emission from stable nuclei like Ba, Ce, Xe and Nd which leads to the daughter nuclei ^{100}Sn or the one in its vicinity. Sushil Kumar et al. [115, 116] also used PCM for analysing the phenomenon of cluster decay in rare earth nuclei which leads to the formation of ^{100}Sn as daughter nuclei.

1.2.3 Neutron skin

With the development of experimental facilities like Radioactive Ion Beams, research in nuclear structure have entered into a new era. They enable us to study the wide range of nuclei in the chart of nuclides. The study of nuclei far from the stability line is an interesting field nowadays. Experimental data are available only for light nuclei. So studies on heavy nuclei in this region mostly rely on theoretical models. In neutron-rich nuclei, as the neutron number increases, the asymmetry between neutron and proton radii increases. This leads to the emergence of new phenomena like neutron skin, neutron halos, shell melting etc[117]. The phenomenon of neutron skin had been experimentally observed in light mass nuclei like ^{6}He and ^{8}He [118].

The description of nuclei near the drip-lines is a very challenging task. Nuclear stability is determined by the interplay between strong nucleon-nucleon interaction and the repulsive Coulomb force. Nuclei near the neutron drip-line are weakly bound and this results in the spatial extension of neutrons around the nuclei. Neutron distribution diffuses out making nuclear surface less defined. It is known that the sum of neutron and proton density in the interior of the nucleus remains constant. So on increasing the neutron number, the proton distribution will extend inorder to keep this constant. As the n-p interaction is much stronger than n-n or p-p, the mean potential of protons will become deeper and neutron potential, more shallower as shown in fig. 1.6[119]. So with the increase of neutron number, the neutron Fermi energy goes up and neutrons will be bounded very loosely. This results in the expansion of neutron density and the proportionality of neutron and proton density breaks. As a result of this a layer of neutrons called the n-skin arises outside the bulk nuclear matter[120]. To analyse the spatial extension of neutron density, the quantities which are usually employed are the neutron and proton root mean square radius(rms). The neutron skin thickness is defined as the difference between neutron and proton

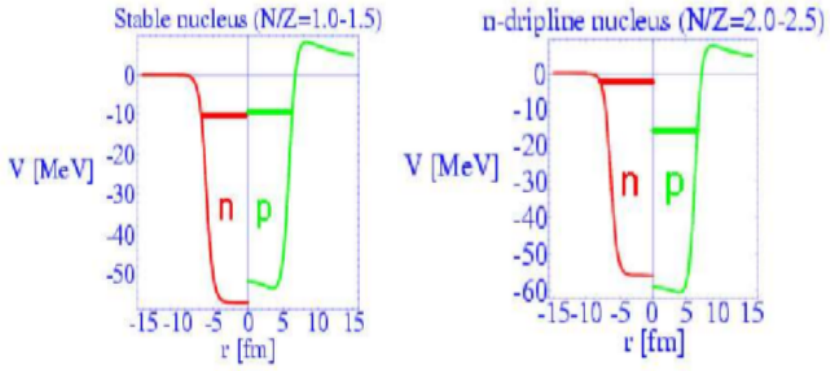

Figure 1.6: Neutron and proton potential for stable as well as drip-line nuclei

rms radii,

$$\Delta R_{np} =< r_n^2 >^{1/2} - < r_p^2 >^{1/2} \tag{1.19}$$

Conventionally, for nuclei near the beta-stability line, this difference will be of the order of 0.1 to 0.2 fm. But in the case of neutron-rich systems, this quantity increases due to the formation of neutron skin or halos.

A brief review of theoretical as well as experimental studies on the neutron skin is given below.

Survey on experimental studies of neutron skin

The direct evidence of neutron skin can be obtained by high energy proton scattering experiment. The PREX (Pb Radius EXperiment) Collaboration at JLab used parity-violating electron scattering (PVES) to study the neutron distribution of ^{208}Pb and provided us with the first results of the neutron radius through an electroweak probe that gives a value of $0.33^{+0.16}_{-0.18}$ fm for the neutron skin thickness[121]. Proton elastic scattering experiment on ^{58}Ni gives skin thickness of $0.211^{+0.054}_{-0.063}$ for ^{208}Pb[122]. Trzcinska et al.[123] have proposed a method using antiprotonic atoms to study the neutron distribution of different isotopes. Later, with the help of antiprotonic X-ray data, skin thickness of ^{208}Pb and ^{209}Bi

were estimated[124]. Another experimental technique for the determination of neutron skin thickness is the excitation of spin dipole resonance (SDR). The skin thickness of ^{120}Sn was estimated using SDR method[125]. Krasznahorkay et al.[126] estimated the neutron skin thickness in Sn and Pb isotopes using spin dipole resonance (SDR) and giant dipole resonance (GDR) excitation by inelastic scattering of α particles . The coherent pion photoproduction measurement, which provides the result of the first determination of a nuclear matter form factor with an electromagnetic probe, shows the formation of neutron skin around ^{208}Pb with a thickness of $0.15 \pm 0.03^{+0.01}_{-0.03}$ fm. The results also showed that it has a halo character [127].

Survey on theoretical studies of neutron skin

The emergence of neutron skin thickness in exotic nuclei have been studied by different groups using different microscopic as well as phenomenological theories in recent decades. A brief description of these theoretical works are given below.

Myers et al.[128, 129] developed a droplet model to study the neutron skin, which is a modified form of the liquid drop model. This model assumed that the densities are approximately constant inside the bulk region and at the boundary, the surface diffuses so that the density decreases to zero slowly. This model suggests that the neutron skin is related to the surface symmetry energy, giant dipole resonance and isotope and isotone shifts. It is assumed that the neutron skin is formed as a result of the interplay between the bulk symmetry energy and the nuclear surface energy [130].

Sharma et al.[131] analysed the neutron skin in closed shell as well as in open shell nuclei within the spherical relativistic and non-relativistic mean field theories. Their study concludes that relativistic results overestimate when compared to the non-relativistic ones. Fukunishi et al.[120] studied the formation of neutron and proton skin formation in Cs nuclei using spherical Hartree-Fock theory. They presented various defintions for the formation of neutron skin in terms of neutron and proton density. They defined n-skin based on three criteria. They

suggested that ratio of neutron to proton density should be greater than 4. R_1 is the radius where this condition is satisfied. The density of neutrons in the skin should not be very small. It should be greater than 1/100 times the central density. This happens at a radius R_2. Finally, the difference of R_1 and R_2, defined as skin thickness should be greater than 1 fm. Dobaczewski et al.[132] had carried out a global calculation of neutron and proton radii and hence the neutron skin thickness using Skyrme Hartree-Fock-Bogoliubov theory. Chen et al.[133] with the help of relativistic Hartree and relativistic Hartree-Fock theory, studied the properties of stable as well as neutron-rich nuclei. They found that the inclusion of Fock exchange term have very large influence on exotic nuclei. Patyk et al.[134] had used various microscopic approaches like Hartree-Fock-Bogoliubov (HFB) with both zero range Skyrme as well as finite range Gogny interaction, relativistic mean field (RMF), extended Thomas-Fermi model with Strutinski integral (ETFSI) and macroscopic-microscopic (MM) method for investigating some spherical nuclei in the mass range $16 \leq A \leq 220$ (light to heavy mass nuclei). They studied how different models affect the masses and radii of these nuclei.

With the help of spherical Skyrme-Hartree-Fock-Bogoliubov and relativistic Hartree-Bogoliubov theories, Mizutori et al.[135] studied nuclear skin and halos in even-even nuclei. They describe the spatial characteristics of nucleonic densities of nuclei far from beta-stability line, with the help of Helm model. They also observed that neutron surface thickness increases with neutron number, but in the vicinity of magic numbers it reduces because of pairing. Vretenar et al.[136] analyzed the neutron distributions of Cs, Ba, Yb, and Pb isotopes using the relativistic Hartree-Bogoliubov model, with the NL3+D1S effective interaction. Furnstahl [137] had investigated the variation of neutron radii by analysing the correlations between basic properties of the mean-field models. Neutron skin thickness in lead has also been analysed. They observed that skin thickness depends mainly on the density dependence of symmetry energy. Neutron skin thickness of ^{208}Pb had been studied using nonrelativistic and relativistic mean-

field models by Meucci et al.[138]. They had analysed the dependence of neutron skin thickness with symmetry energy, slope and curvature coefficient of symmetry energy. Schunck et al.[139] had made a review of nuclear halos and nuclear skins in drip-line nuclei with the help of the spherical Hartree-Fock-Bogoliubov theory with continuum effects and projection on good particle number with the Gogny force. Structural evolution of Sr, Zr and Mo isotopes and its relation with nuclear charge radii have been analysed by Rodriguez et al.[140] with the help of HFB theory with Gogny interaction.

1.3 Organisation of the thesis

The thesis is organised as follows.

In chapter 2, we have explained the theoretical method adopted for the study. We gave a brief introduction of Hartree-Fock theory and BCS theory before going into the Hartree-Fock-Bogoliubov theory. A brief description of the zero range effective Skyrme interaction is also given. The main works are given in the rest of the chapters.

In chapter 3, we have presented the details of the studies carried out on the shape evolution of the transitional nuclei with respect to different Skyrme forces. With the help of quadratic constraint method we obtained potential energy curves(PEC). As some signatures of triaxiality is found to be exhibited by these nuclei, we have done triaxial calculations. Potential energy surfaces (PES) are also computed which clearly shows the presence of triaxiality.

In chapter 4, we have presented the study on the feasibility of alpha and cluster decay in the transitional nuclei. We have studied the sensitviy of different Skyrme forces in predicting the half-lives.

In chapter 5, we tried to analyse the behaviour of W, Os and Pt nuclei, away from the beta-stability line. We studied the phenomenon of neutron skin evolution in these nuclei. Also analysed how different Skyrme forces affect it. We have also predicted the neutron magic number N=184, next to N=126.

Summary and future outlook of the work are presented in chapter 6.

References

[1] K. Heyde, Basic ideas and concepts in Nuclear physics - An introductory approach, ed. Douglas F Brewer (Overseas Press, India, Pvt. Ltd. 1998).

[2] A. Bohr and B. R. Mottelson, Nuclear Structure, Vol. I (World Scientific Publishing Co. Pte.Ltd. Singapore 1998).

[3] A. Bohr and B. R. Mottelson, Nuclear Structure, Vol. II (World Scientific Publishing Co. Pte.Ltd. Singapore 1998).

[4] S. G. Nilsson and I. Ragnarsson, Shapes and shells in nuclear structure, (Cambridge University Press, Cambridge 1995).

[5] W. Nazarewicz, *Nucl. Phys. A*, **574**, 27c(1994).

[6] B. N. Lu, J. Zhao, E. G. Zhao and S. G. Zhou, *Phys. Scr.*, **89**, 054028(2014).

[7] P. Cejnar, J. Jolie and R. F. Casten, *Rev. Mod. Phys.*, **82**, 2155(2010).

[8] F. Iachello, *Phys. Rev. Lett.*, **87**, 052502(2001).

[9] F. Iachello, *Phys. Rev. Lett.*, **85**, 3580(2000).

[10] A. M. Khalaf and A. M. Ismail, *Prog. in Phys.*, **2**, 51(2013).

[11] http://www.nndc.bnl.gov.

[12] Y. Tanaka, R. M. Steffen, E. B. Shera, W. Reuter, M. V. Hoehn and J. D. Zumbro, *Phys. Rev. C*, **29**, 1830(1984).

[13] P. R. John et al., *Phys. Rev. C*, **90**, 021301(R)(2014).

[14] N. Alkhomashi, et al., *Phys. Rev. C*, **80**, 064308(2009).

[15] C. Wheldon, et al., *Phys. Rev. C*, **63**, 011304(R)(2000).

[16] G.D. Dracoulis, et al. *Phys. G: Nucl. Phys.*, **12**, L97(1986).

[17] H. T. Guong et al., *Phys. Lett. B*, **217**, 401 (1989).

[18] A. Rohilla et al., *Eur. Phys. J. A*, **53**, 64(2017).

[19] S. K. Chamoli, *Acta Phy. Pol. B*, **48**, 337(2017).

[20] K. Kumar and M. Baranger, *Phys. Rev. Lett.*, **17**, 1146 (1966).

[21] A. Ansari, *Phys. Rev. C*, **33**, 321 (1986).

[22] R. Bengtsson, T. Bengtsson, J. Dudek, G. Leander, W. Nazarewicz and J. Zhang, *Phys. Lett. B*, **183**, 1 (1987).

[23] P. Bonche, S. J. Krieger, P. Quentin, M. S. Weiss, J. Meyer, M. Meyer, N. Redon, H. Flocard and P-H Heenen, *Nucl. Phys. A*, **500**, 308(1989).

[24] P. D. Stevenson, M. P. Brine, Zs. Podolyak, P. H. Regan, P. M. Walker and J. Rikovska Stone, *Phys. Rev. C*, **72**, 047303(2005).

[25] P. Sarriguren, R. Rodriguez-Guzman and L. M. Robledo, *Phys. Rev. C*, **77**, 064322(2008).

[26] L. M. Robledo, R. Rodriguez-Guzman and P. Sarriguren, *J. Phys. G: Nucl, Part, Phys*, **36**, 115104(2009).

[27] Z. Naik, B. K. Sharma, T. K. Jha, P. Arumugam and S. K. Patra, *Pramana-J Phys.*, **62**, 827(2004).

[28] R. Rodriguez-Guzman, P. Sarriguren, L. M. Robledo and J. E. Garcia-Ramos, *Phys. Rev. C*, **81**, 024310(2010).

[29] K. Nomura, T. Otsuka, R. Rodriguez-Guzman, L. M. Robledo and P. Sarriguren, *Phys. Rev. C*, **84**, 054316(2011).

[30] K. Nomura, T. Otsuka, R. Rodriguez-Guzman, L. M. Robledo and P. Sarriguren, *Phys. Rev. C*, **83**, 014309(2011).

[31] K. Nomura, T. Otsuka, R. Rodriguez-Guzman, L. M. Robledo, P. Sarriguren, P. H. Regan, P. D. Stevenson and Zs. Podolyak, *Phys. Rev. C*, **83**, 054303(2011).

[32] K. Nomura, R. Rodriguez-Guzman and L. M. Robledo, *Phys. Rev. C*, **97**, 064314(2018).

[33] C. A. Radha, V. Ramasubramanian and E. J. J. Samuel, *Turk J Phys*, **34**, 159(2010).

[34] S. Mahapatro, C. Lahiri, B. Kumar, R. N. Mishra and S. K. Patra, *Int. J. Mod. Phys. E*, **25**,1650062(2016).

[35] D.N. Poenaru and W. Greiner, C. Beck (ed.) Clusters in Nuclei, Lecture Notes in Physics 818, **1**, 1-56 (Springer-2010).

[36] D.N. Poenaru, M. Ivascu, A. Sandulescu and W. Greiner, *Phys. Rev. C*, **32**, 572(1985).

[37] D.N. Poenaru, M. Ivascu, A. Sandulescu and W. Greiner, *J. Phys. G: Nucl. Part. Phys.*, **10**, 183(1984).

[38] D.N. Poenaru and W. Greiner, *J. Phys. G: Nucl. Part. Phys.*, **17**, 443(1991).

[39] G. Shanmugam and B. Kamalaharan, *Phys. Rev. C*, **38**, 1377(1988).

[40] Y. J. Shi and W. J. Swiatecki, *Nucl. Phys. A*, **438**, 450(1985).

[41] Y. J. Shi and W. J. Swiatecki, *Nucl. Phys. A*, **464**, 205(1987).

[42] G. A. Pik-Pichak, *Sov. J. Nucl. Phys.*, **44**, 923(1986).

[43] G. Royer and B. Remaud, *Nucl. Phy. A*, **444**, 477(1985).

[44] M. Goncalves and S. B. Duarte, *Phys. Rev. C*, **48**, 2409 (1993).

[45] M. Gaudin, *J. Phys. (France)*, **35**, 885(1974).

[46] G. Gamow, *Z. Phys.*, *51*, 204(1928).

[47] M. Wang, G. Audi, A. H. Wapstra, F. G. Kondev, M. MacCormick, X. Xu, and B. Pfeiffer, *CPC*, **36**, 12(2012).

[48] D. N. Poenaru, J. A. Maruhn, W. Greiner, M. Ivascu, D. Mazilu and I. Ivascu, *Z. Phys. A*, **325**, 435(1986).

[49] Yi-Jin Shi and W. J. Swiatecki, *Nucl. Phys. A*, **464**, 205(1987).

[50] R. Blendowske, T. Fliessbach and H. Walliser, *Nucl. Phys. A*, **464**, 75(1987).

[51] R. Blendowske and H. Walliser, *Phy. Rev. Lett.*, **66**, 1930(1988).

[52] R. Blendowske, T. Fliessbach and H. Walliser, *Z. Phys. A*, **339**, 121(1991).

[53] S. S. Malik and R. K. Gupta, *Phys. Rev. C*, **39**, 1992(1989).

[54] B. Buck and A. C. Merchant, *Phys. Rev. C*, **39**, 2097(1989).

[55] B. Buck and A. C. Merchant and S. M. Perez, *Nucl. Phys. A*, **512**, 483(1990).

[56] A. Sandulescu, R. K. Gupta, W. Greiner, F. Carstoiu and M. Horoi, *Int. J. Mod. Phys. E*, **1**, 379(1992).

[57] D. T. Akrawy, H. Hassanabadi, S. Hosseini and K. P. Santhosh, *Nucl. Phys. A*, **971**, 130(2018).

[58] H. Geiger and J. M. Nuttall, *Philos. Mag.*, **22**, 613(1911).

[59] B. A. Brown, *Phys. Rev. C*, **46**, 811(1992).

[60] V. E. Viola, Jr and G. T. Seaborg, *J. Inorg. Nucl. Chem*, **28**, 741(1966).

[61] A. Sobiczewski and Z. Patyk, *Phys. Lett. B*, **224**, 1(1989).

[62] M. Horoi, *J. Phys. G: Nucl. Part. Phys.*, **30**, 945(2004).

[63] M. Balasubramaniam, S. Kumarasamy, N. Arunachalam and R. K. Gupta, *Phys. Rev. C*, **70**, 017301(2004).

[64] C. Qi, F. R. Xu, R. J. Liotta, R. Wyss, M. Y. Zhang, C. Asawatangtrakuldee, and D. Hu, *Phys. Rev. C*, **80**, 044326(2009).

[65] D.N. Poenaru, R.A. Gherghescu and W. Greiner, *Phys. Rev. C*, **83**, 014601(2011).

[66] H. J. Rose and G. A. Jones, *Nature (London)* **307** 245(1984).

[67] D. V. Aleksandrov, A. F. Belyatskii, Yu. A. Glukhov, E. Yu. Nikol'Skii, B. G. Novataskii, A. A. Ogloblin and D. N. Stepanov (1984), *JETP Lett.*, **40**, 4(1984).

[68] S. Gales, E. Hourany, M. Houssonnois, J. P. Shapira, L. Stab and M. Vergnes, *Phys. Rev. Lett.*, **53**, 759(1984).

[69] W. Kutschera, I. Ahmad, S. G. Armato, A. M. Friedman, J. E. Gindler, W. Henning, T. Ishii, M. Paul and K. E. Rehm, *Phys. Rev. C*, **32**, 2036(1985).

[70] S. W. Barwick, P. B. Price, H. L. Ravn, E. Hourani and Hussonnois, *Phys. Rev. C*, **34**, 362(1986).

[71] S. W. Barwick, P. B. Price and J D. Stevenson, *Phys. Rev. C*, **31**, 1984(1985).

[72] P. B. Price, *Nucl. Phys. A*, **502**, 41c(1989).

[73] P. B. Price, R. Bonetti, A. Guglielmetti, C. Chiesa, R. Matheoud, C. Migliorino and K. J. Moody, *Phys. Rev.C*, **46**, 1939(1992).

[74] P. B. Price, J. D. Stevenson and S. W. Barwick, *Phys. Rev. Lett.*, **54**, 297(1985).

[75] R. Bonetti, C. Chiesa, A. Guglielmetti, C. Migliorino, A. Cesana and M. Terrani , *Nucl. Phys. A*, **556**, 115(1993).

[76] R. Bonetti, C. Chiesa, A. Guglielmetti, C. Migliorino, R. Matheoud, A. L. Pasinetti and H. L. Ravn, *Nucl. Phys. A*, **562**, 32(1993).

[77] R. Bonetti, C. Chiesa, A. Guglielmetti, C. Migliorino, P. Monti, A. L. Pasinetti and H. L. Ravn, *Nucl. Phys. A*, **576**, 21(1994).

[78] S. P. Tretyakova, *Nucl. Tracks Radiat. Meas*, **19**, 667(1991).

[79] S. P. Tretyakova, V. L. Mikheev, V. A. Ponomarenko, A. N. Golovchenko, A. A. Ogloblin and V. A. Shigin, *JEPT Lett*, **59**, 397(1994).

[80] K. J. Moody, E. K. Hulet, Shicheng Wang, P. B. Price and S. W. Barwick, *Phys. Rev. C*, **36**, 2710(1987).

[81] Yu. Ts. Oganessian, Yu. A. Lazarev, V. L. Mikheev, Yu. A. Muzychka, V. Shirokovsky, S. P. Tretyakova and V. K. Utyonkov, *Z. Phys. A: Hadrons Nucl.*, **349**, 341(1994).

[82] A. Guglielmetti, R. Bonetti, G. Poli, P. B. Price, A. J. Westphal, Z. Janas, H. Keller , R. Kirchner, O. Klepper, A. Piechaczek, E. Roeckl, K. Schmidt, A. Plochocki, J. Szerypo and B.Blank, *Phys. Rev. C*, **52**, 740(1995).

[83] A. Guglielmetti, B. Blank, R. Bonetti, Z. Janas, H. Keller, R. Krichner, O. Klepper, A. Piechaczek, A. Plochocki, G. Poli, P. B. Price, E. Roeckl, K. Schmidt, J. Szerypo and A. J. Westphal, *Nucl. Phys. A*, **583**, 867(1995).

[84] M. La Commara et al., *Nucl. Phys. A*, **669**, 43(2000).

[85] A. Sandulescu, D. N. Poenaru and W. Greiner, *Sov. J. Part. Nucl.*, **11**, 528 (1980).

[86] R. K. Gupta, *Pramana-J. Phys.* **53** 3(1999).

[87] W. Greiner, H. J. Fink, J. A. Maruhn and W. Scheid, *Zeitschrift fuer Physik*, **268**, 321(1974).

[88] D. N. Poenaru, W. Greiner, K. Depta, M.Ivascu, D. Mazilu and A. Sandulescu, *At. Data. Nucl. Data Tables*, **34**, 423(1986).

[89] D. N. Poenaru, M.Ivascu and W. Greiner, *Nuclear Tracks*, **12**, 313(1986).

[90] D. N. Poenaru, W. Greiner and M.Ivascu, *Nucl. Phys. A*, **502**, 59c(1989).

[91] A. Sandulescu, *Phys. Scr. T*, **23**, 43(1988).

[92] A. Sandulescu, *J. Phys. G: Nucl. Part. Phys.*, **15**, 529(1989).

[93] B. Buck, A. C. Merchant and S. M. Perez, *J. Phys. G: Nucl. Part. Phys.*, **17**, L91(1991).

[94] B. Buck, A. C. Merchant, S. M. Perez and P. Tripe, *Phys. Rev. C*, **47**, 1307(1993).

[95] B. Buck, A. C. Merchant, S. M. Perez and P. Tripe, *J. Phys. G. Nucl. Part. Phys.*, **20**, 351(1994).

[96] S. K. Patra, R. K. Gupta, B. K. Sharma, P. D. Stevenson and W. Greiner, *J. Phys. G: Nucl. Part. Phys.*, **34**, 2073(2007).

[97] K. P. Santhosh, R. K. Biju and Sabina Sahadevan, *Pramana-J. Phys.* **73**, 1059(2009).

[98] K. P. Santhosh, R. K. Biju and Sabina Sahadevan, *Nucl. Phys. A*, **838**, 38(2010).

[99] K. P. Santhosh, Sabina Sahadevan, B. Priyanka and M. S. Unnikrishnan, *Nucl. Phys. A*, **882**, 49(2012).

[100] K. P. Santhosh, B. Priyanka, M. S. Unnikrishnan, *Nucl. Phys. A*, **889**, 29(2012 b)

[101] K. P. Santhosh and B. Priyanaka, *Eur. Phys. J. A*, **49**, 66(2013).

[102] D. N. Poenaru, W. Greiner, M.Ivacu and A. Sndulescu, *Phys. Rev. C*, **32**, 2198(1985).

[103] D. N. Poenaru, D. Schnabel, W. Greiner, D. Mazilu and R. Gherghescu, *At. Data. Nucl. Data Tables*, **48**, 231(1991).

[104] D. N. Poenaru, W. Greiner and R. Gherghescu, *Phy. Rev C*, **47**, 2030(1993).

[105] D. N. Poenaru, W. Greiner and E. Hourani, *Phy. Rev C*, **51**, 594(1995).

[106] D. N. Poenaru, W. Greiner and E. Hourani, *J. Phys. G: Nucl. Part. Phys.*, **22**, 621(1996).

[107] R. K. Gupta, S. Singh, R. K. Puri and W. Scheid (1993), *Phys. Rev. C*, **47**, 561.

[108] Satish kumar and R. K. Gupta, *Phys. Rev. C*, **49**, 1922(1994).

[109] Sathish Kumar, Dharam Bir and R. K. Gupta, *Phys. Rev. C*, **51**, 1762(1995).

[110] Satish Kumar, J. S. Batra and R. K. Gupta, *J. Phys. G: Nucl. Part. Phys*, **22**, 215(1996).

[111] K. P. Santhosh and Antony Joseph,*Pramana-J. Phys.*, **55**, 375(2000).

[112] K. P. Santhosh and Antony Joseph, *Pramana-J. Phys.*, **58**, 611(2002).

[113] K. P. Santhosh and Antony Joseph, *Indian J. Pure Appl. Phys.*, **42**, 806(2004).

[114] K. P. Santhosh and Antony Joseph, *Pramana-J. Phys.*, **64**, 957(2004).

[115] Sushil Kumar, *Proc. Int. Sym Nucl. Phys.*, **54**, 204(2009).

[116] Sushil Kumar, Ramna Rani and Rajesh Kumar, *J. Phys. G: Nucl. Part. Phys.*, **36**, 015110(2009).

[117] N. Schunck and J. L. Edigo, *Phys. Rev. C*, **78**, 064305(2008).

[118] I. Tanihata, *Phys. Lett. B*, **289**, 261(1992).

[119] E. T. Balbuena, Ph.D Thesis, Graduate School of Vanderbilt University, (2003).

[120] N. Fukunishi, T. Otsuka and I. Tanihata, *Phys. Rev. C*, **48**, 1648(1993).

[121] S. Abrahamyan et al. (PREX Collaboration), *Phys. Rev. Lett.*, **108**, 112502(2012).

[122] J. Zenihiro et al., *Phys. Rev. C*, **82**, 044611(2010).

[123] A. Trzcinska et al., *Phys. Rev. Lett.*, **87**, 082501(2001).

[124] B. Klos et al., *Phys. Rev. C*, **76**, 014311(2007).

[125] A. Krasznahorkay et al., *Phys. Rev. Lett.*, **82**, 3216(1999).

[126] A. Krasznahorkay et al., *Nucl. Phys. A*, **31**, 224(2004).

[127] C. M. Tarbert et al., *Phys. Rev. Lett.*, **112**, 242502(2014).

[128] W. D. Myers and W. J. Swiatecki, *Ann. of Phys.*, **55**, 395(1969).

[129] W. D. Myers, *Phys. Lett.*, **30B**, 451(1969).

[130] W. D. Myers and W. J. Swiatecki, *Nucl. Phys. A*, **336**, 267(1980).

[131] M. M. Sharma and P. Ring, *Phys. Rev. C*, **45**, 2514(1992).

[132] J. Dobaczewski, W. Nazarewicz and T.R. Werner, *Z. Phys. A*, **354**, 27(1996).

[133] B.Q. Chen, Z.Y. Ma, F. Grummer and S. Krewald, *Phys. Lett. B*, **455**, 13(1999).

[134] Z. Patyk, A. Baran, J. F. Berger, J. Decharge, J. Dobaczewski, P. Ring and A. Sobiczewski, *Phys. Rev. C*, **59**, 704(1999).

[135] S. Mizutori, J. Dobaczewski, G. A. Lalazissis, W. Nazarewicz, and P.-G. Reinhard, *Phys. Rev. C*, **61**, 044326(2000).

[136] D. Vretenar, G. A. Lalazissis, and P. Ring, *Phys. Rev. C*, **62**, 045502(2000).

[137] R.J. Furnstahl, *Nucl. Phys. A*, **706**, 86(2002).

[138] A. Meucci, M. Vorabbi, C. Giusti and P. Finelli, *Phys. Rev. C*, **90**, 027301(2014).

[139] N. Schunck and J. L. Egido, *Phys. Rev. Lett.*, **78**, 064305(2008).

[140] R. Rodriguez-Guzman, P. Sarriguren, L. M. Robledo, S. Perez-Martin, *Phys. Lett. B*, **691**, 202(2010).

Chapter 2

Methodology

2.1 Introduction

Self consistent mean field models belong to one of the prominent theories in explaining and predicting the properties of the structure of medium and heavy mass nuclei nowadays. The basis of all mean field theories is the Hartree-Fock (HF) theory. Pairing correlations are included with the help of BCS (Bardeen-Cooper-Schrieffer) theory. HF+BCS theory is well suited for nuclei around the beta stability line but fails towards the drip-line due to their inability to account for the continuum effect there. A generalized version of HF+BCS theory is the Hartree-Fock-Bogoliubov (HFB) theory, in which mean field and pairing part are given equal status. The advantage of HFB theory is that it can successfully describe nuclei away from the beta-stability line. In mean field theories, instead of the bare interaction, zero range Skyrme or finite range Gogny effective interactions are used. Pairing correlations play an inevitable role in the case of open shell nuclei. Pairing interaction is included by density dependent delta interaction.

Our work has been carried out with the help of HFB theory with Skyrme effective interaction. Before going directly into HFB theory, a brief description of HF and BCS is given below.

2.2 Hartree-Fock theory

A general nuclear Hamiltonian is given by the sum of one and two-body interaction[1]

$$H = t_{ij}a_i^\dagger a_j + \sum V_{ijkl}a_i^\dagger a_j^\dagger a_k a_l \tag{2.1}$$

where V_{ijkl} is the two-body interaction and $a^\dagger$ and a are the creation and annihilation single particle operator. The main aim of HF equation is to generate average one-body potential U from V. The eigen state of this H can be expanded as the sum over states, having equal number of total nucleons and the nucleons should occupy all the available single particle states with all possible combinations. Since nucleons are fermions, the wave function Ψ can be written as the Slater determinant of single particle orthonormal wave functions ϕ_k, which are unknown.

$$\Psi = \begin{pmatrix} \phi_1(r_1) & \phi_2(r_1) & \cdots & \phi_A(r_1) \\ \phi_1(r_2) & \phi_2(r_2) & \cdots & \phi_A(r_2) \\ \vdots & \vdots & \ddots & \vdots \\ \phi_1(r_A) & \phi_2(r_A) & \cdots & \phi_A(r_A) \end{pmatrix} \tag{2.2}$$

Since the correct wave function is unknown, variational pronciple is used for finding HF ground state energy,

$$E = \frac{<\Psi|H|\Psi>}{<\Psi|\Psi>} \tag{2.3}$$

HF wave function should be the one which minimizes this energy ie. $\delta E = 0$. Choosing a trial wave function, we calculate U, then solve Schrodinger equation with U to obtain a new wave function. The procedure is repeated till the process converges (ie a self consistent solution is obtained).

Slater determinant can be represented in terms of their single particle density

matrix ρ. The single particle densities have only eigen values 0 or 1. That is,

$$\rho^2 = \rho \tag{2.4}$$

With the help of Wick's theorem, HF energy can be calculated as a function of ρ. In matrix form, HF energy can be expressed as,

$$E^{HF}[\rho] = Tr(t\rho) + \frac{1}{2}Tr_1Tr_1(\rho\bar{v}\rho) \tag{2.5}$$

The minimization of HF energy gives the HF-basis. i.e, $\delta E[\rho] = 0$. The variation leads to a set of equations,

$$h_{kl} = t_{kl} + \sum \bar{v}_{kili} \tag{2.6}$$

and

$$h = t + \Gamma \tag{2.7}$$

where, Γ is the self-consistent field. In the matrix formulation HF equation can be represented as

$$[h, \rho] = 0 \tag{2.8}$$

2.3 BCS Approximation

HF method takes into account particle-hole part of the interaction (long range interaction). Pairing effect plays an important role in structure studies of open shell as well as deformed nuclei. The short range particle-particle or pairing correlation (short range interaction) cannot be explained using HF method. Pairing correlation in nuclei is explained using the BCS theory, which was first developed to explain superconductivity. Certain assumptions are made in this context[2]. They are a. pairing force has a short range b. pair correlation are expected in

the neighbourhood of Fermi surface. c. pairing energy is significant for energy spectra of intermediate and heavy nuclei for which separation of single particle energies are sufficiently small.

A many-body Hamiltonian containing single particle part plus a residual interaction part[1] ie. pairing interaction is expressed as

$$H = \sum_i a_i^\dagger a_i + \sum_{ii'>0} V_{i-ii'-i'} a_i^\dagger a_{-i}^\dagger a_{-i'} a_{i'} \tag{2.9}$$

with pairing potential matrix elements

$$V_{i,-i,i',-i'} =< i,-i|V|i',-i' >= -G \tag{2.10}$$

where G is the constant matrix element, and (i, i') represents the single particle state and its time reversal.

An approximate solution for the above equation based on BCS state is given by

$$|BCS >= \Pi_{i>0}^{\infty}(u_i + v_i a_i^\dagger a_{-i}^\dagger)|0 > \tag{2.11}$$

here v_i^2 is the probability the a certain pair state $(i, -i)$ is occupied and u_i^2 is the probability that the state is not occupied. Normalization of BCS equation gives the condition

$$u_i^2 + v_i^2 = 1 \tag{2.12}$$

Particle number N is not a good quantum number for the BCS state. For particle number conservation we represent it using the expression

$$< BCS|N|BCS >= 2\sum_{i>0} v_i^2 = N \tag{2.13}$$

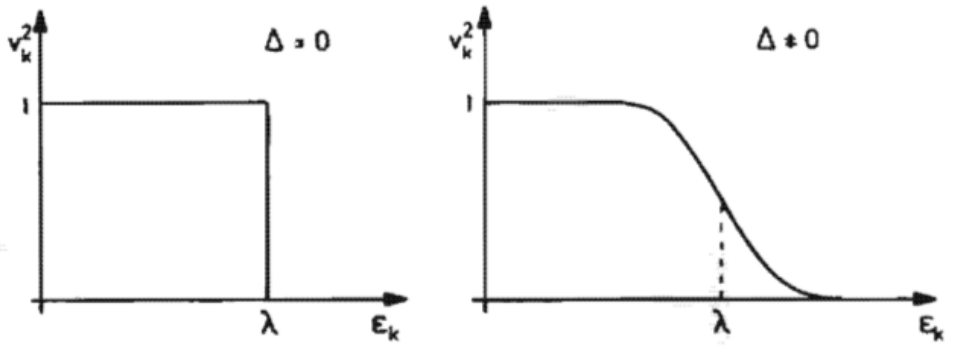

Figure 2.1: The occupation probabilities for non-interacting case ($\Delta = 0$) and for the interacting case ($\Delta \neq 0$).

This is achieved by adding a constraint to Hamiltonian

$$H' = H - \lambda N \tag{2.14}$$

where λ is the Lagrange multiplier. It is called Fermi energy or chemical potential because it represents the increase of the energy

$$E =< BCS|H|BCS > \tag{2.15}$$

for change in particle number N ie. $\lambda = dE/dN$. Applying variational principle,

$$\delta < BCS|H - \lambda N|BCS >= 0$$

we obtain a set of BCS equation

$$2\varepsilon_i u_i v_i + \Delta(v_i^2 - u_i^2) = 0 \tag{2.16}$$

Here Δ, the constant pairing gap is given by,

$$\Delta = G(\sum_{i>0} u_i v_i) \tag{2.17}$$

where G is the pairing strength. Pairing gap (Δ) is basically of the order of

spacing between single particle energies near to Fermi energy. From the BCS equation, we get the expression for occupation probability

$$v_i^2 = \frac{1}{2}(1 - \frac{\varepsilon_i - \lambda}{\sqrt{(\varepsilon_i - \lambda)^2 + \Delta^2}}) \tag{2.18}$$

and non occupation probability

$$u_i^2 = \frac{1}{2}(1 + \frac{\varepsilon_i - \lambda}{\sqrt{(\varepsilon_i - \lambda)^2 + \Delta^2}}) \tag{2.19}$$

In the limit $G \to 0$, ie. $\Delta \to 0$ (non interacting) for occupied levels $v_i^2 = 1$ and for unoccupied levels $u_i^2 = 0$. In this case v_i^2 is a step function. When $\Delta \neq 0$, due to interaction, particles are scattered in the neighbourhood of Fermi surface, which results in a partial depletion of states below and a partial filling of the states above Fermi level as shown in fig. 2.1[1].

The gap equation can be written using the above expression as

$$\Delta = \frac{G}{2} \sum_{i<0} \frac{\Delta}{\sqrt{(\varepsilon_i - \lambda)^2 + \Delta^2}} \tag{2.20}$$

Using all the above equations, we can express the pairing energy as

$$E_{pair} = -\Delta \sum_{i=1}^{A} u_i v_i \tag{2.21}$$

It is found that BCS wave function cannot be used for states with odd number of particles. For describing odd-A systems, an extended BCS ie. blocked BCS is introduced[1]. The ground state of the odd system is described by the wave function

$$\alpha_{i_1}^\dagger |BCS> = a_{i_1}^\dagger \Pi_{i \neq i_1} (u_i + v_i a_i^\dagger a_{\bar{i}}^\dagger)|- > \tag{2.22}$$

The unpaired particles is in i_1 state and this level is blocked. Pauli principle prevents this level from particpating in scattering process of nucleons. Thus i_j

is always occupied and i empty. Only difference found in blocked BCS is that while calculating pairing gap, one level is blocked. The pairing gap is given by

$$\Delta = G \sum_{i \neq i_1} u_i v_i \tag{2.23}$$

The level k_1 has to be excluded as it does not contribute to E_{pair}. BCS approximation gives good results for nuclei on and near to the stability line.

2.4 Hartree-Fock-Bogoliubov theory

Hartree-Fock-Bogoliubov theory (HFB) is the generalized single particle model which is a combination of both HF and BCS theory. In HFB method, Hamiltonian reduces to two average potentials, the self consistent field Γ (HF theory) and pairing field Δ (BCS theory). The field Γ contains all the long range p-h correlations and Δ contains the short range pairing correlations. The many body Hamiltonian expressed in terms of the annihilation and creation operator is given by,

$$H = \sum_{ij} t_{ij} a_i^\dagger a_j + \frac{1}{4} \sum_{ijkl} V_{ijkl} a_i^\dagger a_j^\dagger a_k a_l \tag{2.24}$$

Instead of single particle states, independent quasi-particles are used in HFB approximation. Nuclear wavefunction is defined as a vacuum of suitable quasi-particle operators[1]. The ground state of a many-body system is represented as vacuum w.r.t quasi-particles.

$$\beta_k |\Phi >= 0 \tag{2.25}$$

for all k=1.....M.

These quasi-particle states are related to single particle states using Bogoliubov transformation[1]. Quasi-particles are represented as linear combination of

particle and hole operators.

$$\beta_k = \sum_l V_{lk}^* a_l + U_{lk}^* a_l^\dagger \tag{2.26}$$

$$\beta_k^\dagger = \sum_l U_{lk} a_l^\dagger + V_{lk} a_l \tag{2.27}$$

In matrix form, the transformation is given by

$$\begin{pmatrix} \beta \\ \beta^\dagger \end{pmatrix} = \begin{pmatrix} U^\dagger & V^\dagger \\ V^T & U^T \end{pmatrix} \begin{pmatrix} a \\ a^\dagger \end{pmatrix} = W^\dagger \begin{pmatrix} a \\ a^\dagger \end{pmatrix} \tag{2.28}$$

where

$$W = \begin{pmatrix} U & V^* \\ V & U^* \end{pmatrix} \tag{2.29}$$

is a unitary matrix. A general Bogoliubov transformation is nothing but a BCS transformation in an appropriate basis (canonical basis).

In HFB, Hamiltonian differ from that in HF. Here an additional constraint on number operator is included. ie.

$$H' = H - \lambda N \tag{2.30}$$

where λ is the Lagrange multiplier and $N = a^\dagger a$ is the number operator.

The purpose of the constraining term is to ensure that the expectation value of the nucleon number relative to HFB quasiparticle vacuum state $|0>$ is the nucleon number of the nucleus under investigation.

$$< \phi|\hat{N}|\phi >= n \tag{2.31}$$

Such a constraint is needed in HFB and BCS approximation in which states of different nucleon number are mixed. Making use of the above transformation, Hamiltonian can be written as

$$\begin{aligned}\hat{H} - \lambda\hat{N} &= \hat{H}^0 + \sum_{ij} \hat{H}_{ij}\beta_i^\dagger\beta_j + \sum_{i<j}(\hat{H}_{ij}\beta_i^\dagger\beta_j^\dagger + h.c) + \hat{H}_{int} \\ &= \hat{H}^0 + \hat{H}^{11} + \hat{H}^{20} + \hat{H}^{40} + \hat{H}^{31} + \hat{H}^{22}\end{aligned} \tag{2.32}$$

where the indices denote the number of creation and annihilation operators. $\hat{H}^0$ is the quasi-particle vacuum expectation value, $\hat{H}^{11}$ denotes dependence of energy of quasi-particle-quasi hole excitations, $\hat{H}^{20}$ violates quasi-particle numbers and it is chosen as zero. All the other terms are included in $\hat{H}_{int}$. Two quantities, density matrix ρ (normal density) and pairing tensor κ (abnormal density) are introduced to define the wavefunction. They are represented as

$$\rho_{ij} =< \Phi|a_j^\dagger a_i|\Phi > \tag{2.33}$$

$$\kappa_{ij} =< \Phi|a_j a_i|\Phi > \tag{2.34}$$

In matrix form these can be represented as $\rho = V^*V^T$ and $\kappa = V^*U^T$. The normal density ρ is Hermitian and the abnormal density κ is skew symmetric. For convenience a generalised matrix $\mathcal{R}$ of the form

$$\mathcal{R} = \begin{pmatrix} \rho & \kappa \\ -\kappa^* & 1-\rho^* \end{pmatrix} \tag{2.35}$$

can be introduced. The generalised matrix $\mathcal{R}$ is Hermitian as well as idempotent and and have eigen values 0 or 1. In terms of ρ and κ, expectation value of Hamiltonian can be expressed as energy functional:

$$E[\rho,\kappa] = \frac{< \Phi|H - \lambda N|\Phi >}{< \Phi|\Phi >} = Tr[(\varepsilon + \frac{1}{2}\Gamma)\rho] - \frac{1}{2}Tr[\Delta\kappa^*] \tag{2.36}$$

where HF potential Γ and pairing potential Δ are defined as

$$\Gamma_{kl} = \sum_{i,j} \bar{v}_{kjli}\rho_{ij} \tag{2.37}$$

$$\Delta_{kl} = \frac{1}{2}\sum_{i,j} \bar{v}_{kjli}\kappa_{ij} \tag{2.38}$$

HFB equations are obtained by applying variational principle to equation (2.36). In matrix form HFB equation is given by

$$\begin{pmatrix} h-\lambda & \Delta \\ -\Delta^* & -h^*+\lambda \end{pmatrix} \begin{pmatrix} U_n \\ V_n \end{pmatrix} = E_n \begin{pmatrix} U_n \\ V_n \end{pmatrix} \tag{2.39}$$

where $h = t + \Gamma$, E_n is the quasiparticle energy and λ is the chemical potential.

Similar to the case of equation (2.8), here the HFB equation can be represented in terms of generalised density matrix as

$$[\mathcal{H}, \mathcal{R}] = 0 \tag{2.40}$$

where $\mathcal{H}$, the generalised single particle Hamiltonian is given by,

$$\mathcal{H} = \begin{pmatrix} h-\lambda & \Delta \\ -\Delta^* & -h^*+\lambda \end{pmatrix} \tag{2.41}$$

2.4.1 Pairing Interaction

In the p-p channel, phenomenological density dependent contact interaction is used. The commonly used density independent delta interaction which leads to volume pairing is

$$V^{\delta}_{vol}(\mathbf{r}, \mathbf{r}') = V_0\delta(\mathbf{r} - \mathbf{r}') \tag{2.42}$$

A modified form of the above interaction is the density dependent delta interaction (DDDI)[6].

$$V^{\delta}_{surf}(\mathbf{r}, \mathbf{r}') = f_{pair}(r)\delta(\mathbf{r} - \mathbf{r}') \tag{2.43}$$

where the pairing strength factor is

$$f_{pair}(r) = V_0[1 - (\frac{\rho(\mathbf{r}+\mathbf{r}')}{\rho_c})^{\alpha}] \tag{2.44}$$

where V_0, ρ_c, and α are constants. The density $\rho_c \approx \rho_0$, where the saturation density $\rho_0 = 0.16fm^{-3}$, and $\alpha = 1, 1/2, 1/3$ and $1/6$. The other parameters are adjusted to reproduce the experimental pairing gap Δ.

The pairing interaction is very well described by the combination of volume and surface interaction[7], which is the mixed variant of DDDI, i.e.,

$$V^{\delta}_{mix}(\mathbf{r}, \mathbf{r}') = \frac{1}{2}(V^{\delta}_{vol} + V^{\delta}_{surf}) \tag{2.45}$$

$$V^{\delta}_{mix}(\mathbf{r}, \mathbf{r}') = V_0^{n/p}[1 - \frac{1}{2}(\frac{\rho(\mathbf{r}+\mathbf{r}')}{\rho_c})^{\alpha}]\delta(\mathbf{r}-\mathbf{r}') \tag{2.46}$$

The other parameters are adjusted to reproduce the experimental pairing gap Δ.

2.5 Effective interaction

The bare n-n force does not behave well in many-body techniques because the interaction is modified by complicated many-body effects. The interaction usually used in nucleon-nucleon scattering is not used in many-body problems. This is because the presence of hard core(repulsive core) would have a matrix element with infinite value. So, here an effective interaction which is the infinite sum of scattering process of two nucleon inside a nucleus is considered. This interaction help to get rid of the hard core problem and is well behaved at short distances. Effective interaction depends on the density of nuclei which results in different forces in the interior and outer region of nuclei. There exist a number of phenomenological interactions, based on their range, which are valid for specific problems. The most important ones are the zero range Skyrme interaction[8] and the finite range Gogny interaction[9].

Here we are dealing with Skyrme effective interaction. It is the sum of 2 and 3-body interactions,

$$V = \sum_{i<j} V(i,j) + \sum_{i<j<k} V(i,j,k) \tag{2.47}$$

The two body interaction is given by[8],

$$\begin{aligned} V(i,j) &= t_0(1 + x_0\hat{P}_\sigma)\delta(\mathbf{r}_i - \mathbf{r}_j) \\ &+ \frac{1}{2}t_1(1 + x_1\hat{P}_\sigma)[\delta(\mathbf{r}_i - \mathbf{r}_j)\hat{k}^2 + \hat{k}'^2\delta(\mathbf{r}_i - \mathbf{r}_j)] \\ &+ t_2(1 + x_2\hat{P}_\sigma)k'.\delta(\mathbf{r}_i - \mathbf{r}_j)\hat{k} \\ &+ \frac{1}{6}t_3(1 + x_3\hat{P}_\sigma)\rho^\alpha\delta(\mathbf{r}_i - \mathbf{r}_j) \\ &+ iW_0(\hat{\sigma}_i + \hat{\sigma}_j).\hat{k}' \times \delta(\mathbf{r}_i - \mathbf{r}_j)\hat{k} \end{aligned} \tag{2.48}$$

where

$$\hat{k} = \frac{1}{2i}(\nabla_i - \nabla_j), \hat{k}' = -\frac{1}{2i}(\nabla_i - \nabla_j) \tag{2.49}$$

is the operator of relative momentum. The three-body interaction is given by

$$V(i,j,k) = t_3\delta(\mathbf{r}_i - \mathbf{r}_j)\delta(\mathbf{r}_i - \mathbf{r}_k) \tag{2.50}$$

where $t_0, t_1, t_2, t_3, x_0, x_1, x_2, x_3, W_0$ and α are Skyrme parameters which are fitted to reproduce the properties of finite nuclei. There exits more than 200 Skyrme forces in literature. Among the wide variety of Skyrme forces, we selected SkP[10], SIII[11], SkM*[12], SLY5[13], SLY6[14], UNEDF0[15] and UNEDF1[16]. Table 2.1 shows the nuclear matter properties of these Skyrme forces. The values of the Skyrme parameters can be obtained in the respective references.

Table 2.1: Nuclear matter properties at saturation density for different Skyrme parameters

Force	ρ_0	E/A	E_{sym}	K_0	m^*/m
SkP	0.163	-15.95	30.0	201.0	1.00
SIII	0.145	-15.85	28.16	355.4	0.76
SkM*	0.16	-15.77	30.03	216.6	0.79
Sly5	0.161	-15.99	32.01	230.0	0.70
Sly6	0.159	-15.62	31.96	230.0	0.69
UNEDF0	0.16	-16.05	30.54	230.0	0.90
UNEDF1	0.158	-15.8	28.98	220.0	0.99

2.6 Skyrme energy density functional

In Skyrme Hartree-Fock-Bogoliubov approximation, the total energy of the nucleus can be represented as the integral of local energy density functional.

$$\varepsilon = \int d^3r \mathcal{H}(r) \tag{2.51}$$

where $\mathcal{H}(r)$, the total Hamiltonian density is the sum of mean field and pairing energy density[18]. i.e,

$$\mathcal{H}(r) = H(r) + \tilde{H}(r) \tag{2.52}$$

Total energy can be explicitly represented as the sum of kinetic, Skyrme, spin-orbit, Coulomb and pairing energy densities[7]. They can be expressed as,

$$\mathcal{H}_{kin}(r) = \frac{\hbar^2}{2m}\left[1 - \frac{1}{A}\right]\tau_0 \tag{2.53}$$

$$\mathcal{H}_{Sky}(r) = \sum_{t=0,1}\left[\mathcal{C}_t^{\rho}(\rho_0)\rho_t^2 + \mathcal{C}_t^{\Delta\rho}\rho_t\Delta\rho_t + \mathcal{C}_t^{\tau}\rho_t\tau_t\right] \tag{2.54}$$

$$\mathcal{H}_{S-O}(r) = \sum_{t=0,1}\left(\mathcal{C}_t^{\nabla J}\rho_t\nabla.J_t\right) \tag{2.55}$$

$$\mathcal{H}_{Coul}(r) = V_{Coul}(\rho_p) - \frac{3e^2}{4}\left(\frac{3}{\pi}\right)^{1/3}\rho_p^{4/3} \tag{2.56}$$

$$\mathcal{H}_{Pair}(r) = \frac{1}{4}f_{pair}(\rho_0)\sum_{t=0,1}\kappa_t^2 \tag{2.57}$$

where ρ is the particle density, τ is the kinetic density, κ is the pairing density, J is the spin current density and $\mathcal{C}$ is the coupling constant. Their respective expressions can be obtained from ref. [19] The scalar and isoscalar part of particle density ρ_t, are defined as the sum ($\rho_0 = \rho_n + \rho_p$) and ($\rho_1 = \rho_n - \rho_p$)difference of neutrons and protons densities[20, 21]. f_{pair} is the pairing strength factor which is given by equation (2.44).

References

[1] P. Ring and P. Shuck, *The Nuclear Many-Body Problem*, (Springer, Berlin, 1980).

[2] W. Greiner and J. A. Maruhn, *Nuclear Models*, (Springer, Berlin, 1996).

[3] M. Bender, P.-H. Heenen and P-G. Reinhard, *Rev. Mod. Phys*, **75**, 121(2003).

[4] D. J. Rowe and J.L. Wood, *Fundamentals of Nuclear Models*, (World Scientific, 2010).

[5] M. A. Preston and R. K. Bhaduri, *Structure of the Nucleus*, (Addison-Wesley, 1975).

[6] R.R. Chasman, *Phys. Rev. C*, **14**, 1935(1976).

[7] J. Dobaczewski, W. Nazarewicz and M.V. Stoitsov, *Eur. Phys. J. A*, **15**, 21(2002).

[8] T. H. R. Skyrme, *Nucl. Phys.*, **9**, 615(1959).

[9] J. Decharge and D. Gogny, *Phys. Rev. C*, **21**, 1568(1980).

[10] J. Dobaczewski, H. Flocard and J. Treiner, *Nucl. Phys. A*, **422**, 103(1984).

[11] M. Beiner, H. Flocard, N. Van Giai, and P. Quentin, *Nucl. Phys. A.*, **238**, 29(1975).

[12] J. Bartel, P. Quentin, M. Brack, C. Guet, and H. B. Hakansson, *Nucl. Phys. A*, **386**, 79 (1982).

[13] E. Chabanat, P. Bonche, P. Haensel, J. Meyer and R. Schaeffer, *Nucl. Phys. A*, **627**, 710(1997).

[14] E. Chabanat, P. Bonche, P. Haensel, J. Meyer and R. Schaeffer, *Nucl. Phys. A*, **635**, 231(1998).

[15] M. Kortelainen, T. Lesinski, J. More, W. Nazarewicz, J. Sarich, N. Schunck, M.V. Stoitsov and S. Wild, *Phys. Rev. C*, **82**, 024313(2010).

[16] M. Kortelainen, J. McDonnell, W. Nazarewicz, P.G. Reinhard, J. Sarich, N. Schunck, M.V. Stoitsov and S. Wild, *Phys. Rev. C*, **85**, 024304(2012).

[17] N. Schunck, J. Dobaczewski, J. McDonnell, W. Satua, J.A. Sheikh, A. Staszczak, M. Stoitsov and P. Toivanen, *Comp. Phys. comm.*, **183**, 166(2012).

[18] M.V. Stoitsov, J. Dobaczewski, W. Nazarewicz and P. Ring, *Comp. Phys. comm.*, **167**, 43(2005).

[19] E. Perliska, S. G. Rohoziski, J. Dobaczewski, and W. Nazarewicz, *Phys. Rev. C*, **69**, 014316(2004).

[20] J. Dobaczewski and J. Dudek, *Phys. Rev. C*, **52**, 1827(1995).

[21] J. Dobaczewski and J. Dudek, *Phys. Rev. C*, **55**, 3177(E)(1997).

Chapter 3

Shape transition in transitional nuclei W, Os and Pt

3.1 Introduction

The shape is one of the fundamental properties of a nucleus which gives an insight into the nucleonic distribution. The nuclear shape is a consequence of the interplay between the single-particle energy and the collective degree of freedom. Nuclei are found to exhibit various shapes like spherical, axially symmetric prolate and oblate configurations, axially asymmetric triaxial configurations etc. Nuclei having either magic neutron or proton number or both are found to have a spherical configuration. Increasing or decreasing the nucleonic number leads to deviation from this stable spherical state. Quantitatively, this deviation of the nucleus is expressed in terms of multipole moments. In the nuclear chart, there are some regions where we can find nuclei exhibiting various shapes along the isotopic chain. The sudden change in the shape of nuclei with a change in nucleon number is referred to as quantum phase transition [1]. The study of nuclei belonging to these transitional regions have got importance as they paved the way to the analysis of nuclear structure.

Recent years have seen many experimental and theoretical studies analysing the shape transition in these transitional nuclei. Due to the difficulty in populating these nuclei beyond N=126, the experimental data in this particular region

is not available at present.

This chapter aims at studying the structural evolution in some nuclei which belongs to the sub-lead region, such as W, Os and Pt, around neutron shell closure (N=126). Many earlier works related to this region showed that nuclei in this region ($A \sim 190$) are prone to exhibit a transition in the shape between prolate and oblate via spherical configuration. Moreover, it is found that in this region oblate configuration is energetically favoured. The study of shape transition of these nuclei beyond N=126 have not been done so far within the framework of Skyrme Hartree-Fock-Bogoliubov theory. In the present study, we look for the shape evolution of isotopes with neutron number in the range N=110 to 138.

3.2 Theoretical Formalism

We have computed potential energy curves and surfaces using constrained HFB theory. In the particle-hole channel, we have used the zero range Skyrme effective interaction, with the recent UNEDF1 [2] parametrization. In the pairing part, the density dependent delta interaction (DDDI)[3, 4] in its mixed form is used. The mixed variant of density dependent delta interaction (DDDI) is given by[5],

$$V_{\delta}^{n/p}(\mathbf{r_1}, \mathbf{r_2}) = V_0^{n/p}[1 - \frac{1}{2}(\frac{\rho(\mathbf{r_1} + \mathbf{r_2})}{\rho_0})^{\alpha}]\delta(\mathbf{r_1} - \mathbf{r_2}) \tag{3.1}$$

where the saturation density[6] ρ_0=0.16 fm^{-3} and α=1. But in the case of UNEDFs pairing strength has been optimized using Lipkin-Nogami prescription[7, 8]. The pairing strength is taken to be $V_0^n = -186.065$ MeV and $V_0^p = -206.580$ MeV, according to the ref.[2]. With the help of UNEDF1 parametrizations, we tried to analyse the role played by the triaxial degrees of freedom in these nuclei. Triaxial calculations have been carried out with the aid of symmetry unrestricted code HFODD(v2.49t)[9]. Here shape of the nucleus can be obtained

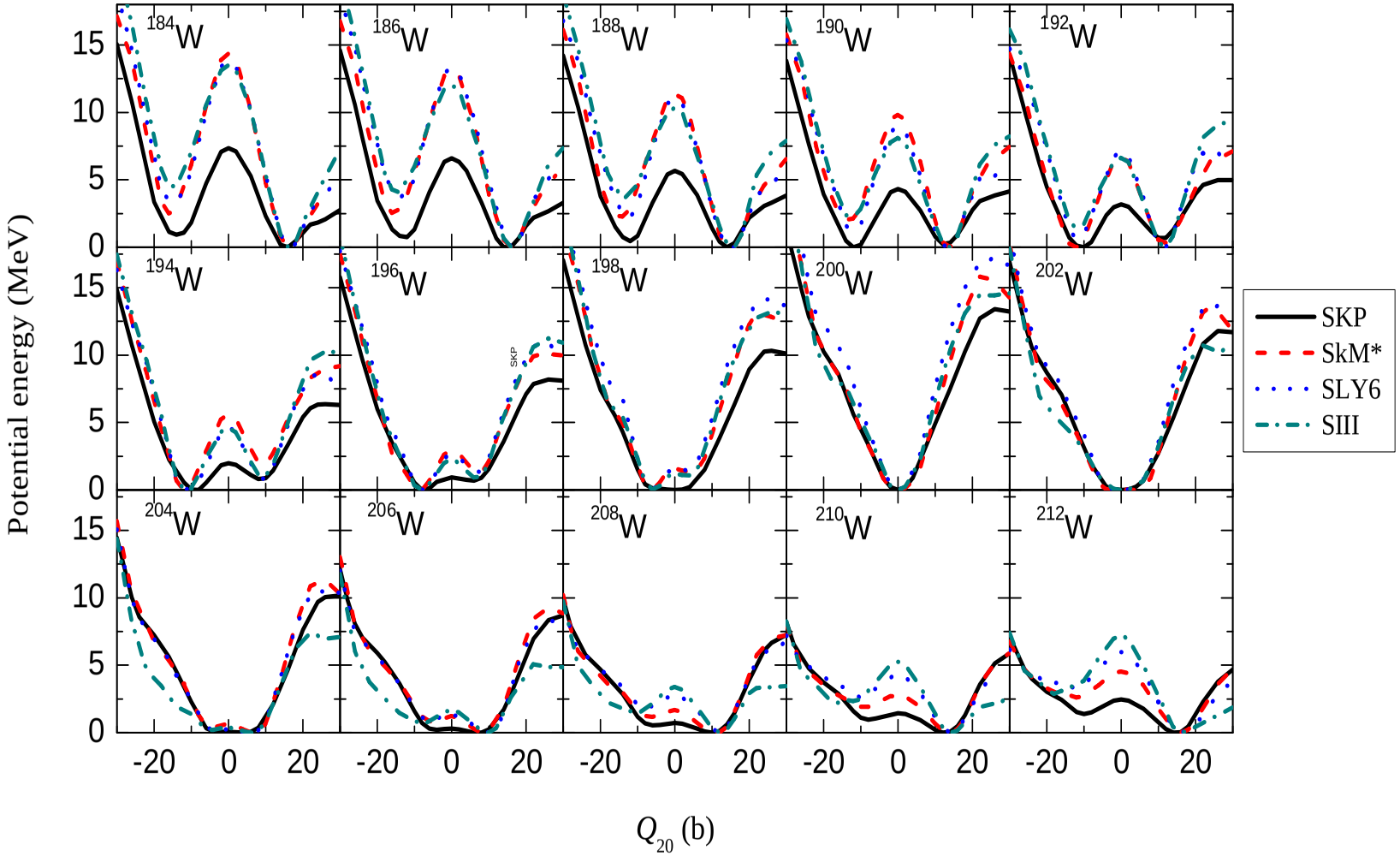

Figure 3.1: Potential energy curves for W isotopes as a function of quadrupole moment Q_{20} for various Skyrme forces

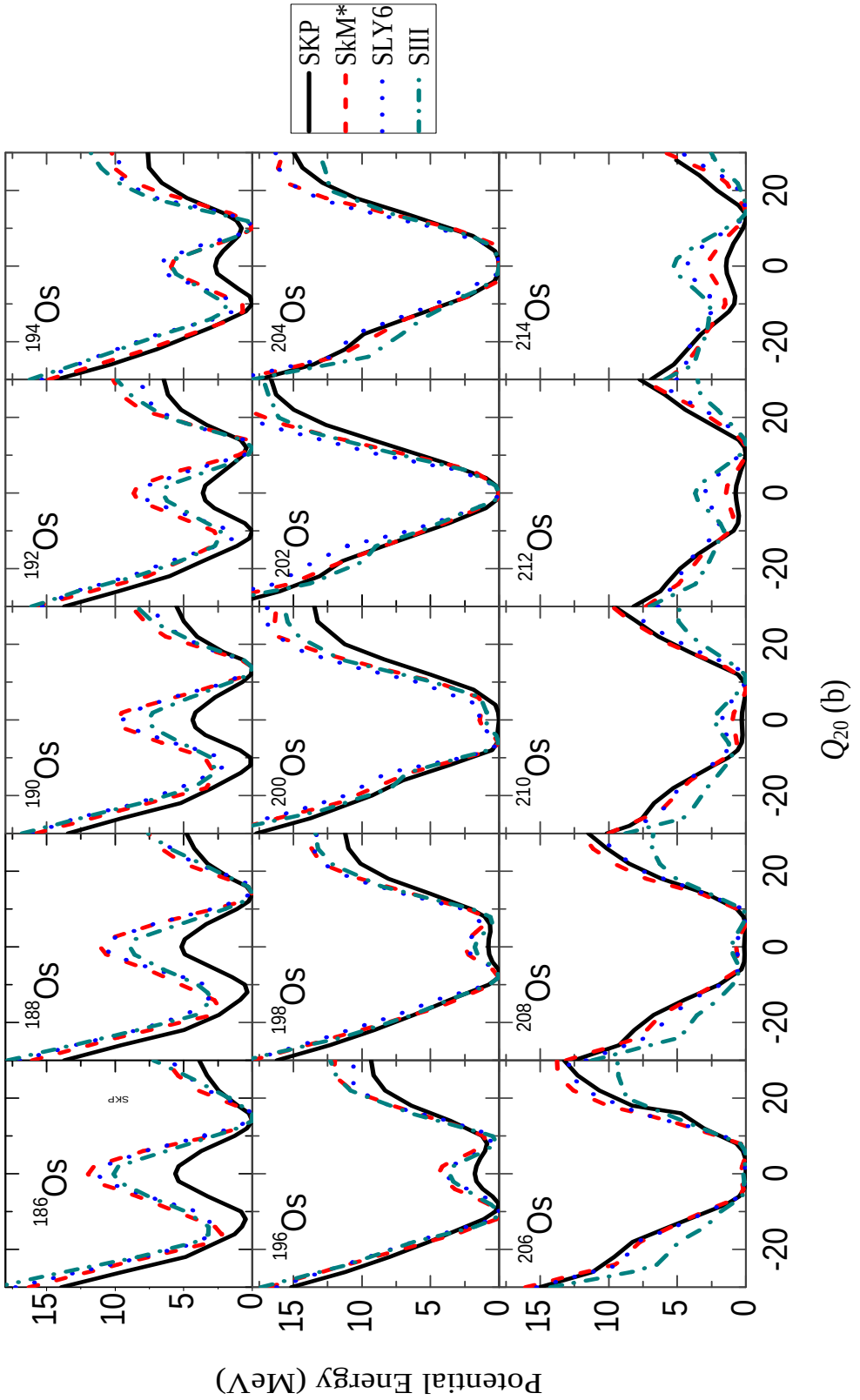

Figure 3.2: Same as fig. 3.1 but for Os isotopes

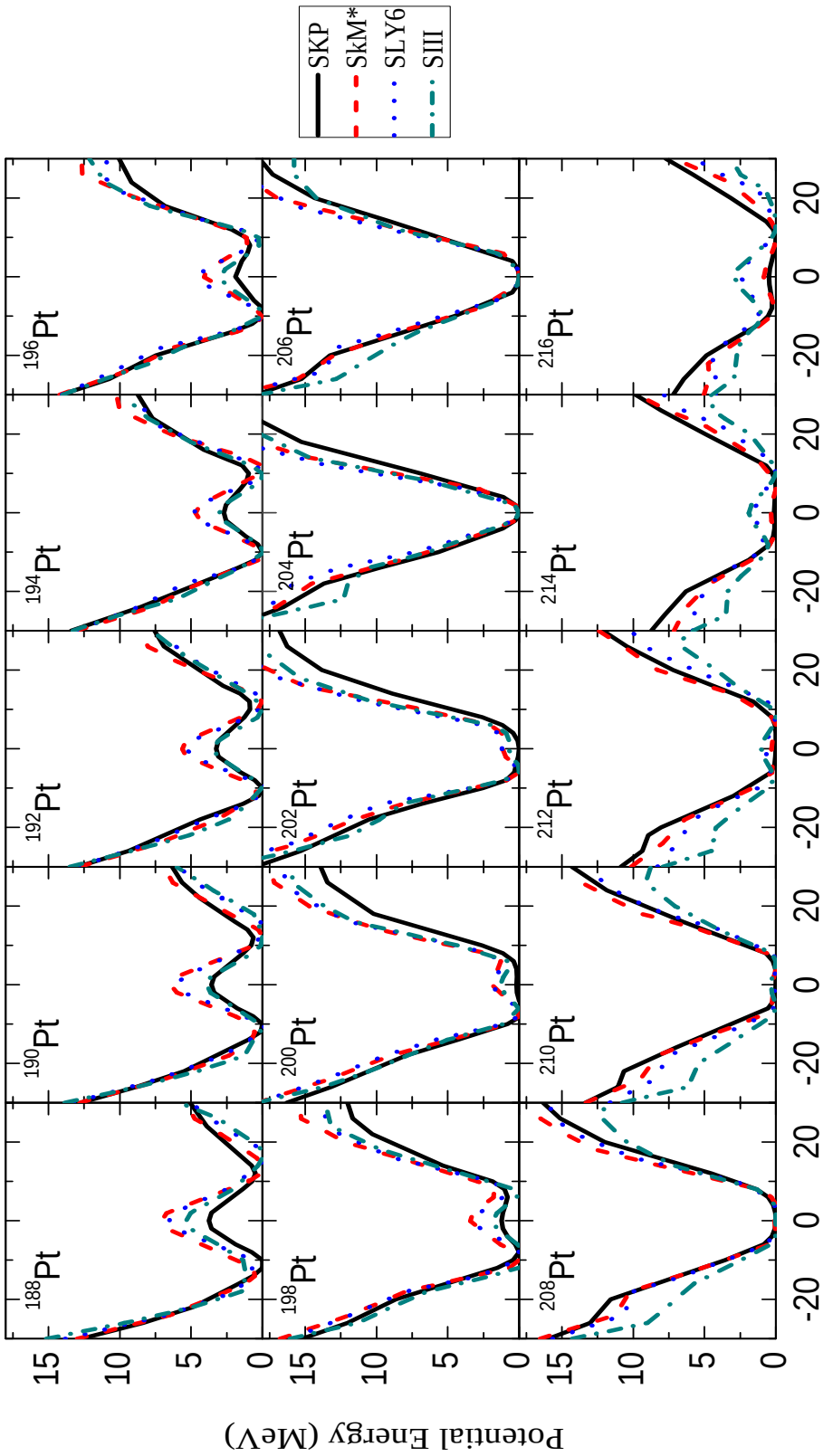

Figure 3.3: Same as fig. 3.1 but for Pt isotopes

by constraining the quantities, Q_{20} and Q_{22}.

$$Q_{20} = \frac{1}{2} < \phi|2z^2 - x^2 - y^2|\phi > \tag{3.2}$$

$$Q_{22} = \frac{\sqrt{3}}{2} < \phi|x^2 - y^2|\phi > \tag{3.3}$$

We have also carried out the analogous calculations to find the axially symmetric solutions of HFB equations. Potential energy curves for the respective isotopic chains corresponding to various Skyrme parametrizations are computed by imposing constraint on quadrupole moment Q_{20}. We have employed some of the widely used Skyrme forces like SIII[10], SkP[11], SkM*[12] and SLy6[13] for this.

We also calculated the nucleon localization function (NLF) which gives an insight into the nuclear shell effects. The nucleon localization function is based on the inverse conditional probability of finding a nucleon with same spin and isospin in the vicinity of another nucleon located at r. NLF, which is derived from the density matrix, depends not only on local mass density, but also on kinetic-energy density and current density[14]. The localization measure is given as,

$$\mathcal{C} = [1 + \Big(\frac{\tau_{q\sigma}\rho_{q\sigma} - \frac{1}{4}|\nabla\rho_{q\sigma}|^2 - j_{q\sigma}^2}{\rho_{q\sigma}\tau_{q\sigma}^{TF}}\Big)^2]^{-1} \tag{3.4}$$

where $\rho_{q\sigma}$, $\tau_{q\sigma}$, $j_{q\sigma}$, $\nabla\rho_{q\sigma}$ and $\tau_{q\sigma}^{TF}$are the particle density, kinetic energy density, current density, density gradient and Thomas-Fermi kinetic density respectively. If the value of $\mathcal{C}$ is close to 1, we can expect that the probability of finding two particles close to each other is very low. A high $\mathcal{C}$ value shows the spatial regions corresponding to shell separations. $\mathcal{C} = \frac{1}{2}$ corresponds to the homogeneous Fermi gas, where the individual orbits are delocalized. α- particle, where one particle of each spin and isospin combination is found, is the perfectly localized system with $\mathcal{C} = 1$. More details can be obtained from ref. [15, 16, 17].

The energy required to remove nucleons from the nuclei is termed as separation energy. While considering the odd-even effects, it is good to use the term

2n-separation energy. And the 2n-separation energy can be obtained from the ground state binding energies of two neighbouring even-even isotopes, using the expression,

$$S_{2n} = B(Z,N) - B(Z,N-2) \tag{3.5}$$

where B(Z,N) is the binding energy of the nucleus, Z is the atomic number and N is the neutron number.

Nuclear radii is yet another important quantity which is helpful in studying the structural properties of a nucleus. The mean square radius of neutron and proton can be obtained from nucleonic density ($\rho_{p,n}$)[18] and are given by

$$< r^2_{p,n} >= \frac{\int R^2 \rho_{p,n}(R) d^3R}{\int \rho_{p,n}(R) d^3R} \tag{3.6}$$

and finally rms radii is given by

$$r^{p,n}_{rms} = \sqrt{< r^2_{p,n} >} \tag{3.7}$$

In exotic nuclei, the neutron number is much greater than the proton number. This leads to the spatial extension of neutron around the proton distribution which results in the formation of a layer of neutrons around the core. This is termed as neutron skin. Quantitatively, this skin thickness is characterized by the difference between the rms radii of neutron and proton[19].

$$skin\ thickness \equiv < r^2_n >^{1/2} - < r^2_p >^{1/2} \tag{3.8}$$

Pairing plays an important role in open-shell nuclei. The odd-even staggering of nuclear binding energy is associated with pairing correlation [20]. The pairing gap is given by

$$\Delta = G \sum_{i>0} u_i v_i \tag{3.9}$$

where u_i and v_i are the occupation numbers and G is the matrix element.

3.3 Results and Discussion

We have made an attempt to analyse the evolution of shapes in transitional nuclei W, Os and Pt which are near to doubly magic nuclei ^{208}Pb. The study has been carried out for isotopes having neutron number in the range N=110 to 138 around the N=126 neutron shell closure.

3.3.1 Potential Energy Curves

Isotopes in the range $^{184-212}$W, $^{186-214}$Os and $^{188-216}$Pt are selected for the investigation. We have considered even-even isotopes of W, Os and Pt nuclei in this mass range.

In the first stage, we have done calculations corresponding to the axially symmetric case. Here the constrained calculations have been done by imposing the constraint on Q_{20} only. The potential energy curves (PEC) obtained in the case of W, Os and Pt isotopes are shown in fig. 3.1, 3.2 and 3.3 respectively. We have used various Skyrme parametrizations in order to analyse their sensitivity in predicting the shape evolution with an increase of neutron number.

From PECs, we have observed a systematic transition in the shape of all the three nuclei along the isotopic chain. In the case of lighter isotopes, among the selected region, we have seen that they exhibit a prolate configuration. And, as the neutron number increases, the shape of the isotopes changes gradually to an oblate configuration. This transition is observed to occur at neutron number N=116-118. It is also visible from the plot that as the magic number is approached, the quadrupole moment Q_{20} decreases. At N=126, the spherical configuration is attained as expected. Then beyond this, all the three nuclei exhibit prolate nature with an increase of Q_{20} with neutron number. Our observation based on axially symmetric calculations matches well with the earlier works [21, 22]. Moreover, all the selected Skyrme forces show almost similar trend

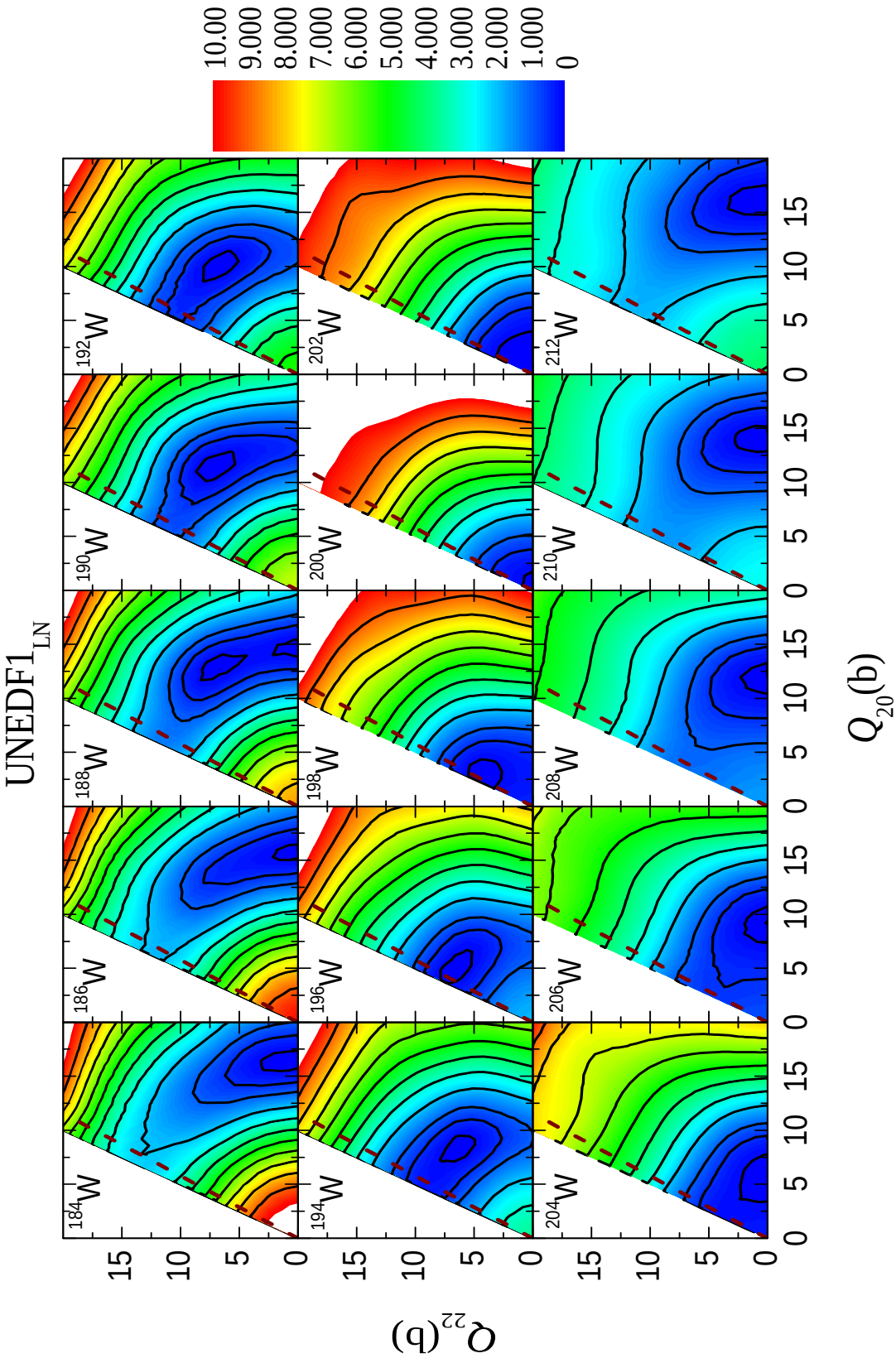

Figure 3.4: Potential energy surface for W isotopes as a function of quadrupole moment Q_{20} and Q_{22}

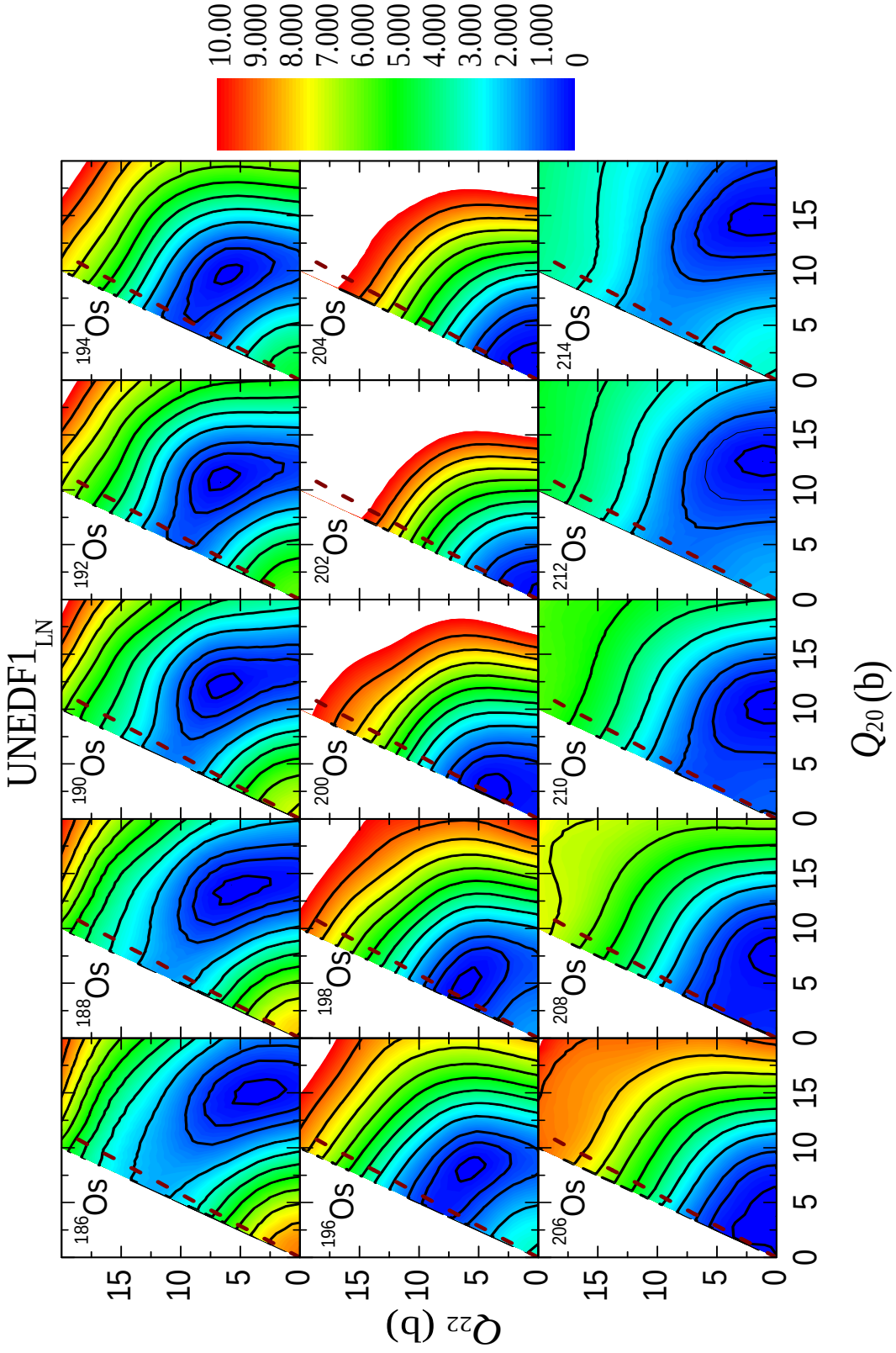

Figure 3.5: Same as fig. 3.4 but for Os isotopes

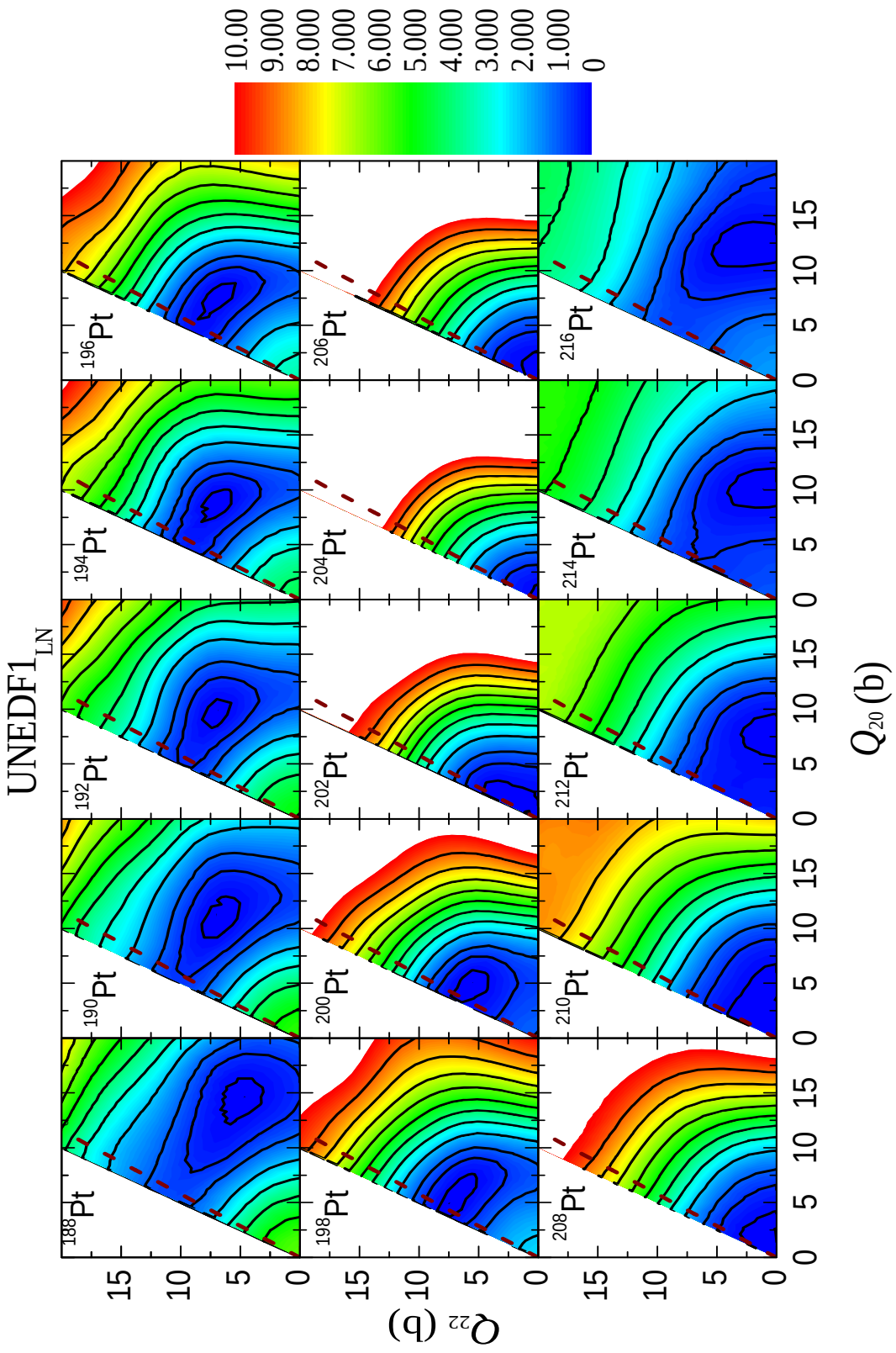

Figure 3.6: Same as fig. 3.4 but for Pt isotopes

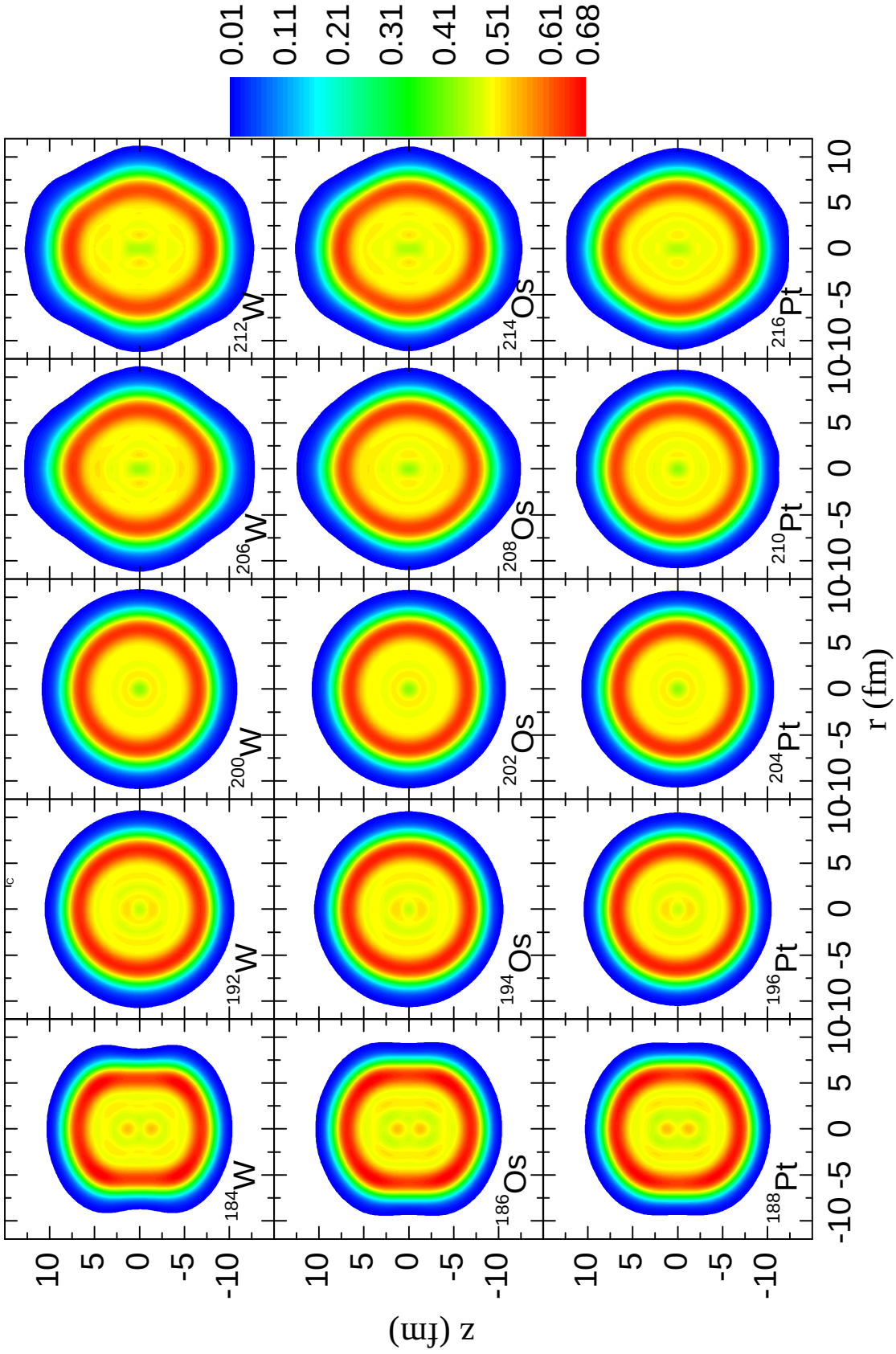

Figure 3.7: Nucleon localization function for selected W, Os and Pt isotopes

in the evolution of the shape except for some isotopes for the SKP parametrization. The difference is seen to be prominent in predicting the spherical barrier height.

To find the signatures of triaxiality in these respective nuclei, we have done triaxial calculations. This has been carried out using the recent UNEDF1 parametrization. By constraining Q_{20} and Q_{22}, we have plotted the potential energy surfaces (PES) for W, Os and Pt isotopes. The PESs are shown in fig 3.4, 3.5 and 3.6. From fig. 3.4, we observed that W isotopes have prolate shape at A=184-188. The calculation predicts a triaxial shape for isotopes falling in the mass range A=190-196. ^{198}W shows oblate nature while ^{200}W (N=126) is spherical as expected. Beyond ^{200}W, isotopes in the selected region shows a prolate shape. In the case of ^{188}W we observed two minima in the PES plot. It shows that ^{188}W exhibit the feature of shape isomerism. Fig. 3.5, shows that Os isotopes with A= 186 to 196 are triaxial in nature and then we find a shape transition to oblate for ^{198}Os and ^{200}Os. After that for the isotope with N=126 shows spherical shape. A similar variation is observed for Pt also. For all the three nuclei, isotopes beyond N=126, shows prolate configuration.

In order to examine the nucleonic shell structure, we have computed nucleonic localization function (NLF) for certain selected isotopes, which fall on either regions of the isotopes with N=126. NLFs are shown in fig. 3.7. In the case of ^{200}W, ^{202}Os and ^{204}Pt (N=126), we can see concentric circles. When comparing with the particle density, NLFs shows the shell structures much more clearly. When $\mathcal{C} = 1$, localization is perfect and when $\mathcal{C} = 0.5$, there won't be any particular shell structure, i.e, similar to Fermi gas.

Some of the important quantities which are helpful in investigating the structural properties of a nucleus are also being studied. They have been obtained from the PES plots of the three nuclei. We are interested only in the ground state of the selected isotopes. We have analysed the following quantities related to these nuclei.

Fig. 3.8 shows the 2n-separation energy which is obtained from the ground

state binding energy using the equation (3.5). Separation energy is the quantity used to find the shell closure in nuclei. A sudden fall in the value of separation energy points towards the shell closure, ie, the magic number. From the figure, we can see a sudden fall in the value of 2n-separation energy at N=126. Our results have been compared with the available experimental values [23]. The calculated results are in close agreement with the experimental values. The decrease in the value of separation energy beyond N=126 shows the reduced binding of valence nucleons.

Another important quantity which is of interest is the rms radii. It shows a clear signature of the shape evolution in nuclei. Instead of the total rms radii, we have computed the rms radii along the three different axes. This help us to understand the change ocurring in the nuclei in a more clear way. Rms radii along x, y and z-axis is depicted in fig. 3.9. Upper panel shows the rms radii of W. From that, we can see that isotopes with A=184-188 and A=202-212 exhibit prolate shapes with same rms radii along x and y-axis. Isotopes in the range A=190-196 have different rms radii along x, y and z- axes which show their triaxial nature. Oblate shape is observed for isotope with A=198 which is having same x and z-axis. And finally A=200 shows spherical shape with rms radii same in all the directions. Similarly, in the case of Os isotopes (middle panel), we found triaxial shape in the mass region A=186-196 and oblate shape for A=198-200. Here, we observed two spherical isotopes, A=202-204 and beyond that we have prolate configuration. A similar observation can be seen in the case of Pt also (lower panel), with A=188-196 having triaxiality and A=198-202 having oblate shape. Also, A=202 and 206 exhibit spherical configurations and mass number A=208 to 216 shows prolate nature. This observation supports the nature of the PES plots.

Neutron skin thickness is another quantity which is having importance in the case of neutron rich nuclei. It is calculated from neutron and proton rms radii using equation (3.8). In the case of nuclei belonging to beta stability line, this difference is around 1-2 fm. When this difference exceeds this limit, we can

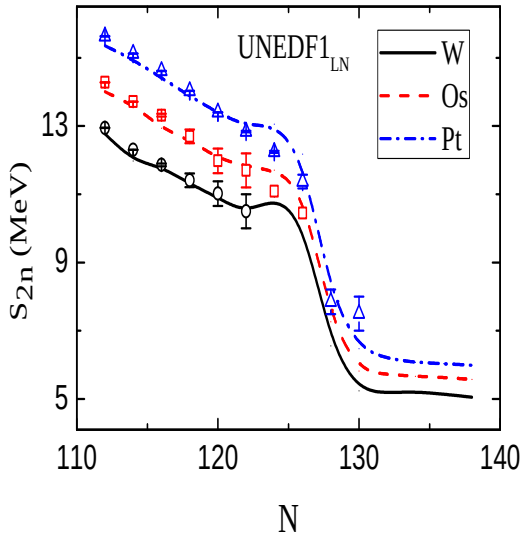

Figure 3.8: 2n-separation energy as a function of neutron number. The corresponding experimental values are shown by symbols along with error bar

expect the formation of neutron skin around the nucleus [19]. The computed values corresponding to the skin thickness is shown in fig. 3.10. From the figure we can observe that, this difference is greater for W compared to other two isotopes. In the selected region, the formation of neutron skin is found to be prominent in the case of W. The skin thickness depends on a systematic way on the atomic number also.

Fig. 3.11 shows the proton and neutron pairing gaps of W, Os and Pt isotopes. From the figure, the proton pairing gap shows a hump around the shell closure while the neutron pairing gap shows a depression. The value of Δ_p shows a systematic decrease with atomic number. It is very small for Pt isotopes as it is more near to proton shell closure compared to W isotopes. An entirely opposite feature is observed for Δ_n.

3.4 Conclusion

With the help of constrained HFB equation, we tried to understand the shape evolution in transitional nuclei W, Os and Pt. The analysis have been carried out

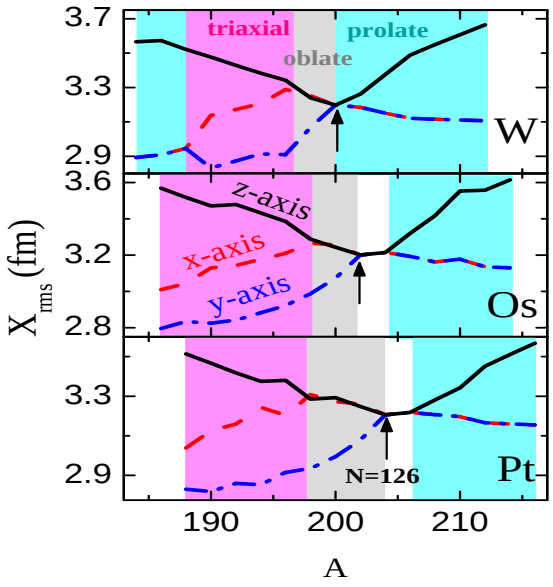

Figure 3.9: Total rms radii of W, Os and Pt along x, y and z-axis

for isotopes having neutron number in the range N=110 to 138. PECs have been plotted for the selected isotopes, with the aid of axially symmetric HFB equation. The PECs have been drawn for some selected Skyrme parametrizations like SKP, SKM*, SIII and sLy6. We observed an evolution of shape in the concerned nuclei with the increase of neutron number. It is found that the shape of these nuclei changes in a systematic way from prolate to oblate (N=116-118), then to spherical at N=126, and then again become prolate.

In the second part, we have analysed the role of triaxial degrees of freedom in these nuclei. PES have been generated in order to analyse the signature of triaxiality. Triaxiality have been analysed with the help of recent UNEDF1 parametrization. PESs have shown a smooth evolution of shape from prolate to spherical through a triaxial γ-soft region. We have also studied some of the quantities like 2n-separation energy, rms radii, skin thickness and pairing gap, which are useful in analysing the structural properties of nuclei. Rms radii along the x, y and z directions also show the shape evolution along these isotopic chains. We also found the signatures of the formation of neutron skin in neutron rich nuclei.

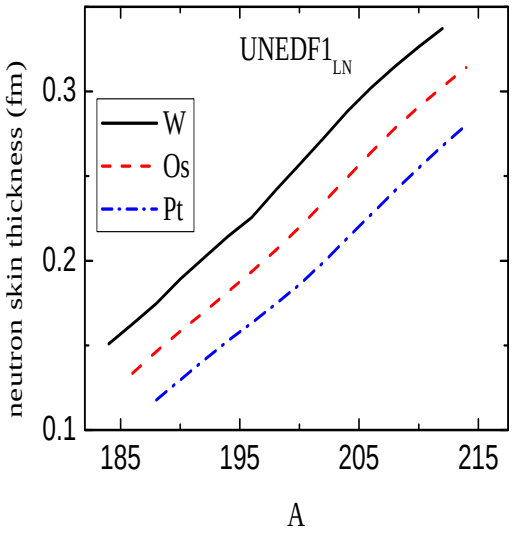

Figure 3.10: Neutron skin thickness of W, Os and Pt as a function of mass number

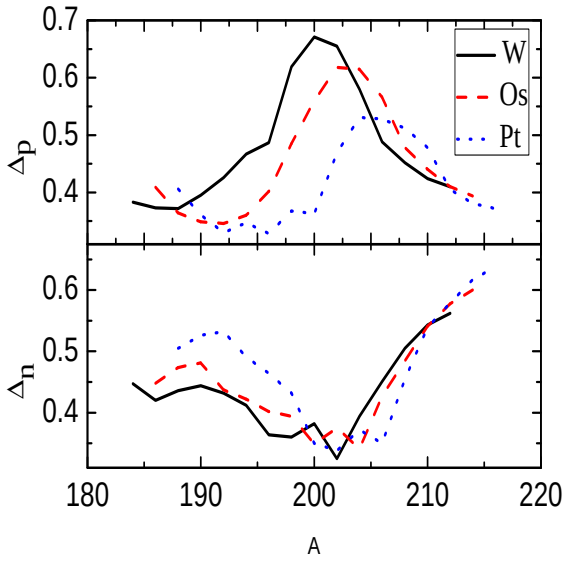

Figure 3.11: Proton and neutron pairing gap in the case of W, Os and Pt as a function of mass number

References

[1] P. Cejnar, J. Jolie, and R. F. Casten, *Rev. Mod. Phys.*, **82**, 2155(2010).

[2] M. Kortelainen, J. McDonnell, W. Nazarewicz, P.G. Reinhard, J. Sarich, N. Schunck, M.V. Stoitsov and S. Wild, *Phys. Rev. C*, **85**, 024304(2012).

[3] R.R. Chasman, *Phys. Rev. C*, **14**, 1935(1976).

[4] J.Terasaki, P.H. Heenen, P. Bonche, J. Dobaczewski and H. Flocard, *Nucl. Phys. A*, **593**, 1(1995).

[5] J. Dobaczewski, W. Nazarewicz and M.V. Stoitsov, *Eur. Phys. J. A*, **15**, 21(2002).

[6] J.Terasaki, H. Flocard, P.H. Heenen and P. Bonche, *Nucl. Phys. A*, **621**, 706(1997).

[7] P. G. Reinhard, W. Nazarewicz, M. Bender and J. A. Maruhn, *Phys. Rev. C*, **53**, 2776(1996).

[8] M. V. Stoitsov, J. Dobaczewski, R. Kirchner, W. Nazarewicz and J. Terasaki, *Phys. Rev. C*, **76**, 014308(2007).

[9] N. Schunck, J. Dobaczewski, J. McDonnell, W. Satua, J.A. Sheikh, A. Staszczak, M. Stoitsov, P. Toivanen, *Comp. Phys. Commun.*, **183**, 166 (2012).

[10] M. Beiner, H. Flocard, N. Van Giai, and P. Quentin, *Nucl. Phys. A.*, **238**, 29(1975).

[11] J. Dobaczewski, H. Flocard and J. Treiner, *Nucl. Phys. A*, **422**, 103(1984).

[12] J. Bartel, P. Quentin, M. Brack, C. Guet, and H. B. Hakansson, *Nucl. Phys. A*, **386**, 79 (1982).

[13] E. Chabanat, P. Bonche, P. Haensel, J. Meyer and R. Schaeffer, *Nucl. Phys. A*, **635**, 231(1998).

[14] P. Jerabek, B. Schuetrumpf, P. Schwerdtfeger and W. Nazarewicz, *Phys. Rev. Lett.*, **120**, 053001(2018).

[15] P.G. Reinhard, J. A. Maruhn, A. S. Umar and V. E. Oberacker, *Phys. Rev. C*, **83**, 034312(2011).

[16] C. L. Zang, B. Schuetrumpf and W. Nazarewicz, *Phys. Rev. C*, **94**, 064323(2016).

[17] B. Schuetrumpf and C. Zhang, *EPJ Web of Conf.*, **163**, 00050(2017).

[18] N. Schunck and J. L. Edigo, *Phys. Rev. C*, **78**, 064305(2008).

[19] S. Mizutori, J. Dobaczewski, G. A. Lalazissis, W. Nazarewicz, and P.-G. Reinhard, *Phys. Rev. C*, **61**, 044326(2000).

[20] P. Ring and P. Shuck, *The Nuclear Many-Body Problem*, (Springer, Berlin, 1980).

[21] P. D. Stevenson, M. P. Brine, Zs. Podolyak, P. H. Regan, P. M. Walker and J. Rikovska Stone, *Phys. Rev. C*, **72**, 047303(2005).

[22] P. Sarriguren, R. Rodriguez-Guzman and L. M. Robledo, *Phys. Rev. C*, **77**, 064322(2008).

[23] M. Wang, G. Audi, F. G. Kondev, W. J. Huang, S. Naimi and X. Xu *CPC*, **41**, 030003(2017).

Chapter 4

Alpha and cluster decay from transitional nuclei W, Os and Pt

4.1 Introduction

Cluster radioactivity is a rare cold nuclear phenomenon intermediate between alpha decay and spontaneous fission. Alpha decay is one of the prominent decay mode exhibited by the atomic nuclei because of its high binding energy. Several theoretical and experimental studies on cluster decay have been carried out in recent years. Different studies show that this phenomenon occurs in those regions where daughter nuclei should either be doubly magic or in its vicinity. In view of this observation, cluster radioactivity falls into two region, trans-tin and trans-lead. Our investigation mainly falls in the vicinity of trans-tin region. As stated in chapter 1, cluster decays are usually studied with the help of phenomenological models like Unified fission model and Preformed Cluster Model. The present work is dedicated to the microscopic description of alpha and cluster decay within the framework of Skyrme Hartree-Fock-Bogoliubov theory.

4.2 Theoretical Formalism

Skyrme HFB equation have been solved using cylindrically deformed HO and THO basis[1]. Numerical calculations have been carried out using 20 oscillator

shells. The cut off energy is taken as 60 MeV. In the particle-hole channel, we have used the effective Skyrme interactions[2]. In the present work we have used different Skyrme forces like SIII[3], SkP[4], SLy5[5], SkM*[6], UNEDF0[7] and UNEDF1[8]. These Skyrme forces are selected as they are very efficient in reproducing the ground state properties. Also they differ in various parameters, and this helps to analyse the effect caused by different factors. They vary in the value of effective mass, surface energy, with the inclusion of J^2 term, centre of mass correction etc.

In the particle-particle (pairing) channel, pairing interaction is included using the density dependent delta interaction[9, 10] of the form[11],

$$V_{\delta}^{n/p}(\mathbf{r_1}, \mathbf{r_2}) = V_0^{n/p}[1 - \frac{1}{2}(\frac{\rho(\mathbf{r_1} + \mathbf{r_2})}{\rho_0})^{\alpha}]\delta(\mathbf{r_1} - \mathbf{r_2}) \tag{4.1}$$

where the saturation density[12] ρ_0=0.16 fm^{-3} and α=1.

The half-lives corresponding to each decay mode is calculated using a standard formula, the Universal decay law(UDL)[13] which has been deduced from WKB approximations, with some modifications. It is given by,

$$log_{10}T_{1/2} = aZ_cZ_d\sqrt{\frac{A}{Q}} + b\sqrt{AZ_cZ_d(A_c^{1/3} + A_d^{1/3})} + c \tag{4.2}$$

where the constants are a=0.4314, b=-0.4087 and c=-25.7725.
Z_c, Z_d are the atomic number of cluster and daughter nuclei, A_c, A_d are the mass number of cluster and daughter nuclei and

$$A = \frac{A_cA_d}{A_c + A_d}$$

And Q is the Q-value of the decay.

4.3 Results and Discussion

In this chapter, we present the theoretical studies on alpha and cluster decay exhibited by transitional nuclei such as W, Os and Pt. We tried to calculate the half-lives of alpha and cluster decay using microscopic theory. The results have been compared with ELDM, which is a phenomenological model.

4.3.1 Alpha decay

As the first stage, we have analysed the feasibility of alpha decay in the isotopic chains of W, Os and Pt because of the availability of the wide range of experimental data. Alpha decay is the dominant decay mode of radioactive nuclei because binding energy of alpha particle is very high and is found to be 28.296 MeV [14]. Any decay mode will be energetically favourable, if and only if the Q-value is positive. We have tried to predict the alpha decay half-lives of W, Os and Pt isotopes by estimating Q-values with the help of Skyrme HFB theory. For each element we have done an extensive survey throughout the isotopic chain from 2p to 2n drip-line. It is observed that isotopes which fall between 2p drip-line and beta-stability line are unstable against alpha decay. The following subsections shows our observations on alpha radioactivity in W, Os and Pt isotopes.

Tungsten isotopes

At first, we have analysed the feasibility of alpha decay in the isotopic chain of W nuclei. It is found that W isotopes within the mass range 158 to 180 are unstable against alpha decay. To identify whether alpha decay is favourable for the W isotopes, we first computed the Q_α-values. Q_α-values are calculated from binding energies using the relation,

$$Q_\alpha(N, 74) = B(N-2, 72) + B(2, 2) - B(N, 74) \tag{4.3}$$

where, B(N,74) and B(N-2,72) are the binding energies of the parent ($_{74}$W) and the daughter nucleus ($_{72}$Hf). B(2,2), the binding energy of $^4_2$He nucleus (28.296

MeV) is taken from Atomic Mass Evaluation table (AME) 2012 [14].

The Q-values obtained in the case of different Skyrme forces are given in Table 4.1. They have been compared with the phenomenological Effective Liquid Drop Model (ELDM) [15, 16] values as well as with the available experimental values[17, 18]. A small discrepency is observed in the estimated Q-values. This is due to the fact that each Skyrme force describes binding energy of W isotopes with slight variation. A small variation in the values of the parameters of the Skyrme forces will affect the values of binding energy. From Table 4.1, we can see that the values obtained by the recent parametrization, UNEDF0 and UNEDF1 as well as the classical Skyrme parametrization SIII agree with ELDM values. Finally, alpha decay half-lives are calculated using UDL. Logarithmic values of half-lives for α decay against mass number of the parent(A) is depicted in fig. 4.1. From this fig. (4.1a), we can observe that the half-life is minimum for ^{158}W, which leads to the magic daughter nuclei ^{154}Hf (N=82). It is also visible that except SKM*, all other Skyrme forces overestimate the alpha decay half-lives.

We have also studied the standard deviation of the half-lives with respect to the experimental values for analysing how much the theoretical values agree with experimental ones. Standard deviations are tabulated in Table 4.2. From this table, it is observed that, SKM* is showing much variation with respect to experimental half-lives, compared to other Skyrme forces.

Osmium isotopes

Here also we have calculated the binding energies mircoscopically using various Skyrme forces and hence estimated the Q_α-values as before, in order to understand whether alpha decay is permissible in this isotopic chain. Q_α-values are calculated from binding energy using the relation,

$$Q_\alpha(N, 76) = B(N-2, 74) + B(2, 2) - B(N, 76) \tag{4.4}$$

Table 4.1: Q-values of alpha decay in even-even W isotopes calculated with Skyrme HFB equations solved using HO(top) and THO(bottom) basis. The results are compared with ELDM and available experimental values.

Alpha decay	Q value							
	SIII	SKP	SkM*	SLy5	UNEDF0	UNEDF1	ELDM	exp
$^{158}W \rightarrow \alpha +^{154}$ Hf	8.2843	7.0719	7.9058	8.3707	6.8296	7.6901	6.6051	
	8.2448	6.9272	7.1c9024	8.3608	6.8330	7.6648		
$^{160}W \rightarrow \alpha +^{156}$ Hf	6.1670	6.1679	6.6801	6.2786	5.9269	6.1993	6.0651	
	6.1674	6.1565	6.6793	6.2924	5.9236	6.1915		
$^{162}W \rightarrow \alpha +^{158}$ Hf	5.4312	5.5584	5.8998	5.4535	5.2839	5.3959	5.6781	5.53
	5.4375	5.5595	5.9009	5.4641	5.2811	5.3908		
$^{164}W \rightarrow \alpha +^{160}$ Hf	5.2161	5.3343	5.5125	5.2823	5.0426	5.0211	5.2781	5.153
	5.2140	5.3451	5.5043	5.2808	5.0586	5.0135		
$^{166}W \rightarrow \alpha +^{162}$ Hf	4.8437	5.0529	5.1203	4.8793	4.8716	4.6123	4.8561	
	4.8417	5.0623	5.1196	4.8811	4.8872	4.6160		
$^{168}W \rightarrow \alpha +^{164}$ Hf	4.5294	4.7429	4.8816	4.5113	4.6839	4.2422	4.5001	
	4.5225	4.7255	4.8851	4.5205	4.6878	4.2600		
$^{170}W \rightarrow \alpha +^{166}$ Hf	4.3104	4.4892	4.8444	4.2749	4.4489	3.9996	4.1441	
	4.3094	4.4941	4.8412	4.2828	4.4591	4.0115		
$^{172}W \rightarrow \alpha +^{168}$ Hf	3.4093	4.2776	4.7594	4.0082	4.2088	-	3.8391	
	3.4486	4.2899	4.7566	4.0265	4.2107	-		
$^{174}W \rightarrow \alpha +^{170}$ Hf	3.6332	4.0139	5.0409	3.8931	3.9625	3.6108	3.6021	
	3.6458	4.0131	5.0231	3.9034	3.9671	3.6265		
$^{176}W \rightarrow \alpha +^{172}$ Hf	3.4270	4.0882	4.9569	4.4733	3.7381	3.6371	3.3351	
	3.4492	4.0904	4.9373	4.4529	3.7501	3.6459		
$^{178}W \rightarrow \alpha +^{174}$ Hf	3.4460	4.0156	4.8358	4.0885	3.5356	3.6378	3.0128	
	3.4257	4.0211	4.8235	4.0597	3.5539	3.6392		
$^{180}W \rightarrow \alpha +^{176}$ Hf	2.4381	3.6434	4.4935	3.2756	3.2196	3.2942	2.5149	2.516
	2.4365	3.6597	4.4771	3.2793	3.2383	3.2923		

Table 4.2: Comparison of standard deviation of alpha decay half-lives of W isotopes calculated for different Skyrme forces

	SKP	SLY5	SIII	SKM*	UNEDF0	UNEDF1
HO	1.0088	0.8719	0.6646	2.0293	0.9245	0.9828
THO	1.0278	0.8850	0.6540	2.0208	0.9281	0.9850

where B(N,76) and B(N-2,74) are the binding energies of the parent ($_{76}$Os) and the daughter nuclei ($_{74}$W). The calculated Q_α along with ELDM values and experimental values[19] are tabulated in Table 4.3. In this case, we found that the SLY5 values understimates all the others. All other parametrizations agree with each other to some extent. The half-lives calculated with the help of UDL are plotted in fig. 4.1(b). It is observed that SLY5 values overestimates and SKM* values underestimates the experimental values compared to all the other parametrizations. The standard deviation of half-lives with respect to experimental values are tabulated in Table 4.4. Table shows that SKM* and SLY5

values are showing very large deviation compared to others. SIII, SKP and UNEDF values very less deviation in predicting the half-lives.

Table 4.3: Q-values of alpha decay in even-even Os isotopes calculated with Skyrme HFB equations solved using HO(top) and THO(bottom) basis. The results are compared with ELDM and available experimental values.

Alpha decay	Q value (MeV)							
	SIII	SKP	SkM*	SLy5	UNEDF0	UNEDF1	ELDM	exp
^{162}Os $\rightarrow \alpha +^{158}$ W	6.9833	6.8709	7.5634	7.1875	6.6728	6.9963	6.7751	
	6.9775	6.8698	7.5607	7.1958	6.6713	6.9846		
^{164}Os $\rightarrow \alpha +^{160}$ W	6.4773	6.4113	7.2721	4.6018	6.1670	6.3907	6.4851	
	6.4725	6.4170	7.2664	4.6351	6.1766	6.3916		
^{166}Os $\rightarrow \alpha +^{162}$ W	6.2453	6.2484	7.1761	4.70300	5.9377	6.2106	6.1381	
	6.2343	6.2551	7.1579	4.7275	5.9616	6.2193		
^{168}Os $\rightarrow \alpha +^{164}$ W	5.8623	6.0754	6.8782	4.5425	5.7419	6.0351	5.8161	
	5.8554	6.0848	6.8649	4.6031	5.7509	6.0496		
^{170}Os $\rightarrow \alpha +^{166}$ W	5.4973	5.8494	6.4858	4.2782	5.4851	5.8075	5.5371	
	5.4947	5.8672	6.4786	4.3199	5.4957	5.8174		
^{172}Os $\rightarrow \alpha +^{168}$ W	5.2105	5.6049	6.1028	3.8939	5.2010	5.5637	5.2241	5.255
	5.2091	5.6187	6.0940	3.9429	5.2136	5.5723		
^{174}Os $\rightarrow \alpha +^{170}$ W	4.2221	5.3433	5.6590	3.1662	4.9184	-	4.8701	4.895
	4.2630	5.3442	5.6543	3.2133	4.9214	4.6068		
^{176}Os $\rightarrow \alpha +^{172}$ W	5.8427	4.8844	5.1933	2.7425	4.6185	-	4.5741	
	5.7850	4.8835	5.1827	2.7830	4.6323	-		
^{178}Os $\rightarrow \alpha +^{174}$ W	5.2869	4.7159	4.6945	3.0558	4.3354	4.3806	4.2581	
	5.2390	4.7096	4.6918	3.0919	4.3495	4.3863		
^{180}Os $\rightarrow \alpha +^{176}$ W	4.4434	4.5974	4.2353	2.6480	4.0361	-	3.5881	
	4.3964	4.6012	4.2448	2.6741	4.0486	-		
^{182}Os $\rightarrow \alpha +^{178}$ W	3.1519	4.0936	4.2462	2.3504	3.5998	3.7918	3.3751	
	3.1584	4.1031	4.2273	2.3745	3.6049	3.7963		
^{184}Os $\rightarrow \alpha +^{180}$ W	3.037	3.4510	3.5056	2.2241	3.0279	3.0511	2.9571	
	3.0402	3.4551	3.5027	2.2411	3.0308	3.0636		
^{186}Os $\rightarrow \alpha +^{182}$ W	3.8500	2.7406	2.9843	1.7362	2.4024	2.4780	2.8204	
	3.8299	2.7351	2.9733	1.7509	2.3951	2.4795		

Table 4.4: Comparison of standard deviation of alpha decay half-lives of Os isotopes calculated for different Skyrme forces

	SKP	SLY5	SIII	SKM*	UNEDF0	UNEDF1
HO	1.2583	6.5259	0.7712	3.8022	0.3788	1.1634
THO	1.2808	6.2523	0.7511	3.7587	0.3768	1.2440

Platinum isotopes

The study has been extended to Pt isotopes. Here also, at first we compute the Q_α-values. Q_α-values are calculated from binding energies using the relation,

$$Q_\alpha(N, 78) = B(N-2, 76) + B(2, 2) - B(N, 78) \tag{4.5}$$

where, B(N,78) and B(N-2,76) are the binding energies of the parent ($_{78}$Pt) and the daughter nucleus ($_{76}$Os). The microscopic values are compared with the phenomenological ELDM values as well as the experimental values [20, 21, 22] and are given in Table 4.5. Predicted half-lives are depicted in fig. 4.1(c) from which we can see that SLY5 values underestimate the experimental values highly compared to other Skyrme forces. UNEDF's predicts half-lives close to experimetal ones. In Table 4.6, we have shown the standard deviation of the predicted values in the case of each Skyrme forces. UNEDF values shows less deviation in predicting alpha decay half-lives compared to others.

Table 4.5: Q-values of alpha decay in even-even Pt isotopes calculated with Skyrme HFB equations solved using HO(top) and THO(bottom) basis along with ELDM and available experimental values.

Alpha decay	Q value (MeV)							
	SIII	SKP	SkM*	SLy5	UNEDF0	UNEDF1	ELDM	exp
^{168}Pt $\rightarrow \alpha +^{164}$ Os	7.5095	6.9677	7.9371	9.3412	6.6857	7.0041	6.9851	
	7.5017	6.9957	7.9191	9.3417	6.7063	6.6421		
^{170}Pt $\rightarrow \alpha +^{166}$ Os	7.4979	6.7617	7.7329	9.0282	6.5111	6.8369	6.7071	
	7.4882	6.7752	7.7270	9.1571	6.5195	6.6326		
^{172}Pt $\rightarrow \alpha +^{168}$ Os	7.7265	6.5345	7.5196	9.0282	6.3062	6.6312	6.4651	
	7.7374	6.5527	7.5182	8.9980	6.3246	5.4551		
^{174}Pt $\rightarrow \alpha +^{170}$ Os	6.0724	6.2828	7.3505	8.8437	6.0872	6.6242	6.1831	6.03
	6.1191	6.2924	7.3454	8.8209	6.1091	5.4946		
^{176}Pt $\rightarrow \alpha +^{172}$ Os	5.0881	6.0046	6.0777	7.9131	5.8545	5.4481	5.8851	5.74
	5.1407	6.0159	6.1019	7.9087	5.8805	-		
^{178}Pt $\rightarrow \alpha +^{174}$ Os	5.7452	5.7459	5.7023	7.5347	5.6046	-	5.5731	5.44
	5.7283	5.7598	5.7227	7.5390	5.6363	4.9739		
^{180}Pt $\rightarrow \alpha +^{176}$ Os	4.6060	5.7321	5.4355	7.4556	5.3591	5.2652	5.2371	5.14
	4.6371	5.7503	5.4566	7.4421	5.3764	-		
^{182}Pt $\rightarrow \alpha +^{178}$ Os	4.3582	5.3930	5.2888	7.0965	5.0605	4.9783	4.9511	4.84
	4.3835	5.5048	5.3127	7.0684	5.0841	4.9739		
^{184}Pt $\rightarrow \alpha +^{180}$ Os	4.2003	4.8019	6.0484	6.6459	4.6734	-	4.5981	4.50
	4.2222	4.8319	6.0461	6.6364	4.6906	-		
^{186}Pt $\rightarrow \alpha +^{182}$ Os	4.4666	4.2332	6.2034	6.5487	4.1855	4.5068	4.3201	4.23
	4.4775	4.2450	6.1889	6.5475	4.1979	4.5043		
^{188}Pt $\rightarrow \alpha +^{184}$ Os	5.7406	3.6178	5.7841	5.9810	6.0632	4.2614	4.0027	3.93
	5.7241	3.6245	5.7536	5.9732	3.6108	2.8270		
^{190}Pt $\rightarrow \alpha +^{186}$ Os	5.3471	2.9960	5.0134	5.1340	2.9514	3.6010	3.2525	3.18
	5.3184	3.0516	4.9977	5.1316	2.9712	3.6045		
^{192}Pt $\rightarrow \alpha +^{188}$ Os	3.9417	2.4168	4.0453	4.0952	2.2386	2.8239	2.4224	2.6
	3.9107	2.4662	4.0434	4.0873	2.2538	2.8269		

Table 4.6: Comparison of standard deviation of alpha decay half-lives of Pt isotopes calculated for different Skyrme forces

	SKP	SLY5	SIII	SKM*	UNEDF0	UNEDF1
HO	1.6367	8.0337	1.9835	2.9102	0.7660	1.4106
THO	1.5632	8.0155	1.9333	2.9088	0.7127	1.5111

4.3.2 Cluster decay

The second stage of the study is devoted to the exotic decay mode which is called cluster radioactivity. We have attempted the feasibility of the emission of clusters like ^{8}Be, ^{12}C, ^{16}O, ^{20}Ne and ^{24}Mg. We are interested only in these alpha-like clusters (A=4n, Z=N). We have considered all the possible parent-cluster combinations for our study. The prediction of possible cluster emissions from W, Os and Pt isotopes are described in the subsequent subsections.

Tungsten isotopes

In W isotopes, we investigated the feasibility of the emission of different clusters like ^{8}Be, ^{12}C, ^{16}O and ^{20}Ne . The respective Q-values are estimated from binding energy using the following expressions,

^{8}Be:

$$Q(N, 74) = B(N-4, 70) + B(4, 4) - B(N, 74) \tag{4.6}$$

^{12}C:

$$Q(N, 74) = B(N-6, 68) + B(6, 6) - B(N, 74) \tag{4.7}$$

^{16}O:

$$Q(N, 74) = B(N-8, 66) + B(8, 8) - B(N, 74) \tag{4.8}$$

^{20}Ne:

$$Q(N, 74) = B(N-10, 64) + B(10, 10) - B(N, 74) \tag{4.9}$$

Table 4.7: Same as Table 4.1, but for various clusters in the case of W isotopes.

Cluster decay	Q value						
	SIII	SKP	SkM*	SLy5	UNEDF0	UNEDF1	ELDM
$^{158}W \rightarrow ^{8}Be + ^{150}Yb$	8.5165	8.6746	8.1450	9.0354	7.9249	7.5949	9.9983
	8.5196	8.5584	8.1576	9.0398	7.9364	8.6686	
$^{160}W \rightarrow ^{8}Be + ^{152}Yb$	14.1145	12.7116	14.1092	14.1472	12.1651	13.3722	11.9983
	14.0845	12.7087	14.0999	14.1462	12.1749	13.3233	
$^{162}W \rightarrow ^{8}Be + ^{154}Yb$	10.9519	11.0198	11.9117	10.8985	10.3995	10.8471	10.9903
	10.9602	11.0270	11.9146	10.9209	10.3887	10.8340	
$^{164}W \rightarrow ^{8}Be + ^{156}Yb$	9.8920	9.9878	10.5721	9.7219	9.3746	9.4569	10.0883
	9.9013	10.0048	10.5653	9.7282	9.3851	9.4439	
$^{166}W \rightarrow ^{8}Be + ^{158}Yb$	9.2564	9.4512	9.8530	9.2583	8.9077	8.6402	9.1803
	9.2178	9.4752	9.8442	9.2523	8.9298	8.6371	
$^{168}W \rightarrow ^{8}Be + ^{160}Yb$	8.3727	8.8660	9.2632	8.5529	8.4527	7.9136	8.3303
	8.3601	8.8807	9.2667	8.5514	8.4652	7.9185	
$^{170}W \rightarrow ^{8}Be + ^{162}Yb$	7.4664	8.3119	9.1163	7.9436	7.9983	7.3057	7.5953
	7.4601	8.3565	9.1158	7.9457	8.0080	7.3135	
$^{158}W \rightarrow ^{12}C + ^{146}Er$	18.0288	18.1709	18.3956	17.7180	17.6459	17.8516	20.622
	18.0469	18.0619	18.4012	17.7474	17.6648	17.8583	
$^{160}W \rightarrow ^{12}C + ^{148}Er$	21.3810	21.4193	21.3479	21.8918	20.3908	21.4069	22.099
	21.3880	21.4263	21.3589	21.9185	20.3914	21.3912	
$^{162}W \rightarrow ^{12}C + ^{150}Er$	26.1713	24.4897	26.5842	25.8829	23.5826	25.0532	23.831
	26.1485	24.4849	26.5816	25.8869	23.5932	25.0148	
$^{164}W \rightarrow ^{12}C + ^{152}Er$	22.3285	22.3276	23.6660	22.1521	21.2683	21.9540	22.266
	22.3298	22.3407	23.6585	22.1721	21.2761	21.9438	
$^{166}W \rightarrow ^{12}C + ^{154}Er$	20.6668	20.7735	21.6400	20.4620	19.8958	19.8242	20.717
	20.6676	20.7931	21.6318	20.4656	19.9143	19.8154	
$^{168}W \rightarrow ^{12}C + ^{156}Er$	19.4806	19.8267	20.6571	19.6931	19.1118	18.5680	19.317
	19.4665	19.8336	20.6541	19.6781	19.1288	18.5744	
$^{170}W \rightarrow ^{12}C + ^{158}Er$	18.1849	19.0182	19.9845	18.7305	18.2899	17.6292	18.014
	18.1726	19.0666	19.9816	18.7168	18.3092	17.649	
$^{158}W \rightarrow ^{16}O + ^{142}Dy$	29.5101	28.8028	30.3917	27.9216	28.4526	28.4691	31.157
	29.5086	28.6975	30.3727	27.9127	28.4691	28.5935	
$^{160}W \rightarrow ^{16}O + ^{144}Dy$	30.1986	30.3007	31.0786	30.0405	29.5483	29.5663	31.927
	30.2093	30.3126	31.0895	30.0739	29.5663	29.8251	
$^{162}W \rightarrow ^{16}O + ^{146}Dy$	32.7798	32.5919	33.1311	32.8781	31.2475	31.2867	33.292
	32.7960	32.5986	33.1432	32.8958	31.2867	32.4321	
$^{164}W \rightarrow ^{16}O + ^{148}Dy$	37.2166	35.0472	37.9786	36.5910	33.7072	33.7293	34.362
	37.2017	35.0540	37.9577	36.5940	33.7293	35.4355	
$^{166}W \rightarrow ^{16}O + ^{150}Dy$	32.3325	32.3992	34.0840	32.2562	30.9283	30.9418	32.158
	32.3346	32.4169	34.0689	32.2685	30.9418	31.8396	
$^{168}W \rightarrow ^{16}O + ^{152}Dy$	29.7736	30.2490	31.4556	29.9717	29.1075	29.1339	29.962
	29.7726	30.2534	31.4505	29.9762	29.1339	28.8249	
$^{170}W \rightarrow ^{16}O + ^{154}Dy$	27.7213	28.7941	30.2402	28.8077	27.9051	27.1763	27.841
	27.7212	28.8416	30.2304	28.7877	27.9333	-	
$^{158}W \rightarrow ^{20}Ne + ^{138}Gd$	37.4084	37.8199	40.2825	37.1795	37.5530	37.0624	35.7945
	37.4142	37.7133	40.2517	37.1381	37.5530	37.0619	
$^{160}W \rightarrow ^{20}Ne + ^{140}Gd$	38.5361	37.8979	40.0555	37.2569	37.2671	37.2925	34.6913
	38.5313	37.9152	40.0393	37.2690	37.2671	37.2945	
$^{162}W \rightarrow ^{20}Ne + ^{142}Gd$	38.6017	38.6360	39.9717	38.4065	37.5541	37.8696	33.3599
	38.6242	38.6508	39.9862	38.4521	37.5541	37.8534	
$^{164}W \rightarrow ^{20}Ne + ^{144}Gd$	40.9146	40.2224	41.6357	40.6858	38.5794	39.8443	32.0253
	40.9272	40.2396	41.6361	40.7305	38.5794	39.8258	
$^{166}W \rightarrow ^{20}Ne + ^{146}Gd$	44.7203	42.0287	45.6637	43.7478	40.3151	-	30.5302
	44.7027	42.0382	45.6402	43.7349	40.3151	-	
$^{168}W \rightarrow ^{20}Ne + ^{148}Gd$	38.6716	38.8529	40.8899	38.7856	37.0623	38.0478	36.3782
	38.6858	38.8553	40.8805	38.7894	37.0623	38.0478	

where, B(N-4,74), B(N-6,68), B(N-8,66), B(N-10,64) are the binding energies of the corresponding daughter nuclei ($_{70}$Yb, $_{68}$Er, $_{66}$Dy and $_{64}$Gd) and B(4,4), B(6,6), B(8,8) and B(10,10) are the binding energies of the clusters ^{8}Be, ^{12}C, ^{16}O and ^{20}Ne respectively. Q-values calculated with respect to different Skyrme forces are given in Table 4.7. We have compared the obtained results with the ELDM values. We have estimated the half-lives of all the decay modes from the binding energies of W isotopes, which are obtained using different Skyrme forces. The calculated half-lives (using UDL) are depicted in fig. 4.2. Each Skyrme force predicts the binding energy with a slight variation in its values and it is reflected in the predicted half-lives. All the half-lives except those obtained by SKM* overestimate the ELDM values. From fig. 4.2, it is observed that Ne radioactivity half-lives do not fall within the experimentally measurable range.

The decay rate for a particular decay mode will be maximum, if the corresponding half-life is minimum. From fig. 4.2, it is found that in the case of ^{8}Be decay, the half-life is minimum for ^{160}W. This shows that the decay rate of ^{8}Be is maximum for ^{160}W isotope. Also, this particular decay leads to the formation of the daughter nucleus ^{152}Yb, which is having magic neutron number (N=82). Similarly for ^{12}C, ^{16}O and ^{20}Ne decay modes, half-lives are minimum for those decays which leads to the formation of daughter nuclei (i.e, ^{150}Er, ^{148}Dy and ^{146}Gd) having magic neutron number (N=82). These results show that the rate of decay will be maximum for those decay modes leading to magic daughter nuclei (N=82). These observations confirm the role of magicity in cluster decay.

From fig. 4.2, it is observed that all the calculations show similar trend in predicting the values, but with minor discrepancy in their magnitudes.

Osmium isotopes

After W isotopes, we have analysed the isotopes of osmium to find if they are unstable against various cluster decay modes. Like W isotopes, here also we looked for the clusters like ^{8}Be, ^{12}C, ^{16}O, ^{20}Ne and ^{24}Mg. To analyse whether a decay mode is energetically favourable, we calculated the Q-values. Q-values

are obtained using the following expressions,
^{8}Be:

$$Q(N,76) = B(N-4,72) + B(4,4) - B(N,76) \tag{4.10}$$

^{12}C:

$$Q(N,76) = B(N-6,70) + B(6,6) - B(N,76) \tag{4.11}$$

^{16}O:

$$Q(N,76) = B(N-8,68) + B(8,8) - B(N,76) \tag{4.12}$$

^{20}Ne:

$$Q(N,76) = B(N-10,66) + B(10,10) - B(N,76) \tag{4.13}$$

^{24}Mg:

$$Q(N,76) = B(N-12,64) + B(12,12) - B(N,76) \tag{4.14}$$

where B(N-4,72), B(N-6,70), B(N-8,68), B(N-10,66), B(N-12,64) are the binding energies of corresponding daughter nuclei ($_{70}$Yb, $_{68}$Er, $_{66}$Dy and $_{64}$Gd) and B(6,6), B(8,8), B(10,10) and B(12,12) are the binding energies of clusters ^{12}C, ^{16}O, ^{20}Ne and ^{24}Mg respectively. The computed Q-values are tabulated in Table 4.8 along with ELDM and experimental values. The half-lives calculated with the help of UDL are plotted in fig. 4.3. Compared to W isotopes, here we found the emission of ^{20}Ne isotopes. Some Skyrme forces predicts the emission of ^{24}Mg cluster also. The shell effects of cluster decay is observed here also. The decay rate is maximum for ^{162}Os, ^{164}Os, ^{166}Os, ^{168}Os and ^{170}Os which correspond to ^{8}Be, ^{12}C, ^{16}O, ^{20}Ne and ^{24}Mg decay modes respectively. In all these case the daughter nuclei have magic neutron number (N=82).

Table 4.8: Same as Table 4.1, but for various clusters in the case of Os isotopes.

Cluster decay	Q value (MeV)						
	SIII	SKP	SkM*	SLy5	UNEDF0	UNEDF1	ELDM
^{162}Os $\rightarrow^{8}$ Be $+^{154}$ Hf	15.1751	13.8419	15.3766	15.4657	134099	14.5939	13.2883
	15.1298	13.8290	15.3706	15.4642	13.4118	14.5569	
^{164}Os $\rightarrow^{8}$ Be $+^{156}$ Hf	12.5518	12.4832	13.8597	10.7878	12.0015	12.4975	12.4583
	12.5474	12.4836	13.8533	10.8349	12.0077	12.4906	
^{166}Os $\rightarrow^{8}$ Be $+^{158}$ Hf	11.5840	11.7265	12.9833	10.0639	11.1292	11.5141	11.7243
	11.5793	11.7193	12.9663	10.0992	11.1502	11.5176	
^{168}Os $\rightarrow^{8}$ Be $+^{160}$ Hf	10.9858	11.3129	12.2982	9.7323	10.6919	10.9637	11.0023
	10.9769	11.3294	12.2737	9.7914	10.7171	10.9706	
^{170}Os $\rightarrow^{8}$ Be $+^{162}$ Hf	10.2485	10.8056	11.5137	9.0649	10.2641	10.3273	10.3013
	10.2440	10.8319	11.5057	9.1085	10.2904	10.3409	
^{172}Os $\rightarrow^{8}$ Be $+^{164}$ Hf	9.6474	10.2513	10.8919	8.3127	9.7924	9.7134	9.6323
	9.6391	10.2678	10.8865	8.3709	9.8089	9.7398	
^{174}Os $\rightarrow^{8}$ Be $+^{166}$ Hf	8.4401	9.7360	10.4108	7.3486	9.2748	-	8.9223
	8.4799	9.7415	10.4031	7.4036	9.2880	8.5257	
^{162}Os $\rightarrow^{12}$ C $+^{150}$ Yb	22.8660	22.8694	23.0746	23.5892	21.9640	23.0310	24.14
	22.8634	22.8685	23.0845	23.6019	21.9740	23.0196	
^{164}Os $\rightarrow^{12}$ C $+^{152}$ Yb	27.9581	26.4511	28.7476	26.1153	25.6984	27.1291	25.85
	27.9233	26.4414	28.7326	26.1476	25.7179	27.0812	
^{166}Os $\rightarrow^{12}$ C $+^{154}$ Yb	24.5635	24.5907	26.4540	22.9678	23.7035	24.4241	24.495
	24.5608	24.5955	26.4387	23.0147	23.7166	24.4196	
^{168}Os $\rightarrow^{12}$ C $+^{156}$ Yb	23.1205	23.3921	24.8165	21.6307	22.4828	22.8584	23.271
	23.1230	23.4015	24.7936	21.6975	22.5024	22.8597	
^{170}Os $\rightarrow^{12}$ C $+^{158}$ Yb	22.1199	22.6330	23.7051	20.9027	21.7591	21.8139	22.084
	22.0788	22.6584	23.6892	20.9385	21.7918	21.8208	
^{172}Os $\rightarrow^{12}$ C $+^{160}$ Yb	20.9495	21.7979	22.7322	19.8131	21.0199	20.8435	20.921
	20.9354	21.8278	22.7269	19.8606	21.0451	20.8571	
^{174}Os $\rightarrow^{12}$ C $+^{162}$ Yb	19.0548	20.0755	22.1415	18.4761	20.2830	-	19.832
	19.0893	21.0054	22.1365	18.5253	20.2957	19.2866	
^{162}Os $\rightarrow^{16}$ O $+^{146}$ Er	32.1736	32.1585	33.1206	32.0671	31.4803	32.0095	34.559
	32.1860	32.1650	33.1234	32.1048	31.4977	32.0042	
^{164}Os $\rightarrow^{16}$ O $+^{148}$ Er	35.0199	34.9488	35.7816	33.6552	33.7195	34.9592	35.746
	34.9542	34.9529	35.7870	33.7152	33.7297	34.9445	
^{166}Os $\rightarrow^{16}$ O $+^{150}$ Er	39.5782	37.8611	40.9218	37.7474	36.6819	38.4255	37.131
	39.5127	37.5863	40.9011	37.7760	36.7165	38.3957	
^{168}Os $\rightarrow^{16}$ O $+^{152}$ Er	35.3523	35.5209	37.7057	33.8561	34.1718	35.1507	35.244
	35.2903	35.5311	37.6821	33.9368	34.1886	35.1550	
^{170}Os $\rightarrow^{16}$ O $+^{154}$ Er	33.3257	33.7447	35.2875	31.9017	32.5425	32.7933	33.416
	33.2671	33.7665	35.2720	31.9472	32.5716	32.7945	
^{172}Os $\rightarrow^{16}$ O $+^{156}$ Er	31.8527	32.5579	33.9215	30.7486	31.4744	31.2933	31.703
	31.7962	32.5788	33.9096	30.7826	31.5041	31.3083	
^{162}Os $\rightarrow^{20}$ Ne $+^{142}$ Dy	41.2229	40.3678	42.6846	39.8387	39.8549	40.3161	42.6619
	41.2156	40.3747	42.6629	39.8381	39.8699	40.3076	
^{164}Os $\rightarrow^{20}$ Ne $+^{144}$ Dy	41.4054	41.3956	43.0802	39.3719	40.4448	40.9534	43.1419
	41.4113	41.4031	43.0855	39.4386	40.4725	40.9463	
^{166}Os $\rightarrow^{20}$ Ne $+^{146}$ Dy	43.7547	43.5262	45.0367	42.3106	41.9148	43.3932	44.1599
	43.7598	43.5328	45.0306	42.3529	41.9779	43.3809	
^{168}Os $\rightarrow^{20}$ Ne $+^{148}$ Dy	47.7547	45.8191	49.5863	45.8630	44.1786	46.2382	44.9079
	47.7867	45.8196	49.5492	45.9266	44.2098	46.2147	
^{170}Os $\rightarrow^{20}$ Ne $+^{150}$ Dy	42.5593	42.9361	45.2994	41.2638	41.1428	42.3826	42.4249
	42.5589	42.9568	45.2771	41.3180	41.1670	42.3866	
^{162}Os $\rightarrow^{24}$ Mg $+^{138}$ Gd	53.7079	53.9871	57.1621	53.6832	53.5421	53.3749	55.0936
	53.7079	53.9878	57.1287	53.6502	53.5780	53.3628	
^{164}Os $\rightarrow^{24}$ Mg $+^{140}$ Gd	54.3297	53.5901	56.6438	51.1749	52.7504	52.9994	55.2456
	54.3201	53.5993	56.6220	51.2203	53.1495	53.0024	
^{166}Os $\rightarrow^{24}$ Mg $+^{142}$ Gd	54.1632	54.1558	56.4640	52.4257	52.8082	53.3965	55.4566
	54.1748	54.1683	56.4603	52.4958	52.8421	53.3889	
^{168}Os $\rightarrow^{24}$ Mg $+^{144}$ Gd	56.0931	55.5728	57.8301	54.5445	53.6375	55.1957	55.7066
	56.0988	55.5861	57.8143	54.6498	53.6599	55.1917	
^{170}Os $\rightarrow^{24}$ Mg $+^{146}$ Gd	59.5338	57.1625	61.4658	57.3422	55.1163	-	56.0936
	59.5137	57.1726	61.4351	57.3711	55.1570	-	

Platinum isotopes

We have extended our calculations to predict the clusters which are likely to be emitted from Pt isotopes. Here also the half-lives are computed using the equation (4.2). Also the Q-values for various clusters are given by,
^{8}Be:

$$Q(N,78) = B(N-4,74) + B(4,4) - B(N,78) \tag{4.15}$$

^{12}C:

$$Q(N,78) = B(N-6,72) + B(6,6) - B(N,78) \tag{4.16}$$

^{16}O:

$$Q(N,78) = B(N-8,70) + B(8,8) - B(N,78) \tag{4.17}$$

^{20}Ne:

$$Q(N,78) = B(N-10,68) + B(10,10) - B(N,78) \tag{4.18}$$

^{24}Mg:

$$Q(N,78) = B(N-12,66) + B(12,12) - B(N,78) \tag{4.19}$$

where, B(N-4,74), B(N-6,72), B(N-8,70), B(N-10,68), B(N-12,66) are the binding energies of the corresponding daughter nuclei (W, Hf, Yb, Er and Dy) and B(4,4), B(6,6), B(8,8), B(10,10) and B(12,12) are the binding energies of the emitted clusters ^{8}Be, ^{12}C, ^{16}O, ^{20}Ne and ^{24}Mg respectively. As in the case of W and Os, we have shown the Q-values of the emitted clusters in Table 4.9. Due to the lack of availability of experimental values, we have compared them with ELDM values. We observed a good agreement among the values with a small discrepency in some cases.

Here also, we have observed that the half-lives are minimum for those decays which have the daughter nuclei with magic neutron number (N=82). This is visbile only for ^{16}O, ^{20}Ne and ^{24}Mg decays and their magic daughters are ^{168}Yb, ^{150}Er and ^{148}Dy respectively with neutron number N=82. For ^{8}Be and ^{12}C, the magic daughter nuclei lies outside the selected region. So it is not shown here.

4.3.3 Geiger-Nuttal plot

As mentioned in chapter 1, Geiger-Nuttal law can be expressed in different forms. Here, we have computed this relation in terms of logarithmic half-lives and disintegration energy (Q-value) of the decays. Geiger-Nuttal law gives a linear relationship between these two quantities. It is expressed as

$$log_{10}T_{1/2} = \frac{X}{\sqrt{Q}} + Y \tag{4.20}$$

where X and Y are the slopes and intercepts of the straight lines respectively.

Fig. 4.5 shows the GN plots for the different clusters emitted from W isotopes corresponding to various Skyrme parameters. The linear nature of the plot is reproduced in the case of all the cluster modes. Each emitted cluster has a specific slope and intercept. They are given in Table 4.10. From the table, we can see that as the emitted cluster becomes massive, the slope as well as the intercept increases.

Similar figures has been plotted for Os and Pt isotopes and are shown in fig. 4.6 and fig. 4.7 respectively. The linear nature of the plot is reproduced in the case of all the cluster modes as expected. But each cluster emission is characterised by specific slope and intercept. The values obtained for Os and Pt are given in Tables 4.11 and Table 4.12 respectively. From these tables also, we have noticed that as the emitted cluster becomes massive, the slope as well as the intercept increases, as in the case of W isotopes.

Table 4.9: Same as Table 4.1, but for various clusters in the case of Pt isotopes.

Cluster decay	Q value (MeV)						
	SIII	SKP	SkM*	SLy5	UNEDF0	UNEDF1	ELDM
^{168}Pt $\rightarrow^{8}$ Be $+^{158}$ W	13.8943	13.2826	15.1167	13.8505	12.7603	13.3022	13.3783
	13.8817	13.2698	15.0931	13.8843	12.7904	13.3093	
^{170}Pt $\rightarrow^{8}$ Be $+^{160}$ W	13.6507	12.9141	14.8164	13.7675	12.3563	12.9551	12.7533
	13.6301	12.9405	13.7924	13.7921	12.3886	12.9713	
^{172}Pt $\rightarrow^{8}$ Be $+^{162}$ W	13.4963	12.5140	14.3053	13.4782	11.9556	12.5739	12.1893
	13.5003	12.5487	14.2876	13.5086	11.9830	12.5992	
^{174}Pt $\rightarrow^{8}$ Be $+^{164}$ W	11.4772	12.0364	13.7439	13.0293	11.4798	12.3392	11.6283
	11.5213	12.0721	13.7315	13.0483	11.5123	12.3575	
^{176}Pt $\rightarrow^{8}$ Be $+^{166}$ W	10.2062	11.5136	12.0880	11.7145	10.9630	10.9194	11.0173
	10.2574	11.5656	12.1034	11.7592	11.0016	10.9349	
^{178}Pt $\rightarrow^{8}$ Be $+^{168}$ W	9.8748	10.9932	11.2687	10.6084	10.4305	9.9887	10.3513
	9.8988	11.0128	11.2845	10.6598	10.4651	10.0089	
^{180}Pt $\rightarrow^{8}$ Be $+^{170}$ W	10.3562	10.5249	10.5363	10.1057	9.8851	-	
	10.3296	10.5282	10.5468	10.1325	9.9162	-	
^{168}Pt $\rightarrow^{12}$ C $+^{156}$ Hf	27.4275	26.8167	29.1631	27.4953	26.0535	26.8678	26.8100
	27.4153	26.7925	29.1387	27.5429	26.0803	26.8670	
^{170}Pt $\rightarrow^{12}$ C $+^{158}$ Hf	26.4482	25.8387	28.0825	26.5873	25.0066	25.7173	25.7980
	26.4338	25.8663	28.0595	26.6225	25.0360	25.7283	
^{172}Pt $\rightarrow^{12}$ C $+^{160}$ Hf	26.0786	25.2146	27.1841	26.1268	24.3644	24.9612	24.8340
	26.0806	25.2601	27.1582	26.1557	24.4079	24.9790	
^{174}Pt $\rightarrow^{12}$ C $+^{162}$ Hf	23.6871	24.4555	26.2305	25.2748	23.7177	24.3177	23.8510
	23.7293	24.5007	26.2174	25.2957	23.7657	24.3398	
^{176}Pt $\rightarrow^{12}$ C $+^{164}$ Hf	22.1017	23.6228	24.3359	23.5920	23.0132	22.5277	22.8840
	22.1461	23.6573	24.3547	23.6459	23.0557	22.5612	
^{178}Pt $\rightarrow^{12}$ C $+^{166}$ Hf	21.5515	22.8486	23.4794	22.2496	22.2457	21.3546	21.8620
	21.5744	22.8731	23.4920	22.3088	22.2905	21.3867	
^{180}Pt $\rightarrow^{12}$ C $+^{168}$ Hf	21.1318	22.1688	22.6619	21.4802	21.4602	20.4886	
	21.1445	22.1844	22.6697	21.5253	21.4932	20.5088	
^{182}Pt $\rightarrow^{12}$ C $+^{170}$ Hf	20.5519	21.3884	22.2981	21.3192	20.6322	20.2435	
	20.5421	21.4945	22.3013	21.3374	20.6745	20.2568	
^{168}Pt $\rightarrow^{16}$ O $+^{152}$ Yb	42.6291	41.1181	43.8462	42.6181	39.5458	41.2947	39.9970
	42.5866	40.5989	43.8134	42.6509	39.5857	41.2530	
^{170}Pt $\rightarrow^{16}$ O $+^{154}$ Yb	39.2229	39.1071	41.3485	39.2865	37.3761	38.4226	38.3640
	39.2106	38.5879	41.3273	39.3334	37.3977	38.4257	
^{172}Pt $\rightarrow^{16}$ O $+^{156}$ Yb	38.0085	37.5935	39.4978	37.8204	35.9506	36.6511	36.8980
	38.0221	37.1739	39.4734	37.8571	35.9885	36.6634	
^{174}Pt $\rightarrow^{16}$ O $+^{158}$ Yb	35.3539	36.4367	38.2173	36.9080	35.0079	35.5997	35.4290
	35.3595	36.1677	38.1962	36.9210	35.0625	35.6150	
^{176}Pt $\rightarrow^{16}$ O $+^{160}$ Yb	33.1992	35.1748	35.9715	34.8878	34.0361	33.4533	33.9680
	33.2378	35.0667	35.9904	34.9310	34.0872	33.4738	
^{178}Pt $\rightarrow^{16}$ O $+^{162}$ Yb	31.9616	33.9330	35.0054	33.1724	33.0492	31.9147	32.567
	31.9792	33.9896	35.0207	33.2259	33.0935	31.9428	
^{168}Pt $\rightarrow^{16}$ Ne $+^{148}$ Er	47.2589	47.1890	48.4482	47.7259	45.1348	46.6928	47.4609
	47.2533	46.6797	48.4356	47.7864	45.1655	46.6841	
^{170}Pt $\rightarrow^{16}$ Ne $+^{150}$ Er	51.8056	49.9402	53.3843	51.6341	47.9225	49.9919	48.5679
	51.7622	49.4091	53.3576	51.6626	47.9655	49.9697	
^{172}Pt $\rightarrow^{16}$ Ne $+^{152}$ Er	47.8083	47.2965	49.9549	47.6138	45.2075	46.5115	46.4389
	47.8137	46.8730	49.9298	47.6643	45.2427	46.5266	
^{174}Pt $\rightarrow^{16}$ Ne $+^{154}$ Er	44.1276	45.1223	47.3675	45.4749	43.3592	44.1470	44.3289
	44.1726	44.8489	47.3469	45.4976	43.4102	44.1566	
^{176}Pt $\rightarrow^{16}$ Ne $+^{156}$ Er	41.6704	43.4988	44.7287	43.3912	42.0585	41.4709	42.3179
	41.7075	43.3828	44.7411	43.4209	42.1141	41.4929	
^{178}Pt $\rightarrow^{16}$ Ne $+^{158}$ Er	40.0433	42.0026	43.2369	41.3226	40.7041	39.6015	40.3489
	40.0550	42.0630	43.2497	41.3603	40.7580	39.6422	
^{168}Pt $\rightarrow^{24}$ Mg $+^{144}$ Dy	58.2312	58.2251	60.3335	58.0293	56.4468	57.2736	59.4436
	58.2292	57.7207	60.3208	58.0965	56.4949	57.2727	
^{170}Pt $\rightarrow^{24}$ Mg $+^{146}$ Dy	60.5688	60.1970	62.0858	60.7839	57.7422	59.5464	60.1836
	60.5643	59.6774	62.0738	60.8262	57.8136	59.5416	
^{172}Pt $\rightarrow^{24}$ Mg $+^{148}$ Dy	64.8511	62.1707	66.4221	64.2074	59.8010	62.1856	60.6896
	64.8403	61.7410	66.3836	64.2409	59.8506	62.1729	
^{174}Pt $\rightarrow^{24}$ Mg $+^{150}$ Dy	57.9479	58.9026	61.9662	59.4237	56.5463	58.3230	57.9246
	57.9942	58.6273	61.9387	59.4552	56.5923	58.3354	
^{176}Pt $\rightarrow^{24}$ Mg $+^{152}$ Dy	54.1181	56.0758	57.6819	55.8244	54.2087	53.8786	55.1176
	54.1682	55.9572	57.6922	55.8736	54.2738	53.8980	
^{178}Pt $\rightarrow^{24}$ Mg $+^{154}$ Dy	51.7344	53.9332	55.6472	53.5544	52.4739	51.3033	52.3306
	51.7582	53.9926	55.6532	53.5857	52.5367	-	

Table 4.10: Slopes and intercepts of even-even W isotopes calculated for different Skyrme forces using HO(top) and THO(bottom) basis

Skyrme	Alpha		Be		C		O		Ne	
force	Slope	Intercept	Slope	Intercept	Slope	Intercept	Slope	Intercept	Slope	Intercept
SKP	119.866	-50.212	330.189	-76.060	580.124	-100.322	879.117	-127.861	1206.770	-155.868
	119.803	-50.182	330.406	-76.060	580.572	-100.422	879.117	-127.861	1206.770	-155.870
SLY5	120.559	-50.524	330.200	-76.062	581.055	-100.525	875.289	-127.181	1190.031	-153.194
	120.546	-50.187	330.198	-76.061	580.972	-100.507	875.271	-127.177	1193.551	-153.683
SIII	121.191	-50.779	330.727	-76.223	580.500	-100.390	872.011	-126.587	1184.827	-152.336
	121.182	-50.776	330.715	-76.219	580.449	-100.378	860.188	-124.536	1185.006	-152.364
SKM*	119.353	-50.063	331.083	-76.390	583.610	-101.112	866.964	-125.747	1193.181	-153.544
	119.605	-50.179	331.793	-76.589	583.614	-101.114	865.863	-125.553	1195.265	-153.856
UNEDF0	120.241	-50.352	329.901	-75.953	584.205	-101.176	876.459	-127.421	1135.247	-144.43
	120.218	-50.343	330.861	-76.254	584.219	-101.179	876.473	-127.422	1132.531	-143.99
UNEDF1	120.561	-50.492	330.377	-76.093	582.262	-100.744	871.549	-126.519	1131.420	-143.772
	120.545	-50.485	330.357	-76.087	582.248	-100.741	871.161	-126.531	1131.304	-143.753

Table 4.11: Slopes and intercepts of even-even Os isotopes calculated for different Skyrme forces using HO(top) and THO(bottom) basis

Skyrme	Alpha		Be		C		O		Ne		Mg	
force	Slope	Intercept	Slope	Intercept	Slope	Intercept	Slope	Intercept	Slope	Intercept	Slope	Intercept
SKP	123.515	-50.805	345.873	-76.717	586.039	-99.314	888.680	-126.651	1143.032	-146.098	1625.492	-184.654
	123.525	-50.811	345.716	76.666	585.839	-99.275	889.178	-126.736	1143.656	-146.196	1626.695	-184.815
SLY5	125.010	-51.336	348.403	-77.375	58.992	-100.016	879.703	-125.079	1141.924	-145.879	1580.745	-178.653
	125.003	-51.335	348.377	-77.369	58.984	-100.002	879.673	-125.076	1142.082	-145.906	1582.022	-178.826
SIII	124.357	-51.162	348.461	-77.486	592.217	-100.568	873.165	-124.086	1131.496	-144.327	1587.232	-179.462
	124.329	-51.149	348.454	-77.483	592.128	-100.549	885.367	-126.084	1139.341	-145.189	1510.485	-169.172
SKM*	123.925	-51.013	345.021	-76.552	583.995	-99.032	862.676	-122.411	1130.279	-144.270	1595.930	-180.494
	123.924	-51.012	345.053	-76.560	591.638	-100.544	872.663	-124.066	1145.609	-146.546	1596.316	-180.546
UNEDF0	125.118	-51.491	347.287	-77.109	58.469	-99.011	861.549	-122.033	1124.486	-143.217	1494.288	-166.907
	125.033	-51.439	347.055	-77.029	58.503	-99.036	872.59	-123.885	1131.362	-144.225	1476.971	-164.459
UNEDF1	124.656	-51.278	347.459	-77.156	59.081	-100.308	870.824	-123.663	1124.486	-143.217	1472.870	-177.524
	124.120	-51.039	347.375	-77.131	59.038	-100.174	874.490	-124.234	1131.136	-144.225	1485.801	165.367

4.4 Conclusion

This chapter is devoted to the study of the feasibility of alpha and cluster decays in W, Os and Pt isotopes. The study has been carried out within the framework of Skyrme HFB theory. Calculations have been done with the help of harmonic and transformed harmonic oscillator basis. Six different Skyrme parametrizations, such as SIII, SKP, SKM*, SLY5, UNEDF0 and UNEDF1 have been used for the study. It is observed that, among the selected isotopes, those falling between the proton drip-line and beta-stability line are unstable against various decay modes. The use of different oscillator basis shows only a very small difference - of the order of a few keV in Q-values and correspondingly a very small difference in their half-lives. The calculated standard deviations show that UNEDF parametrizations lead to less deviation in predicting the half-lives of alpha decay compared to other Skyrme parametrizations. We have observed the

Table 4.12: Slopes and intercepts of even-even Pt isotopes calculated for different Skyrme forces using HO(top) and THO(bottom) basis

Skyrme	Alpha		Be		C		O		Ne		Mg	
force	Slope	Intercept	Slope	Intercept	Slope	Intercept	Slope	Intercept	Slope	Intercept	Slope	Intercept
SKP	128.198	-51.815	341.170	-75.589	594.985	-99.103	874.118	-121.739	1182.924	-145.292	1502.437	-168.592
	128.164	-51.802	341.286	-75.626	594.561	-99.021	873.755	-121.684	1182.939	-145.435	1503.212	-168.696
SLY5	126.993	-51.476	344.951	-76.706	601.635	-100.475	885.710	-123.688	1195.328	-147.306	1521.823	-171.163
	126.995	-51.476	344.878	-76.688	601.508	-100.453	885.611	-123.674	1195.273	-147.300	1521.969	-171.183
SIII	127.470	-51.536	346.225	-77.027	604.065	-100.913	892.051	-124.677	1198.884	147.789	1511.682	-169.807
	127.433	-51.521	346.144	-77.004	603.950	-100.890	891.921	-124.655	1198.797	-147.776	1511.719	-169.813
SKM*	126.690	-51.272	345.174	-76.831	599.912	-100.229	883.933	-123.513	1193.222	-147.108	1509.444	-169.646
	126.664	-51.261	344.881	-76.741	599.801	-100.207	883.725	-123.478	1193.109	-147.091	1509.439	-169.645
UNEDF0	128.445	-51.928	342.563	-75.920	596.366	-99.301	874.512	-121.694	1189.337	-146.265	1485.281	166.209
	128.257	-51.832	342.492	-75.903	596.237	-99.279	874.978	-121.775	1189.256	-146.256	1485.286	-166.214
UNEDF1	127.658	-51.580	345.037	-76.673	603.206	-100.709	888.587	-124.071	1199.454	-147.825	1508.678	-169.371
	127.655	-51.578	344.998	-76.663	603.102	-100.689	888.391	-124.039	1199.341	-147.808	1534.976	-172.800

emission of clusters like ^{8}Be, ^{12}C, ^{16}O, ^{20}Ne and ^{24}Mg from the selected isotopes. The emission of clusters along an isotopic chain depends on neutron number. i.e, as the neutron number increases, the rate of emission of cluster decreases. Also as the atomic number of the parent increases, we can expect the emission of the massive cluster. In the case of W isotopes, we predicted clusters like ^{8}Be, ^{12}C and ^{16}O. But for Os and Pt isotopes, the emission of ^{20}Ne and ^{24}Mg are also predicted. The linear nature of the Geiger-Nuttel plot is also successfully reproduced in the case of all the selected Skyrme forces.

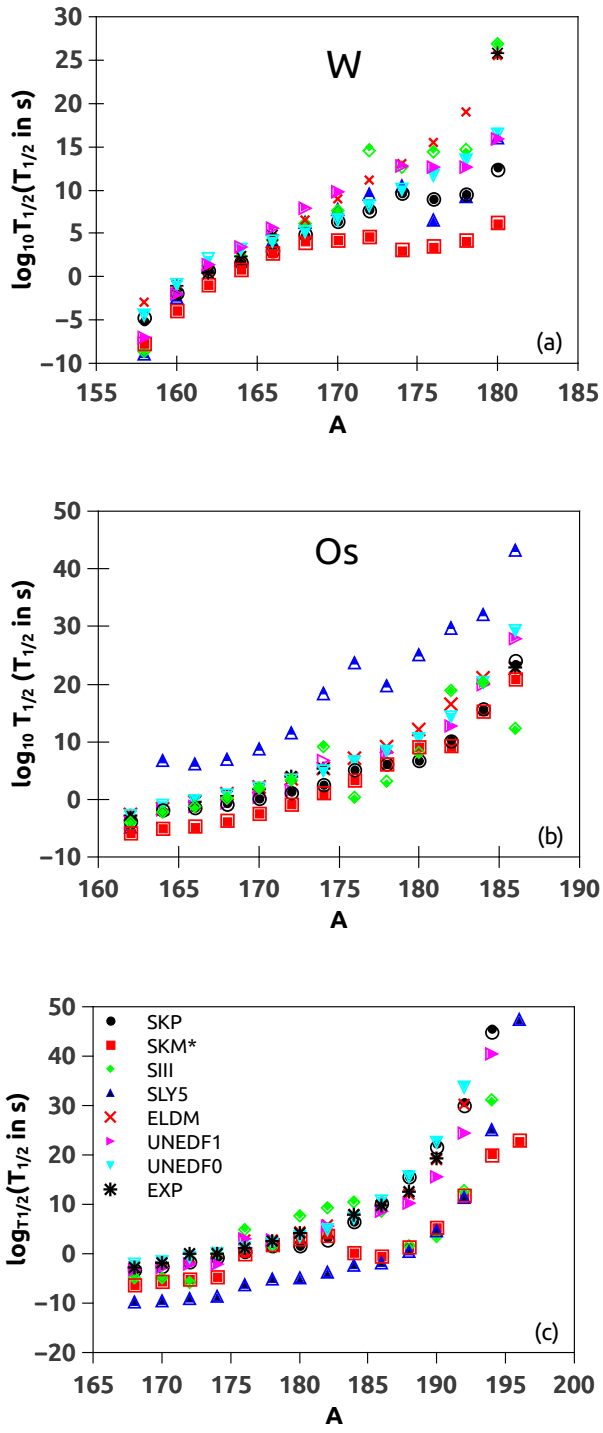

Figure 4.1: Plots showing logarithmic values of half-lives ($T_{1/2}$ in sec) against mass number of parent (A) nuclei, corresponding to alpha decay for HO(solid) and THO(open) basis in the case of (a) W, (b) Os and (c) Pt isotopes for different Skyrme forces.

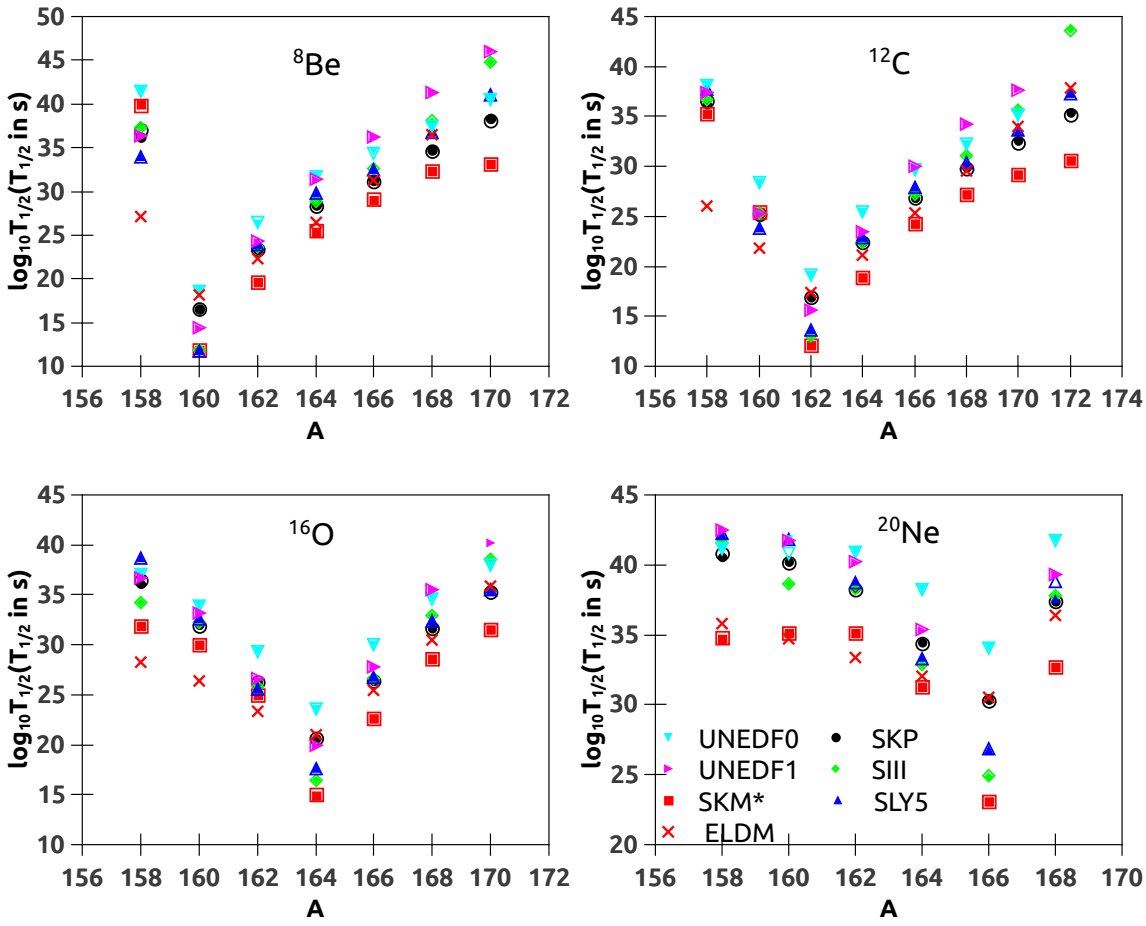

Figure 4.2: Plots showing logarithmic value of half-lives ($T_{1/2}$ in sec) of W isotopes against mass number of parent (A) nuclei, corresponding to different decay modes for HO(solid) and THO(open) basis (for different Skyrme forces).

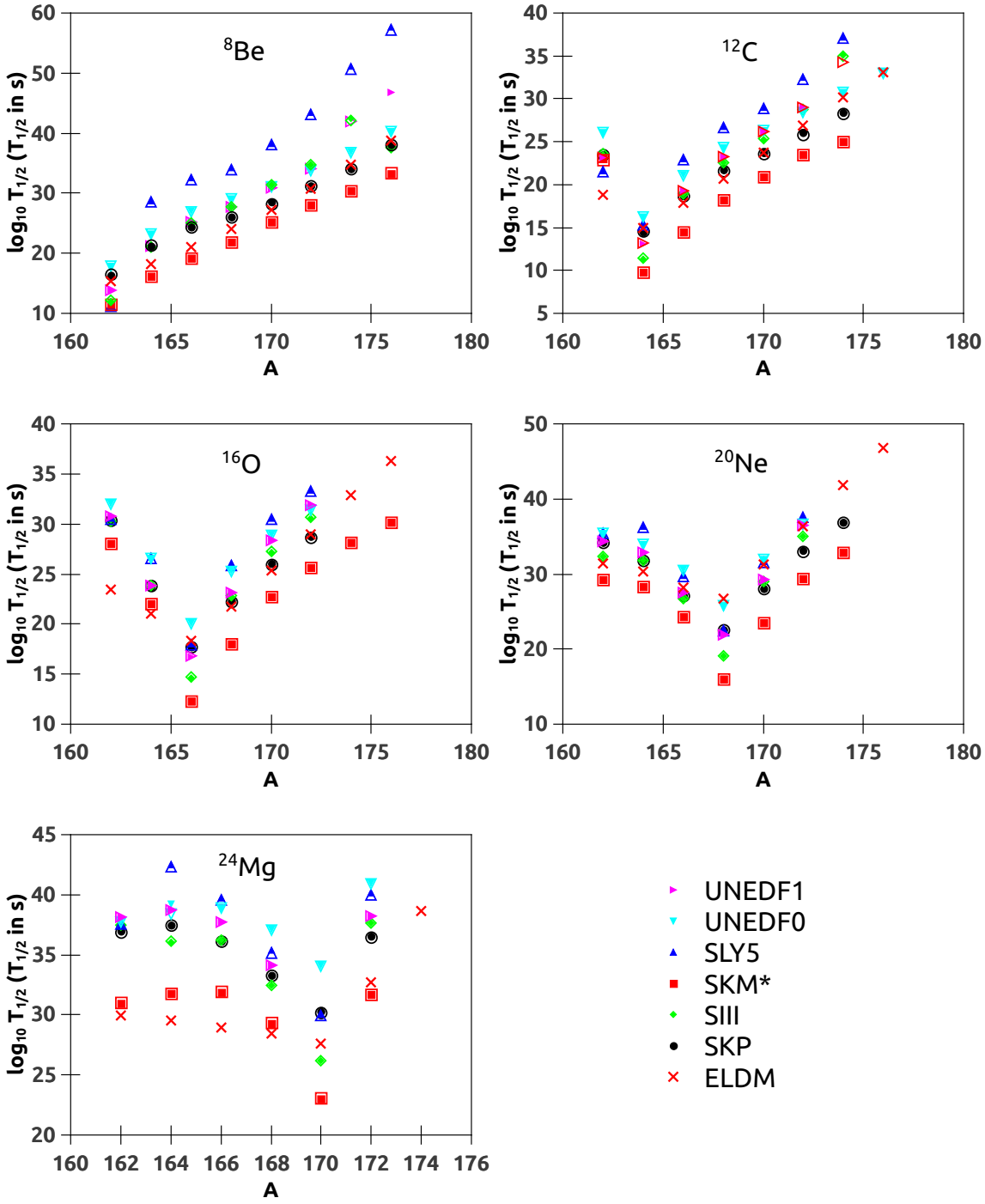

Figure 4.3: Plots showing logarithmic value of half-lives ($T_{1/2}$ in sec) of Os isotopes against mass number of parent (A) nuclei, corresponding to different decay modes for HO(solid) and THO(open) basis (for different Skyrme forces).

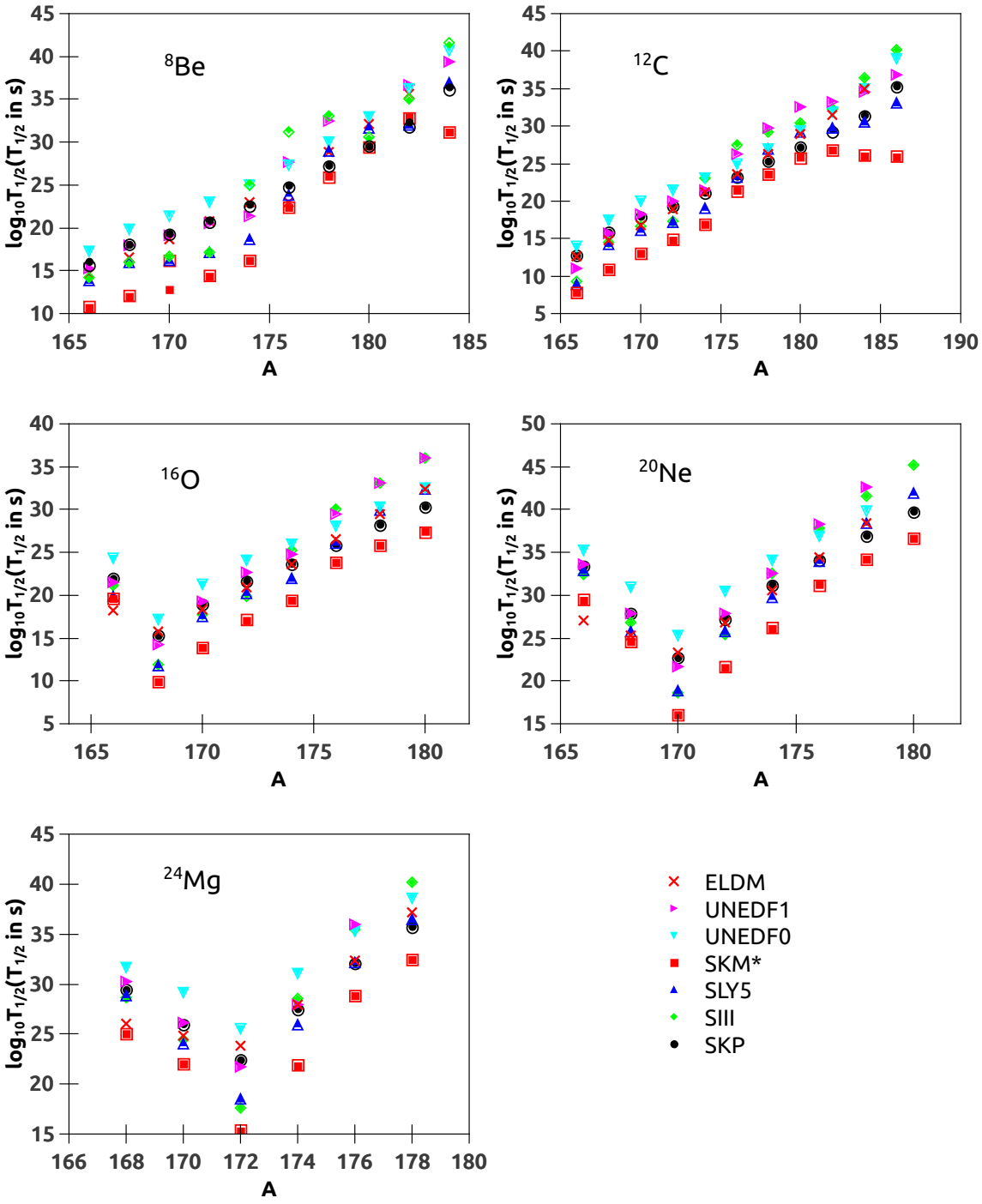

Figure 4.4: Plots showing logarithmic value of half-lives ($T_{1/2}$ in sec) of Pt isotopes against mass number of parent (A) nuclei, corresponding to different cluster decay modes for HO(solid) and THO(open) basis (for different Skyrme forces).

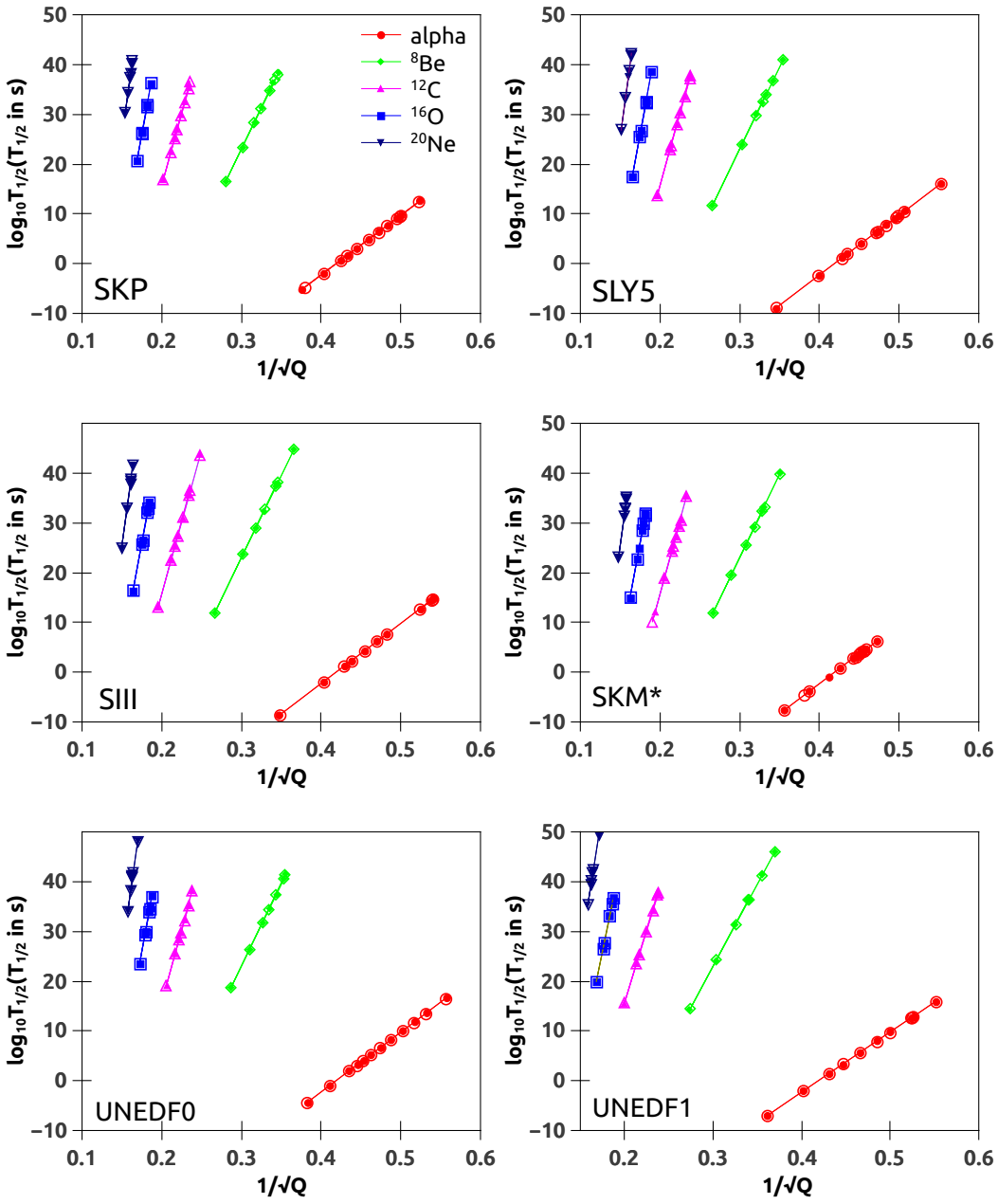

Figure 4.5: Geiger-Nuttal plots for different cluster decay modes of W for HO(solid) and THO(open) basis, corresponding to different Skyrme forces.

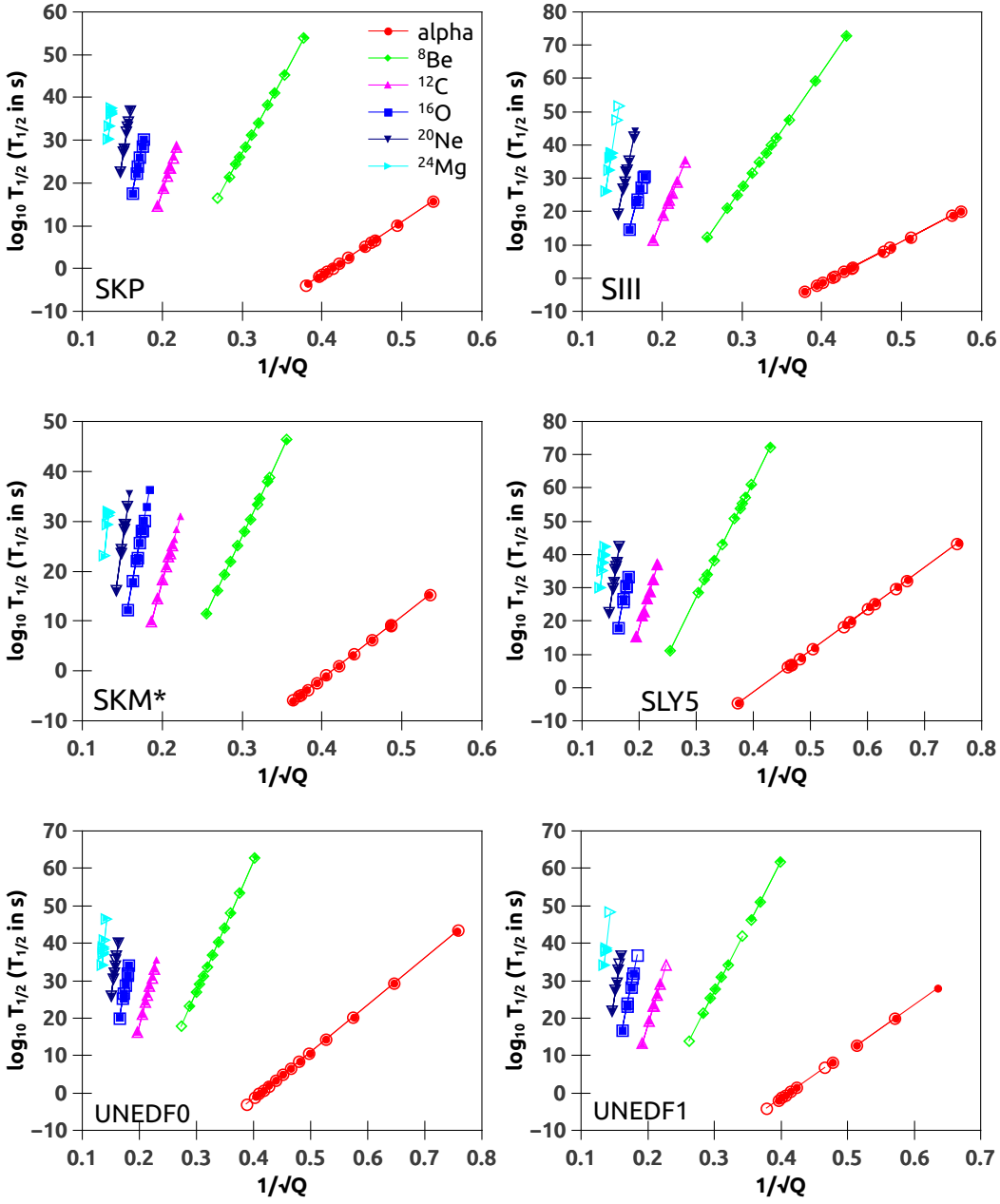

Figure 4.6: Geiger-Nuttal plots for different cluster decay modes of Os for HO(solid) and THO(open) basis, corresponding to different Skyrme forces.

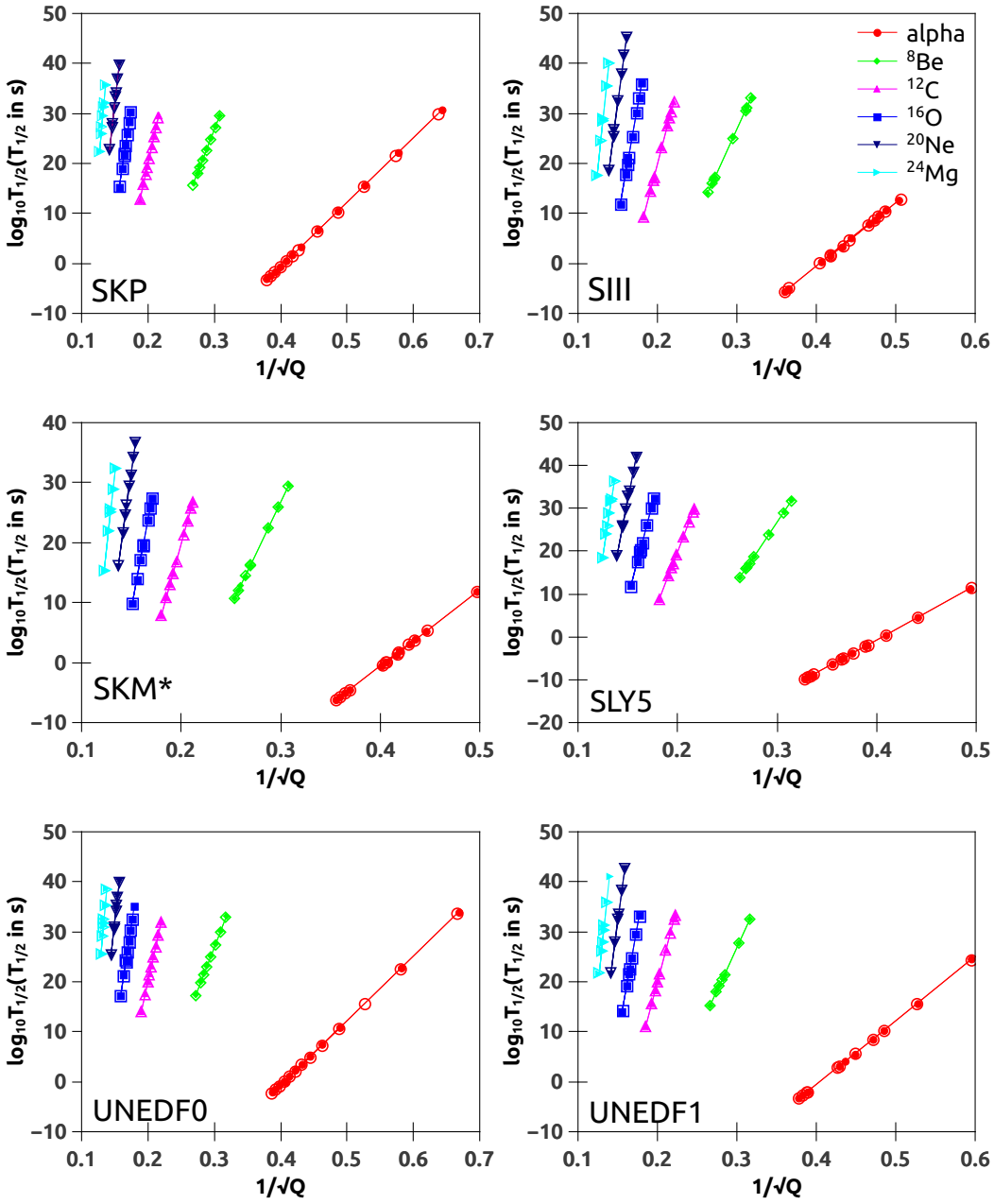

Figure 4.7: Geiger-Nuttal plots of different cluster decay modes of Pt for HO(solid) and THO(open) basis, corresponding to different Skyrme forces.

References

[1] M.V. Stoitsov, N. Schunck, M. Kortelainen, N. Michel, H. Nam, E. Olsen, J. Sarich, S. Wild, *Comp. Phys. Commun.*, **184**, 1592(2013).

[2] T. H. R. Skyrme, *Nucl. Phys.*, **9**, 615(1959).

[3] M. Beiner, H. Flocard, N. Van Giai, and P. Quentin, *Nucl. Phys. A.*, **238**, 29(1975).

[4] J. Dobaczewski, H. Flocard and J. Treiner, *Nucl. Phys. A*, **422**, 103(1984).

[5] E. Chabanat, P. Bonche, P. Haensel, J. Meyer and R. Schaeffer, *Nucl. Phys. A*, **627**, 710(1997).

[6] J. Bartel, P. Quentin, M. Brack, C. Guet, and H. B. Hakansson, *Nucl. Phys. A*, **386**, 79 (1982).

[7] M. Kortelainen, T. Lesinski, J. More, W. Nazarewicz, J. Sarich, N. Schunck, M.V. Stoitsov and S. Wild, *Phys. Rev. C*, **82**, 024313(2010).

[8] M. Kortelainen, J. McDonnell, W. Nazarewicz, P.G. Reinhard, J. Sarich, N. Schunck, M.V. Stoitsov and S. Wild, *Phys. Rev. C*, **85**, 024304(2012).

[9] R.R. Chasman, *Phys. Rev. C*, **14**, 1935(1976).

[10] J.Terasaki, P.-H. Heenen, P. Bonche, J. Dobaczewski and H. Flocard, *Nucl. Phys. A*, **593**, 1(1995).

[11] J. Dobaczewski, W. Nazarewicz and M.V. Stoitsov, *Eur. Phys. J. A*, **15**, 21(2002).

[12] J.Terasaki, H. Flocard, P.-H. Heenen and P. Bonche, *Nucl. Phys. A*, **621**, 706(1997).

[13] Dongdong Ni, Zhongzhou Ren, Tiekuang Dong and Chang Xu, *Phys.Rev. C*, **78**, 044310(2008).

[14] M. Wang, G. Audi, A. H. Wapstra, F. G. Kondev, M. MacCormick, X. Xu, and B. Pfeiffer, *CPC*, **36**, 12(2012).

[15] M. Goncalves and S. B. Duarte, *Phys. Rev. C* **48**, 2409(1993).

[16] M. Goncalves, S. B. Duarte, F. Garcia and O. Rodriguez, *Comp. Phys. Commun.*, **107**, 246(1997).

[17] D. A. Eastham and I. S. Grant, *Nucl. Phys. A*, **208**, 119(1973).

[18] F.A. Danevich, A.Sh. Georgadze, V.V. Kobychev, S.S. Nagorny, A.S. Nikolaiko, O.A. Ponkratenko,

[19] J. Borggreen and E. K. Hyde, *Nucl. Phys. A*, **162**, 407(1971).

[20] A. Siivola, *Nucl. Phys. A*, **84**, 385(1966).

[21] G. Graeffe, *Ann. Acad. Sci. Fenn. A*, **6**, 128(1963).

[22] W. Porschen and W. Riezler, *Z. Naturf.*, **11a**, 143(1956).

Chapter 5

Evolution of Neutron skin in transitional nuclei W, Os and Pt

5.1 Introduction

The developments of experimental facilities like Radioactive Ion Beams (RIB) help us to study the structural properties of a wide range of nuclei in the nuclear chart. Studying the structural properties of nuclei far from the stability line is an interesting area of research nowadays. However, the experimental facilities which exist today are not fully capable of studying nuclei very far from the stability line. In order to explore their properties, we have to rely mainly on theoretical methods. Hartree-Fock-Bogoliubov (HFB) theory [1] is one of the efficient self consistent mean field theories which is used to study nuclei away from the stability line. As we move away from the stability line, asymmetry between proton and neutron number increases. This results in the appearance of new phenomena like n-skin, halos etc.

Nuclear size is one of the important characteristic properties of a nucleus. Nuclear mass and radius are the main quantities used to probe the structure of a nucleus. Nuclear stability is determined mainly due to the interplay between strong nucleon-nucleon interaction and repulsive Coulomb force. Nuclei near the drip-line are weakly bound and this results in the spatial extension of neutrons. Protons do not have sufficient strength to hold the excess neutrons. Neutron

distribution diffuses out making the nuclear surface less defined. One of the interesting features of these nuclei is that, as the radial dimension increases, the separation energy decreases[2]. Approaching towards the neutron drip-line, Fermi energy becomes very close to zero and leads to particle continuum in these nuclei. Theoretical description of such nuclei is a very tedious task. BCS theory is not suitable for the description of nuclei towards drip-line as it fails to incorporate the continuum effects. But HFB theory serves good in this weakly bound region by taking into account the continuum effects fairly well.

We have tried to study these sort of structural properties of W, Os and Pt isotopes using Skyrme Hartree-Fock-Bogoliubov (HFB) theory. This theory serves well in the region away from the drip-line due to the inclusion of pairing correlation and thereby removes the continuum problems[3, 4]. Moreover we have used two different basis to solve HFB equations, the Harmonic Oscillator (HO) and Transformed Harmonic Oscillator (THO). HO basis explains the nuclear properties in the nuclear interior in the case of nuclei near and far from beta-stability line, very well. But in the case of exterior part of drip-line or weakly bound nuclei, HO basis expansion converges slowly and results in the reduction of densities and do not reflect the pairing correlations correctly. Under such situations THO is more appropriate[5, 6, 7].

5.2 The Formalism

For the purpose mentioned above, Skyrme HFB equations are solved using axially deformed cylindrical harmonic oscillator (HO) and transformed harmonic oscillator (THO) basis. As a general approach numerical calculations have been done with 20 oscillator shells. The cut-off energy is taken as 60 MeV. In the mean field part, we used the zero range Skyrme effective interaction. There exists a variety of Skyrme parametrizations. In the present case, we make use of some widely used Skyrme interactions like SIII[8], SKP[9], SKM*[10], SLY6[11], UNEDF0[12] and UNEDF1[13]. These Skyrme forces are found to be very effi-

cient in reproducing nuclear ground state properties. In the pairing part, density dependent delta interaction (DDDI)[14, 15] in the mixed form is used as in our previous studies.

Drip-line is the boundary of nuclear stability. At the drip-line, it is known that, the nucleon separation energy vanishes. Separation energy is the energy required to remove the last nucleon from the nucleus. Here, as we are interested in investigating neutron drip-line, we computed the 2n-separation energy. Neutron drip-line is characterised by $S_{2n} \approx 0$. It is estimated from the binding energy using the relation,

$$S_{2n}(N,Z) = BE(N,Z) - BE(N-2,Z) \tag{5.1}$$

where BE(N,Z) is the binding energy of the nucleus, Z is the atomic number and N is the neutron number.

The quantity which specifies the shape of a nucleus is the quadrupole moment. From the quadrupole moment, we have estimated the deformation parameter β_2 using the expression,

$$\beta_2 = \frac{4\pi}{3R^2A}\sqrt{\frac{5}{16\pi}}Q \tag{5.2}$$

where Q is the quadrupole moment, A is the mass number and $R = R_0A^{1/3}$, with $R_0 = 1.2$ fm.

In this part of our study, we have made an investigation of the neutron and proton distribution in the W, Os and Pt isotopes. The quantity which characterizes these are the neutron and proton radii. The mean square radius of neutron and proton can be obtained from nucleonic density ($\rho_{p,n}$)[16] and are given by

$$< r^2_{p,n} >= \frac{\int R^2\rho_{p,n}(R)d^3R}{\int \rho_{p,n}(R)d^3R} \tag{5.3}$$

and finally rms radii is given by

$$r_{rms}^{p,n} = \sqrt{< r_{p,n}^2 >} \tag{5.4}$$

Nuclear charge radii is obtained by folding the proton distribution with finite size of neutron and proton. Nuclear rms charge radii is evaluated using the simplified form of the expression [17],

$$r_c = \sqrt{r_p^2 + 0.64} \tag{5.5}$$

For the nuclei far from the stability line, the number of neutrons is much greater than that of protons. This leads to the formation of a thin layer of neutrons around the bulk matter of the nucleus. This layer which is termed as the neutron skin is measured as the difference between the neutron and proton rms radii [2].

$$skin\ thickness \equiv < r_n^2 >^{1/2} - < r_p^2 >^{1/2} \tag{5.6}$$

5.3 Results and Discussion

In the present work, we have made an attempt to study systematically the evolution of neutron skin and estimation of its thickness in W, Os and Pt isotopes. The selected isotopes ranges from 2p drip-line to 2n drip-line.

5.3.1 Potential Energy Curves

We have started by computing the Potential Energy Curves (PEC) by using quadratic constrained method[18]. In this method, we have to minimize $E^{'} = E + C(< \hat{Q}_{20} > -Q_{20})^2$, where C is the Stiffness constant and Q_{20} is the quadrupole moment. Thus, binding energy corresponding to a specific Q_{20} is obtained. Total

energy which corresponds to the minimum value is the ground state and all other local minima are the excited intrinsic states. We are interested only in the ground state properties. Fig. 5.1 shows the PEC of W isotopes corresponding to HO basis for some selected Skyrme forces. Similar plots are also there for Os and Pt. Since the PECs follow a similar trend in the case of Os and Pt isotopes, we have not shown them here. From the PECs we can see that the shape of the nuclei systematically changes betweeen prolate, oblate and spherical configurations.

In fig 5.2. we have shown the 2n-separation energy, which is evaluated from the binding energies using the equation (5.1). The calculated results have been compared with the available experimental values [19]. From the figure, we can see that, as the neutron number increases, ie, on approaching towards the drip-line, the separation energy decreases. This is evident from the fact that as the number of neutrons increases, the nucleons becomes less bound with each other and a small amount of energy is required to remove them from the nucleus. From the figure, a sudden fall in the separation energy is observed at the neutron shell closure (N=126). For W, Os and Pt isotopes, again a fall in the separation energy is observed at N=184. We can assume that at this neutron number the next shell closure exits and can be the next magic number after 126. Similar observations have been reported using RMF calculations in the case of super heavy nuclei by several groups [20]. On reaching the boundary, called the 2n-drip-line, separation energy becomes zero. It is observed that the prediction of drip-line nuclei is model dependent. It is found that for W isotopes, the drip-line nuclei varies between ^{248}W and ^{258}W. But in the case of Os and Pt isotopes most of the forces predicts ^{260}Os and ^{262}Pt as the drip-line nuclei.

Nuclear radius is one of the important quantities which helps in studying the structural properties of nuclei. Fig. 5.3 shows the rms radii of proton and neutron distribution. From the figure, we can visualise that as the mass number increases, neutron as well as the proton rms radii increases. Even if the proton number is a constant, the proton radii is also found to be increasing. This is due to the n-p interaction, which makes the proton distribution to extend a little

bit in accordance with the neutron distribution. All the Skyrme forces show the same trend in predicting the neutron and proton rms radii.

Fig. 5.4 shows the nuclear charge radii. We have compared them with the available experimental data. All the Skyrme forces show similar trend in predicting the nuclear charge radii, as before. SIII values overstimates all the other forces in the prediction of charge radii. All the others more or less predicts the values in the same way.

The excess of neutron matter in the case of nuclei far from the stability line indicate the formation of a layer of neutron around the bulk nuclear matter. Mathematically this is expressed as the difference of neutron and proton radii. Fig. 5.5 shows the formation of neutron skin in the selected nuclei as a function of asymmetry parameter. For the nuclei near to the beta-stability line, this difference is found to be 1-2 fm. When the difference of rms radii exceeds this value we can expect the formation of neutron skin around the bulk nuclear matter. Here, we observed that the layer width increases more than this limit and reaches a value around 5-6 fm near the 2n-drip-line. So a thin layer of neutron skin is observed to formed in the case of W, Os and Pt isotopes. We obtain a linear relationship between the skin thickness and mass number (or neutron number). Calculated values shows that SIII values understimates all other Skyrme forces. UNEDF values predicts a large skin thickness for all the nuclei under consideration.

The evolution of neutron skin can also be visualized with the help of density profile. We have plotted the neutron and proton density distribution of some selected isotopes of the isotopic chains in fig. 5.6. We can predict the formation of neutron skin in these isotopes by analysing the distance between the tail of neutron and proton density distributions. To show this difference more clearly, we have plotted the logarithm of density against the nuclear radii. In the case of nuclei near to beta-stability line this distance will be very small. From the figure, we have observed that as neutron number increases, this distance also starts increasing. This shows the formation of neutron skin in the isotopes towards the

neutron drip-line.

We have also estimated the deformation parameter of these nuclei. The computed values are depicted in fig. 5.7. Figure shows that at and near magic number (N=126 and 184), the deformation parameter is zero, showing spherical configuration. We can observe the change in the deformation parameter from prolate to oblate and then to spherical configuration.

5.4 Conclusion

In summary, we have made an attempt to investigate the emergence of neutron skin and its variation in transitional nuclei W, Os and Pt. The study has been carried out with the help of Skyrme HFB theory. Harmonic oscillator and Transformed harmonic oscillator basis have been employed in solving Skyrme HFB equation. In the present work, we made use of some widely used Skyrme interactions like SIII, SKP, SKM*, SLY6, UNEDF0 and UNEDF1. We have studied the 2n-separation energies, neutron and proton rms radii, deformation parameter and neutron and proton density distributions in these isotopes. We have observed a sudden fall in 2n-separation energy at N=126 and 184. So we have concluded that N=184 may be the next neutron magic number. The calculated deformation parameter also shows the spherical nature near N=184. We also searched for the neutron drip-line nuclei and found that they are mainly model dependent. We observed that as the neutron number increases, the neutron and proton rms radii increases. We noticed that, in W, Os and Pt isotopes, on approaching neutron drip-line, the difference between neutron and proton radii increases which results in the formation of neutron skin. The same has been shown with the aid of density profile. In short, we have shown the ability of different Skyrme forces in predicting these properties in the unexplored regions of the nuclear chart.

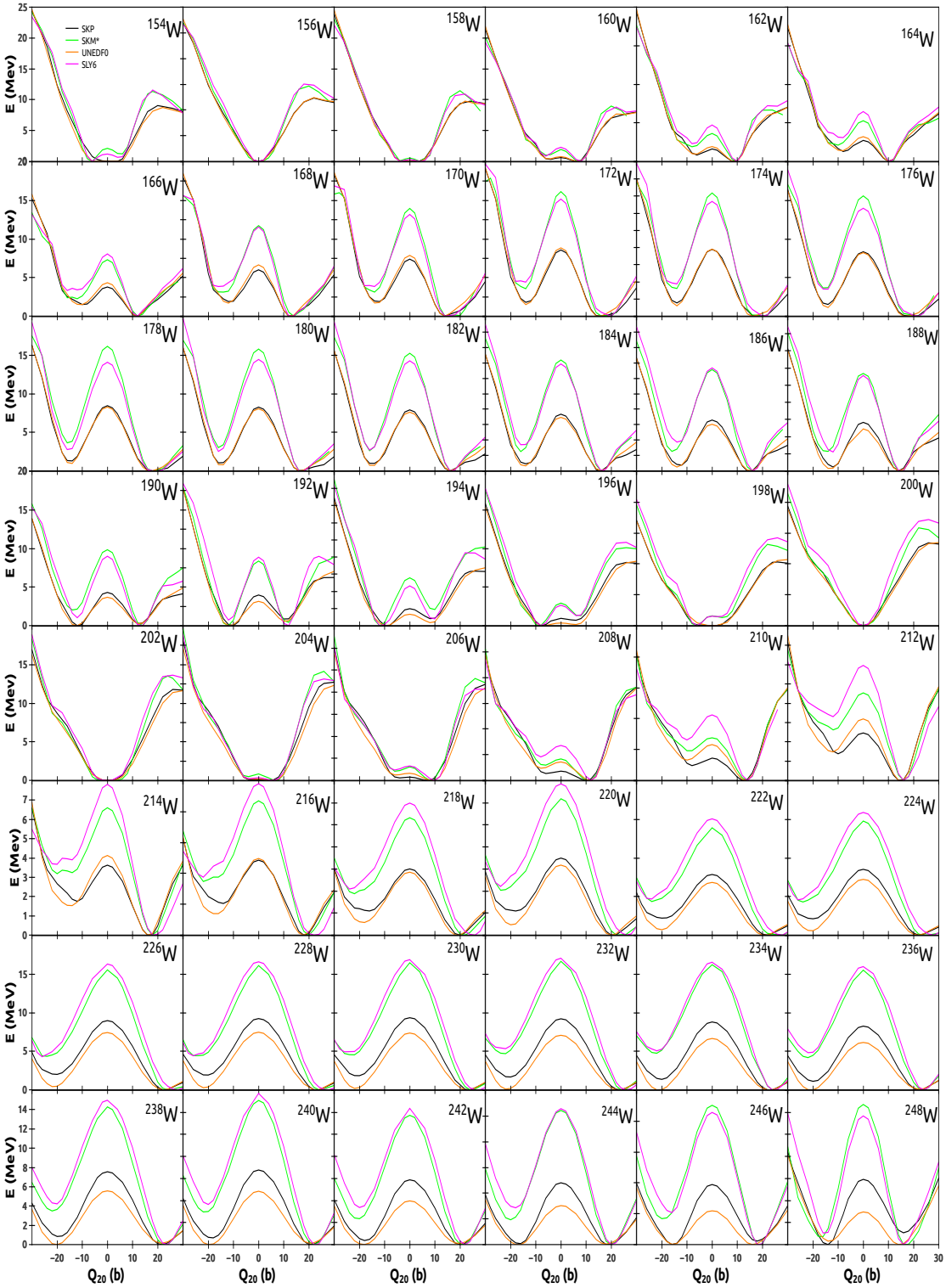

Figure 5.1: Potential energy curves for W isotopes for selected Skyrme forces .

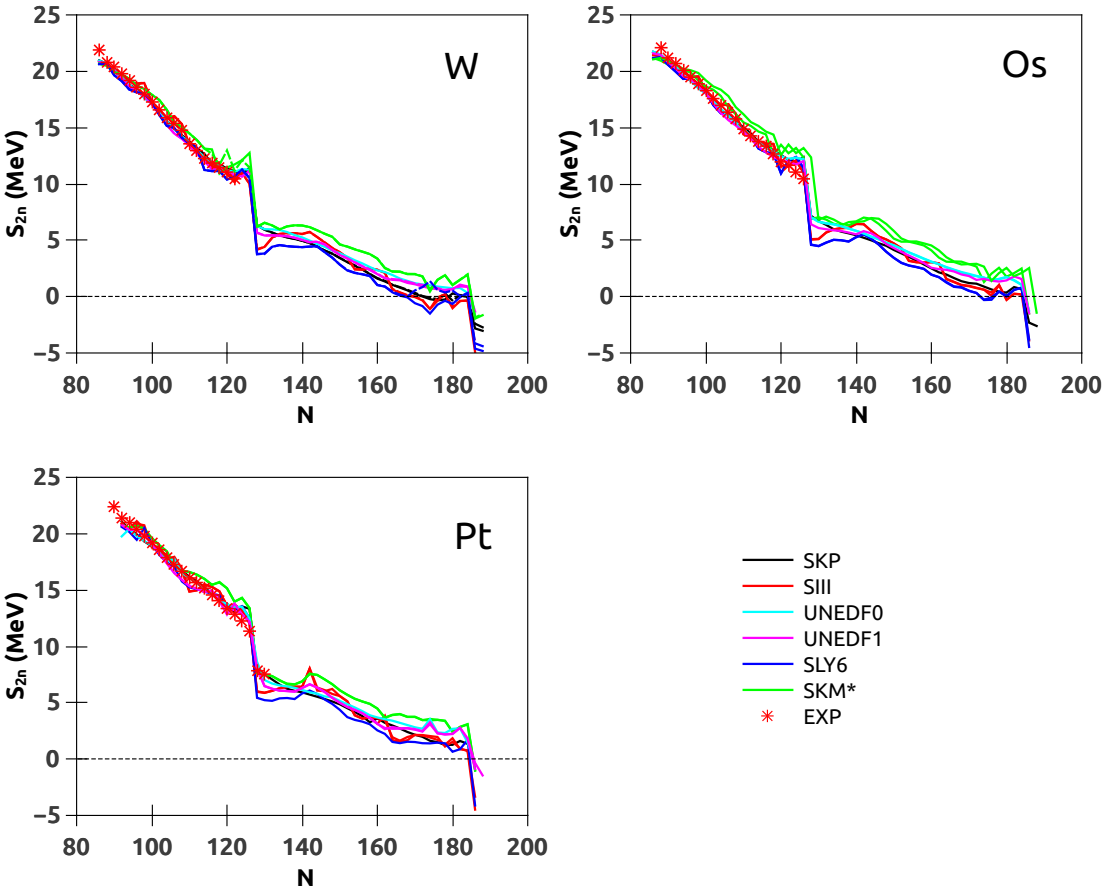

Figure 5.2: 2n-separation energy calculated using HO (solid) and THO (dashed) basis

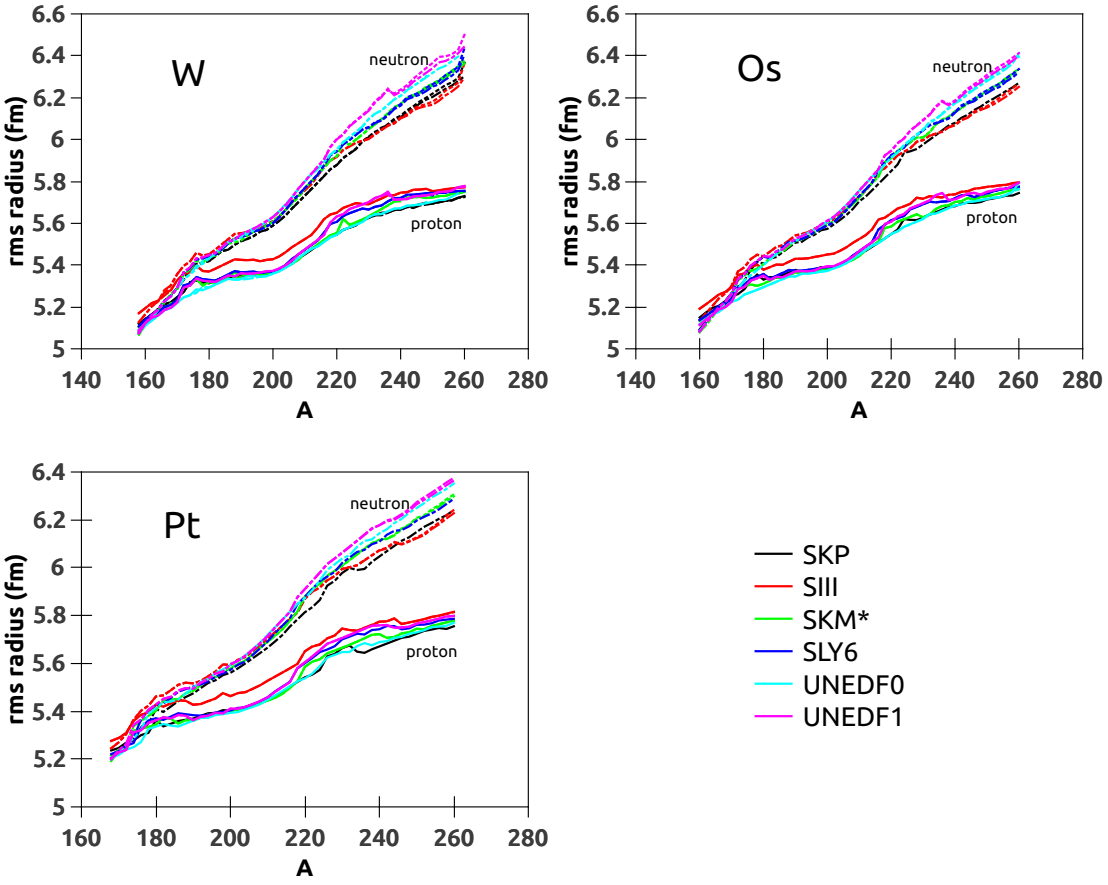

Figure 5.3: Neutron and proton rms radii calculated using HO and THO basis

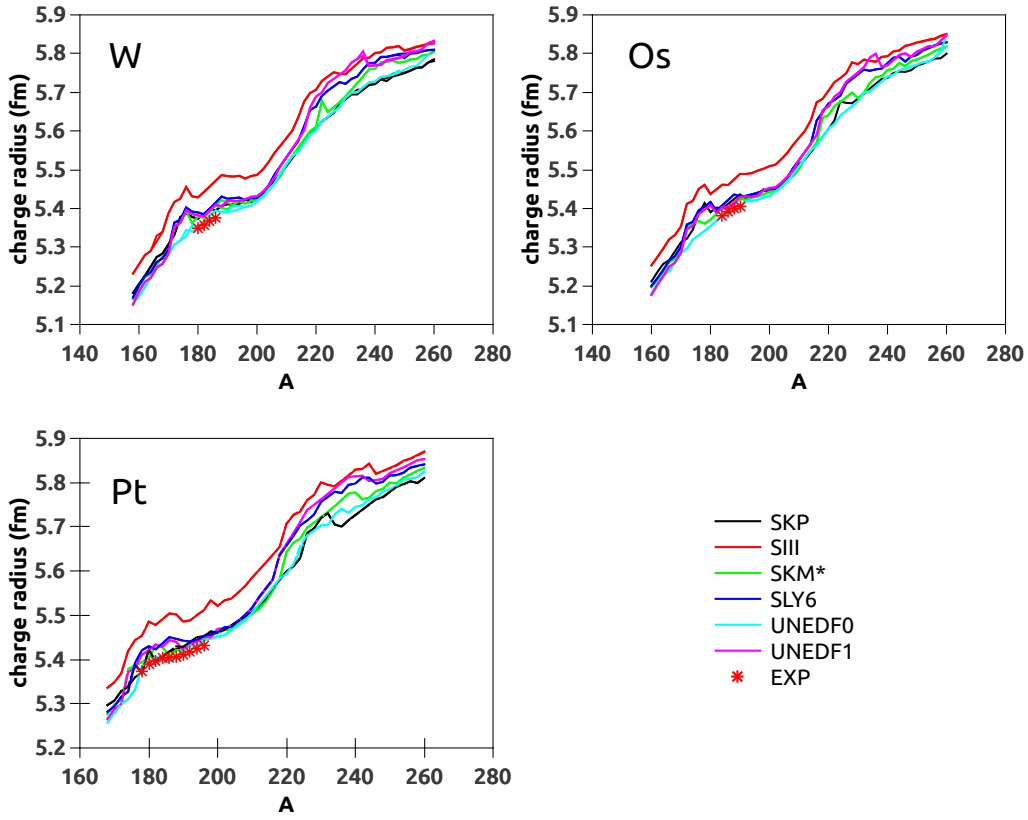

Figure 5.4: Nuclear charge radii calculated using HO (solid) and THO (dashed) basis

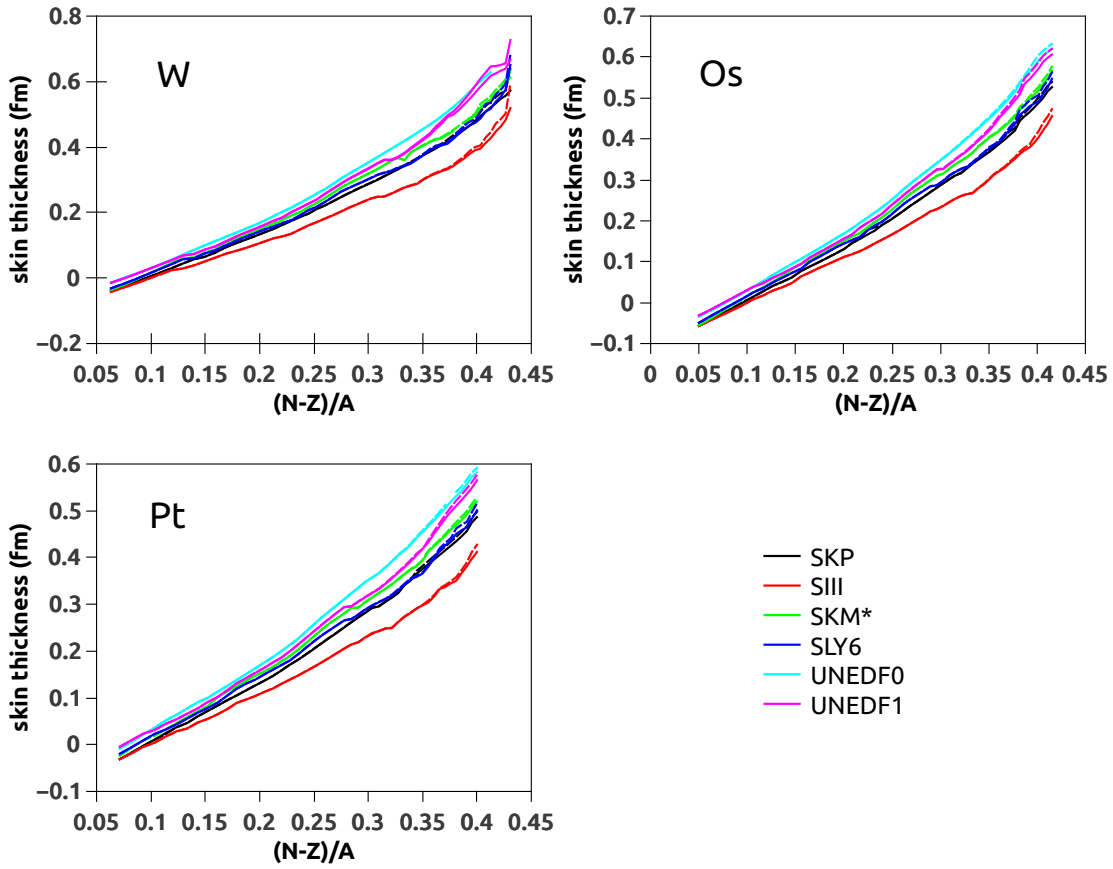

Figure 5.5: Neutron skin thickness calculated using HO (solid) and THO (dashed) basis

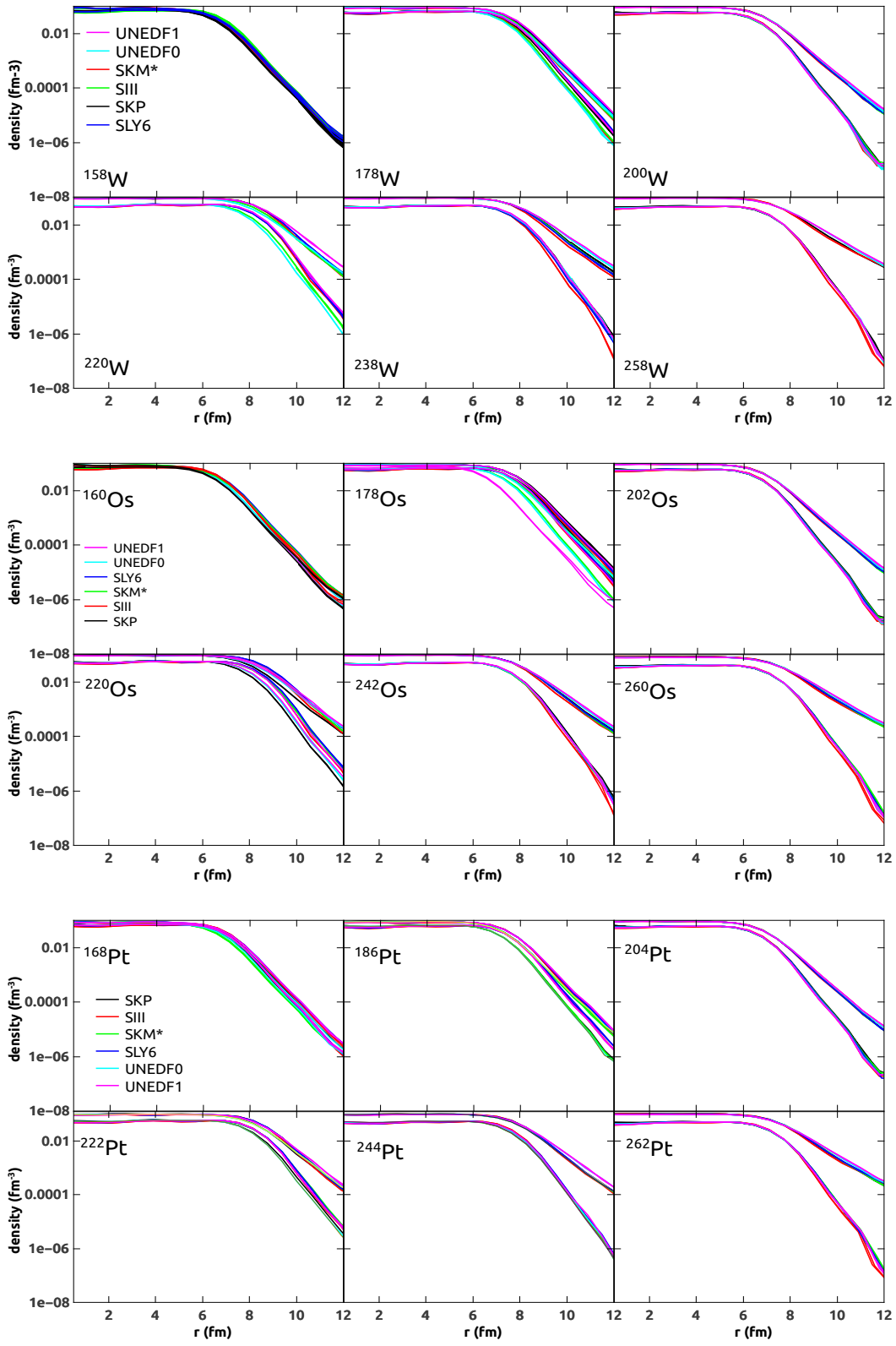

Figure 5.6: Neutron and proton density distribution of W (top), Os (middle) and Pt (bottom) using HO (solid) and THO (dashed) basis

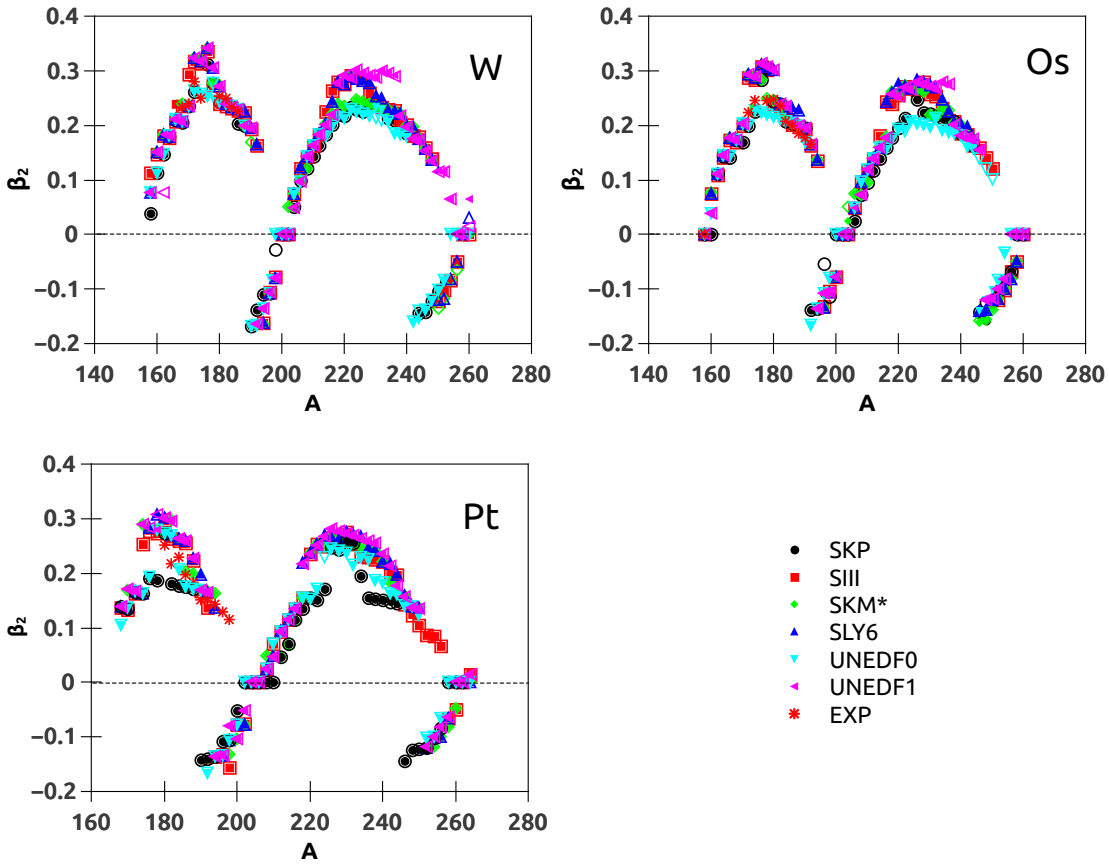

Figure 5.7: Deformation parameter calculated using HO (solid) and THO (dashed) basis

References

[1] P. Ring and P. Shuck, *The Nuclear Many-Body Problem*, (Springer, Berlin, 1980).

[2] S. Mizutori, J. Dobaczewski, G. A. Lalazissis, W. Nazarewicz, and P.-G. Reinhard, *Phys. Rev. C*, **61**, 044326(2000).

[3] J. Dobaczewski, W. Nazarewicz, T.R. Werner, J. F. Berger, C. R. Chinn and J. Decharge, *Phys. Rev. C*, **53**, 2809(1996).

[4] J. Dobaczewski, I. Hamamoto, W. Nazarewicz and J. A. Sheikh, *Phys. Rev. Lett.*, **72**, 981(1994).

[5] M. V. Stoitsov, W. Nazarewicz, and S. Pittel, *Phys. Rev. C*, **58**, 2092(1998).

[6] M. V. Stoitsov, J. Dobaczewski, P. Ring, and S. Pittel, *Phys. Rev. C*, **61**, 034311(2000).

[7] M. V. Stoitsov, J. Dobaczewski, W. Nazarewicz, S. Pittel, and D. J. Dean, *Phys. Rev. C*, **68**, 054312(2003).

[8] M. Beiner, H. Flocard, N. Van Giai, and P. Quentin, *Nucl. Phys. A.*, **238**, 29(1975).

[9] J. Dobaczewski, H. Flocard and J. Treiner, *Nucl. Phys. A*, **422**, 103(1984).

[10] J. Bartel, P. Quentin, M. Brack, C. Guet, and H. B. Hakansson, *Nucl. Phys. A*, **386**, 79 (1982).

[11] E. Chabanat, P. Bonche, P. Haensel, J. Meyer and R. Schaeffer, *Nucl. Phys. A*, **635**, 231(1998).

[12] M. Kortelainen, T. Lesinski, J. More, W. Nazarewicz, J. Sarich, N. Schunck, M.V. Stoitsov and S. Wild, *Phys. Rev. C*, **82**, 024313(2010).

[13] M. Kortelainen, J. McDonnell, W. Nazarewicz, P.G. Reinhard, J. Sarich, N. Schunck, M.V. Stoitsov and S. Wild, *Phys. Rev. C*, **85**, 024304(2012).

[14] R.R. Chasman, *Phys. Rev. C*, **14**, 1935(1976).

[15] J.Terasaki, P.H. Heenen, P. Bonche, J. Dobaczewski and H. Flocard, *Nucl. Phys. A*, **593**, 1(1995).

[16] N. Schunck and J. L. Edigo, *Phys. Rev. C*, **78**, 064305(2008).

[17] M. Bender, P.H. Heenen and P.G. Reinhard, *Rev. Mod. Phys*, **75**, 121(2003).

[18] A. Staszczak, M.Stoitsov, A. Baran, and W. Nazarewicz, *Eur. Phys. J. A*, **46**, 85(2010).

[19] M. Wang, G. Audi, F. G. Kondev, W. J. Huang, S. Naimi and X. Xu *CPC*, **41**, 030003(2017).

[20] M. Bhuyan and S. K. Patra, *Pramana J. Phys.*, **82**, 851(2014).

Chapter 6

Summary and Conclusion

The thesis starts with a basic introduction to the properties of the nuclei and the different models proposed for the study of their structural properties. The aim of the thesis is to study the structural properties of some transitional nuclei like W, Os and Pt along their isotopic chain. The study has been conducted with the help of a microscopic model - Hartree-Fock-Bogoliubov theory. In the mean-field part, we have made use of the zero range effective Skyrme interaction. In the pairing part, we adopted the density-dependent delta interaction (DDDI) in the mixed form where the volume and surface part are given equal importance. We have made a survey on these nuclei along their isotopic chain and found that certain phenomena dominate a particular region of the chain.

In the first part we tried to analyse the shape transition in transitional nuclei W, Os and Pt. As a part of this we have computed the potential energy curves for the selected nuclei and observed a transition in their shape from proton drip-line to neutron drip-line. As some signature of triaxiality is found, we did triaxial calculations also with the help of UNEDF1 parametrization for W, Os and Pt isotopes around the neutron shell closure (N=126). It was observed a transition to spherical at N=126 from prolate via γ -soft region.

In the second part, we studied the decay properties of these nuclei. We analyzed the feasibility of alpha and cluster radioactivity of the isotopes of these nuclei. We surveyed throughout the isotopic chain and found that these decay modes are dominant between the proton drip-line and beta-stability line. The

probability of alpha and cluster emission diminishes with the increase of neutron number. The study emphasised the role of magicity in cluster radioactivity. It was predicted that the rate of decay is maximum for those decays which leads to magic daughter nuclei. It was also observed that as the mass of parent increases, we could expect more massive clusters. The linear nature of the Geiger-Nuttel plot is also reproduced.

In the third part, we extended our study to neutron-rich region of the isotopic chain of W, Os and Pt. It was observed that, as we move towards the neutron drip-line some interesting phenomena starts to occur. Here the number of neutrons will be much greater than protons. The n-p interaction is not sufficient enough to hold the excess neutrons inside the core. This will lead to the formation of a thin layer of neutrons around the bulk nuclear matter. It is characterised by the difference of neutron and proton rms radii. Towards drip-line, this difference increases to about 1-2 % of that at the stability line. We have also computed 2n-separation energy for these nuclei. A sudden fall in its value is observed at neutron shell closure (at the magic number). We found such a sudden fall at N=126 and 184. Deformation parameters are also calculated which shows that around N=184, the isotopes are spherical. So it may be considered that N=184 is the magic number next to N=126.

Future perspectives

- The study can be extended to odd-mass isotopes also. While considering odd-mass isotopes, we have to use either blocking approximation or equal filling approximation.

- In the present case, we have adopted only the zero-range Skyrme interaction. The investigation can be carried out with the help of finite range Gogny interaction also.

- Here we have studied the evolution of neutron skin thickness near the neutron drip-line. Another interesting phenomenon which is gaining current

interest is the neutron halo.

- The superheavy nuclei (SHN) is an exciting area which is having the current interest. We can use the HFB theory to study the structural properties of SHN.

- We can extend our investigations to analyze the phenomena of nuclear fission and other related properties in these nuclei.

- Our present study concentrates only on the ground state properties of nuclei. Nuclei can exist in the excited state as well. So it will be interesting to study the properties of excited states.